Mechanistic Insights into the Auto-Regulation of PTEN and Its Related HECT E3 Ligases

by

Zan Chen

A dissertation submitted to Johns Hopkins University in the conformity with the requirements for the degree of Doctor of Philosophy

Baltimore, Maryland

2017

Abstract

PTEN (phosphatase and tensin homolog deleted on chromosome 10) is a lipid phosphatase that dephosphorylates PIP3 to PIP2, and negatively regulates the PI3K/AKT signaling pathway. PTEN is an essential tumor suppressor gene frequently deactivated in cancer cells. Previous work in our lab and by others has shed light on the regulation of PTEN by a cluster of phosphorylation sites within the C-terminal regulatory tail at residues Ser380, Thr382, Thr383 and Ser385. Tetra-phosphorylation of the C-terminal tail binds to the C2 domain and leads to a closed conformation which inhibits PTEN's lipid phosphatase activity and membrane association, but increases its stability. We continued to investigate the molecular mechanisms of this regulatory mechanism using native chemical ligation. Systematic evaluation of the PTEN C-tail phospho-cluster showed that the conformational closure and autoinhibition was influenced by the aggregate effect of multiple phospho-sites rather than dominated by a single phosphorylation site. The photo-crosslinking results suggested that the phosphorylated C-tail not only interacts with the C2 domain but also the N-terminal phosphatase domain. The ubiquitination assays analyzing PTEN ubiquitination by WWP2 showed that PTEN C-tail phosphorylation could inhibit its ubiquitination by the HECT E3 ligases, presumably by disrupting the protein-protein interaction between PTEN and WWP2.

In the course of analyzing PTEN ubiquitination by WWP2, we noticed that the monomeric WWP2 is autoinhibited. WWP2 is a member of the NEDD4 HECT E3 ligase family, and the autoinhibition mechanisms of this family have been reported as involving intramolecular interactions between C2 or WW domains with the corresponding catalytic HECT domains. However, we found unexpectedly that a peptide linker tethering WW domains is the key regulatory element of WWP2 catalytic activity. Biochemical,

structural, and cellular analyses have revealed that the linker can lock the HECT domain in an inactive conformation and block the proposed allosteric ubiquitin binding site. Such linker mediated autoinhibition can be relieved by linker post-translational modifications, but complete removal of the linker can induce hyperactive autoubiquitination and E3 self-destruction. We further showed that this regulatory mechanism is not limited to WWP2, but also applies to the related HECT family members WWP1, ITCH, and NEDD4-1.

To my family, my friends and my advisor, without whom this never would have been possible.

Acknowledgements

I would like to express my deepest gratitude to my advisor Dr. Philip A. Cole, for his continuous support and guidance during my study at Hopkins. I have many thanks to Dr. Sandra Gabelli, who has been a great collaborator and thesis committee member during the past four years of study. I wish to thank the other committee members, Dr. Cynthia Wolberger and Dr. Peter Devreotes who provided tremendous amount of help. I also want to thank my collaborator Dr. Mario Amzel and rotation mentor Dr. Jun Liu.

I would like to extend my gratitude to my current and former colleagues, Hanjie Jiang, Dr. Daniel Dempsey, Dr. David Bolduc, Wei Xu, Dr. Yun Wang, Dr. Nam Chu, Sam Hanegar, Dawn Hayward, Dr. Mingxuan Wu, Dr. Jay Kalin, Dr. Yousang Hwang, Dr. Beth Zucconi, Dr. Brian Wieser, Dr. Shri Bhat and Dr. Zhihong Wang, for their great support and helpful suggestions on my research project.

I would like to especially thank Yana Li, Xiaoguang Li and Xiangbin Zhang for their technical support in my projects, and thank Amy Paronto, Mimi Guercio, Robin Hart, Brenda Figueroa and Deborah Saylor in the Pharmacology department.

Finally, I would like to thank my parents, mother Yuanshi Li, father Deqiang Chen, for their love and support. I share my happiness and pride in completing my Ph.D. with them.

Intended to be blank

Table of Contents

List of Tables

List of Figures

Chapter 1: Introduction

1.1 Post-translational Modifications

While genes keep and encode the genetic information of life, proteins are the executor of most biological functions. Millions of different protein molecules with various sizes, shapes, structures and functions working together inside and outside of the cell contribute to the well-being of a normal healthy organism. Not only do the proteins have to function proficiently, they also have to adjust their activity precisely in response to different environment stimuli to support biological processes such as cell growth, proliferation, death, differentiation. As new functional groups in the side-chain or terminus of proteins, post-translational modifications expand the chemical repertoire of the 20 natural amino acids utilized by cells.(*1, 2*) The most common post-translational modifications include phosphorylation, ubiquitination, acetylation, glycosylation and methylation.(*3*) Attachment of these groups to the protein can change the size and charge of the unmodified protein and confer alterations in protein conformation, protein-protein interactions, and enzymatic activity.(*3, 4*) Post-translational modifications, as the fundamental character of cell signal transduction, mediates almost all biological processes, and establishes the precise communication within cells.(*5*)

Determining the mechanisms of how post-translational modifications are regulated represent an exciting area of research. In many cases, the enzymes that catalyze protein post-translational modifications are also regulated by post-translational modifications catalyzed by other enzymes, forming cascading pathways and inducing cross-talk among distinct post-translational modifications.(*4, 6*)

1.2 PTEN Phosphorylation and Ubiquitination

PTEN (Phosphatase and Tensin Homolog deleted on chromosome 10) is a lipid phosphatase that hydrolyzes phosphatidylinositol 3,4,5-triphosphate (PIP3), converting it to phosphatidylinositol 4.5-diphosphate (PIP2).(Figure 1)(*7, 8*) PIP3 is the key second messenger in the PI3 kinase-Akt signaling pathway.(*9*) The activation of Akt by PIP3 induces multiple downstream signaling events, including promotion of cell proliferation, growth and survival, and the PI3K-Akt pathway is often perturbed in human cancer.(*8*) PTEN, is the best defined negative regulator of PI3K-Akt pathway that suppresses carcinogenesis.(*10, 11*) PTEN is the second most frequently-mutated gene in cancer, and the activity of PTEN is down-regulated in many types of cancer, such as prostate cancer, breast cancer, glioblastoma, and lung cancer.(*12, 13*) Down-regulation of PIP3 inhibits the activation of Akt, thus arresting cell proliferation. Beyond its lipid phosphatase activity to counteract PI3K action, PTEN protein-protein interactions may also play roles in its anti-tumor activity.(*14, 15*)

Human PTEN is a protein that is composed of 403 amino acids and its architecture consists of three major domains, an N-terminal phosphatase domain, a central C2 domain, and a regulatory C-terminal domain (C-tail). A crystal structure of PTEN solved in 1999 uncovered detailed structural information about the phosphatase domain and C2 domain.(*16*) The phosphatase domain (residues 15-186) contains the catalytic residue signature motif CxxGxR. C124 is a nucleophilic catalyst in the PTEN reaction. Although in the tyrosine phosphatase family, the PTEN structure is different from typical protein tyrosine phosphatases in that its catalytic pocket is much larger and can accommodate the larger phospholipid substrate. The C2 domain (residues 187-351) is involved in membrane binding. A loop enriched in lysines called the CBR III loop within the C2 domain is believed to directly contact phospholipids on membranes. The C-tail of PTEN

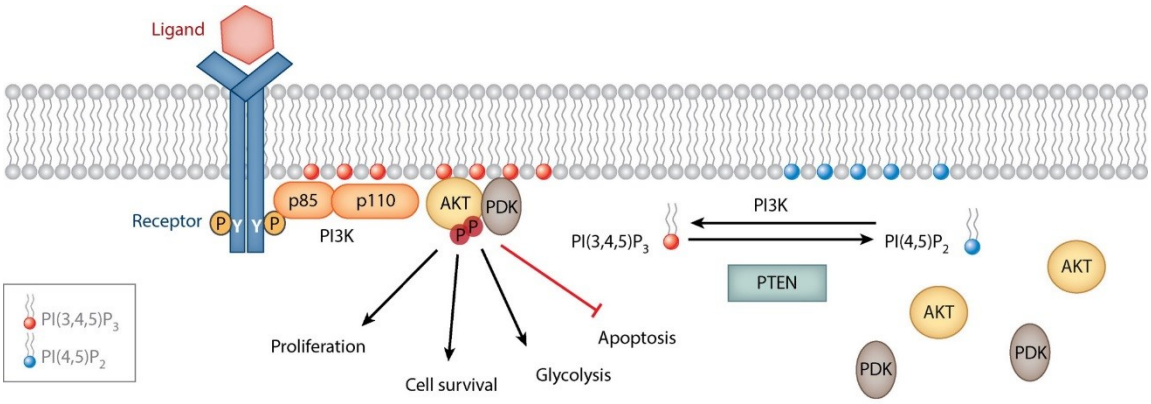

Figure 1: The PI3K/PTEN/AKT signaling pathway. In response to ligand binding (such as growth factor and hormones), receptor tyrosine kinases (RTKs) dimerize, stimulating their kinase activity and autophosphorylation. The phosphorylated tyrosine(s) within RTKs recruits PI3K through binding to the p85 subunit that contains an SH3 domain. While recruited to the plasma membrane, PI3K phosphorylates the lipid $PI(4,5)P_2$, generating $PI(3,4,5)P_3$. PIP3 acts as a second messenger to recruit PDK and AKT to the plasma membrane, where AKT is phosphorylated and activated. The activated AKT phosphorylates downstream targets which promote cell proliferation, cell survival, glycolysis and resistance to apoptosis. PTEN dephosphorylates PIP3 and turns off this pathway(*8*).

(residues 352-403) is a regulatory domain that is highly negatively charged and subject to several post-translational modifications. Although it is widely accepted that the PTEN C-tail has a critical regulatory role, the solved PTEN crystal structure lacked the 49 C-terminal residues, presumably due to the C-tail's intrinsic flexibility.

PTEN is highly post-translationally modified including by phosphorylation, acetylation, Cys oxidation, ubiquitination, and SUMOylation,(*8, 17*) The C-tail of PTEN is rich in serine/threonine residues and a number of these have been shown to be phosphorylated. These phosphorylation sites include S362, T366, S370, S380, T382, T383, S385, and S398,(*8, 18*) and the cluster of residues S380, T382, T383, S385, have been reported to regulate PTEN stability, activity and subcellular localization.(*19-21*) This cluster of serine/threonine residues is believed to be phosphorylated by casein kinase 2 (CK2) in sequential fashion, S385 followed by S380, and then T382/T383.(*22, 23*) These phosphorylation events induce a conformational change in which the C-tail binds to the C2 domain of PTEN and this down-regulates the phosphatase activity and disrupts phospholipid binding, thus inhibiting the localization to plasma membrane.(Figure 2)(*19*) There are reports that C-tail phosphorylation also protects PTEN from proteasomal degradation. Phosphorylated PTEN has also been reported to inhibit its association within protein complexes relative to non-phosphorylated PTEN.(*24*) Phosphorylation on T383 is suggested to be critical for regulating cancer cell migration.(*15*) Thus the available evidence points to the importance of PTEN phosphorylation on S380, T382, T383, S385 and elucidating a more detailed structure of phospho-PTEN could provide key insights into the biology of PTEN and give guidance to new therapy for cancer and other diseases.

Apart from phosphorylation, ubiquitination is another important post-translational modification that regulates PTEN.(*8, 17*) In some cancer cell lines with no mutation in

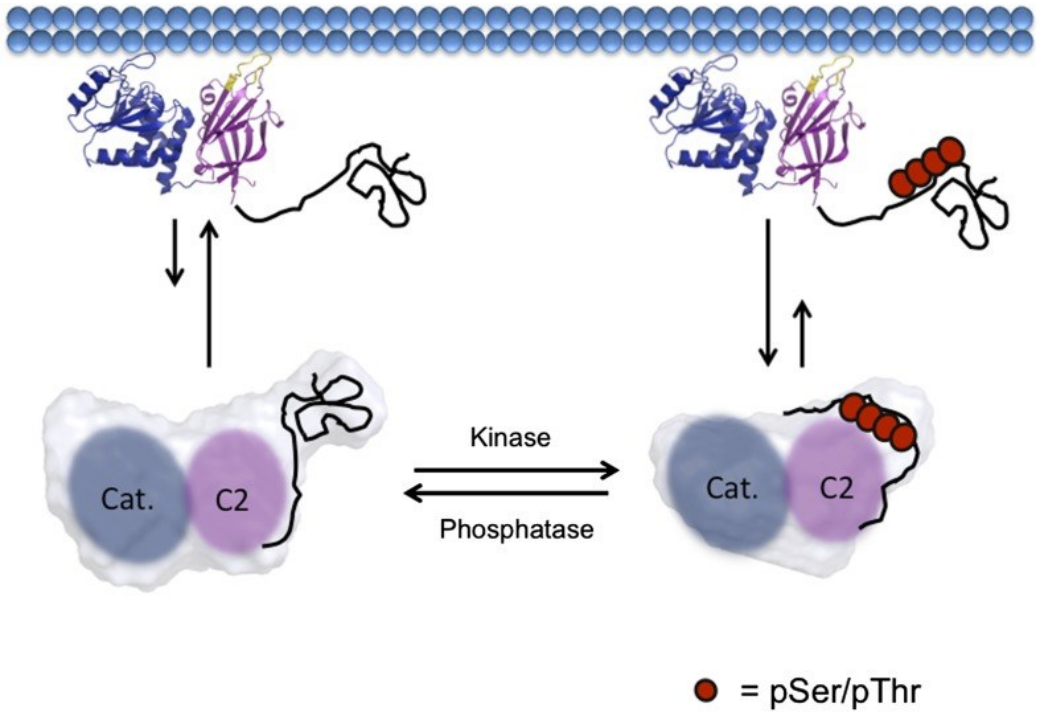

Figure 2: Schematic showing the regulation of PTEN by C-tail phosphorylation. The nonphosphorylated C-tail of PTEN is unstructured and does not interact with the core of the protein, and PTEN stays in the open conformation. This nonphosphorylated form of PTEN has high affinity for the plasma membrane and high enzyme activity. When PTEN is tetra-phosphorylated at residues Ser380, Thr382, Thr383 and Ser385, the phospho-C-tail binds to the C2 domain, rendering a closed conformation. This conformational change decreases PTEN's enzyme activity, membrane association, and enhances its stability(*19*).

the PTEN gene, the loss of PTEN protein is attributed to ubiquitin-mediated degradation.(*25*) Several E3 ligases for PTEN have been discovered, including NEDD4-1, WWP2 and XIAP.(*26-28*) NEDD4-1, a HECT family E3 ligase, was the first discovered E3 ligase to ubiquitylate PTEN promoting both poly- and mono-ubiquitination. Poly-ubiquitination by NEDD4-1 is suggested to regulate PTEN stability through proteasomal degradation, while mono-ubiquitination on K13 and K289 is reported to enhance PTEN's localization into nucleus.(*29, 30*) However, there is a provocative study showing that mice or cells depleted of NEDD4-1 by knockout have unchanged PTEN stability or localization, arguing for the role of other E3 ligases involved in PTEN regulation.(*26*) WWP2 is another HECT E3 ligase for PTEN, regulating PTEN stability through poly-ubiquitination.(*27*) Degradation of PTEN by WWP2 has been shown to be involved in melanoma development after UV exposure.(*31*) Another proposed E3 for PTEN, XIAP, is a Ring-finger family E3 ligase that regulates PTEN stability and nuclear localization by both mono- and poly-ubiquitination.(*28*) Since C-tail phosphorylation has been described to inhibit degradation, we hypothesize that this mechanism may involve phosphorylation mediated changes in the interactions among PTEN and E3 ligases. Biochemical and biophysical study into the details of non-phosphorylated and phosphorylated PTEN with E3 ligases could help better illuminate how PTEN is regulated by phosphorylation and ubiquitination.

Beyond post-translational modifications, PTEN activity and stability is likely regulated by protein-protein interactions. PTEN has been reported to interact with MAGI-2, MAST1,2,3, DLG1, NHERF1,2, P85a, DJ1, Man2C1, Sharpin, PREX2a and Histone H1.(*14, 32-41*) Membrane associated guanylate kinase inverted-2 (MAGI-2) is an adherens junction scaffold protein. PTEN has been reported to bind to MAGI-2 via an interaction between the C-terminal PDZ binding motif of PTEN and a second PDZ

domain of MAGI-2, thus enhancing PTEN stability and activity.(*32*) This interaction may inhibit cancer cell migration and proliferation.(*42*) PTEN-MAGI-1 interaction is proposed to be potentiated by PTEN C-tail phosphorylation at T382/T383.(*43*) Other proteins interacting with PTEN through its PDZ domain are microtubule-associated S and T kinases 1, 2, and 3 (MAST1,-2, and -3), discs large (DLG), and Na+/H+ exchanger regulatory factors 1 and 2 (NHERF1,and 2).(*8*) Another interesting protein interacting with PTEN is p85a, the subunit of PI3K. Although PI3K functionally opposes PTEN, its subunit p85a is suggested, paradoxically, to bind and activate PTEN directly, with a preference for binding non-phosphorylated PTEN.(*36, 44*) Phosphatidylinositol 3,4,5-triphosphate RAC exchanger 2a (pREX2a) is also suggested to interact with PTEN and inhibit PTEN's activity.(*41*) Interestingly, the binding of non-phosphorylated and phosphorylated PTEN (S380, T382, T383) with pREX2a was reported to be similar, but pREX2a was stated to only inhibit the activity of phosphorylated PTEN. This was rationalized by implicating the PH domain of pREX2a binding the PTEN phosphorylated C-tail, releasing it from autoinhibition.(*40*)

1.3 Ubiquitin and Ubiquitination

Ubiquitin is a small regulatory protein containing 76 amino acid residues (~8.5 kDa). The discovery of ubiquitin dates back to 1975 when Gideon Goldstein and co-workers isolated the ‘ubiquitous immunopoietic polypeptide’ from a variety of eukaryotic cells.(*45*) This protein was found to express ubiquitously in all tissues of eukaryotic organisms and thus given the name ‘ubiquitin’. The sequence of ubiquitin is highly conserved among all eukaryotic cells. As an abundant protein, the concentration of

ubiquitin in the cell is estimated to be 10 to 30 μM.(*46*) In the human genome, ubiquitin is expressed by four genes including UBB, UBC, UBA52 and RPS27A.(*47*)

Ubiquitin is a tiny globular protein that has the β-grasp fold, featured by a core structure consisting of beta(2)-alpha-beta(2) (two β-strands followed by an α-helix and then two β-strands).(Figure 3A)(*48-50*) The overall structure of ubiquitin is extremely compact and tightly hydrogen-bonded. Nearly 90% of the polypeptide chain is involved in the hydrogen-bonding of in its secondary structure, and there is a remarkable hydrophobic core formed between the β-strands and the α-helix. These structural features make ubiquitin a highly stable protein. Even after treatment under denaturing conditions, ubiquitin can spontaneously and efficiently fold back to its native conformation. Compared to the core structure, the C-terminal tail of ubiquitin is relatively labile. However, the di-glycine at the C-terminus is a key feature of ubiquitin for its function.

Ubiquitin's role is to serve as a very large PTM that is added to substrate proteins, the process of which is called ubiquitination or ubiquitylation. To be more specific, through a ubiquitination reaction, the C-terminal carboxyl group of ubiquitin is conjugated to the amine sidechain of a lysine in substrate protein, forming an isopeptide bond, so that ubiquitin is covalently attached to the substrate protein.(*51*) Ubiquitination, like phosphorylation, is a fundamental post-translational modification essential for protein function and signal transduction. There are numerous forms of ubiquitination including monoubiquitination and polyubiquitination, and they affect substrate proteins in many different ways such as providing marking for proteosomal degradation, altering sub-cellular localization, changing its catalytic activity, and regulating protein-protein interactions.(*50, 52*)

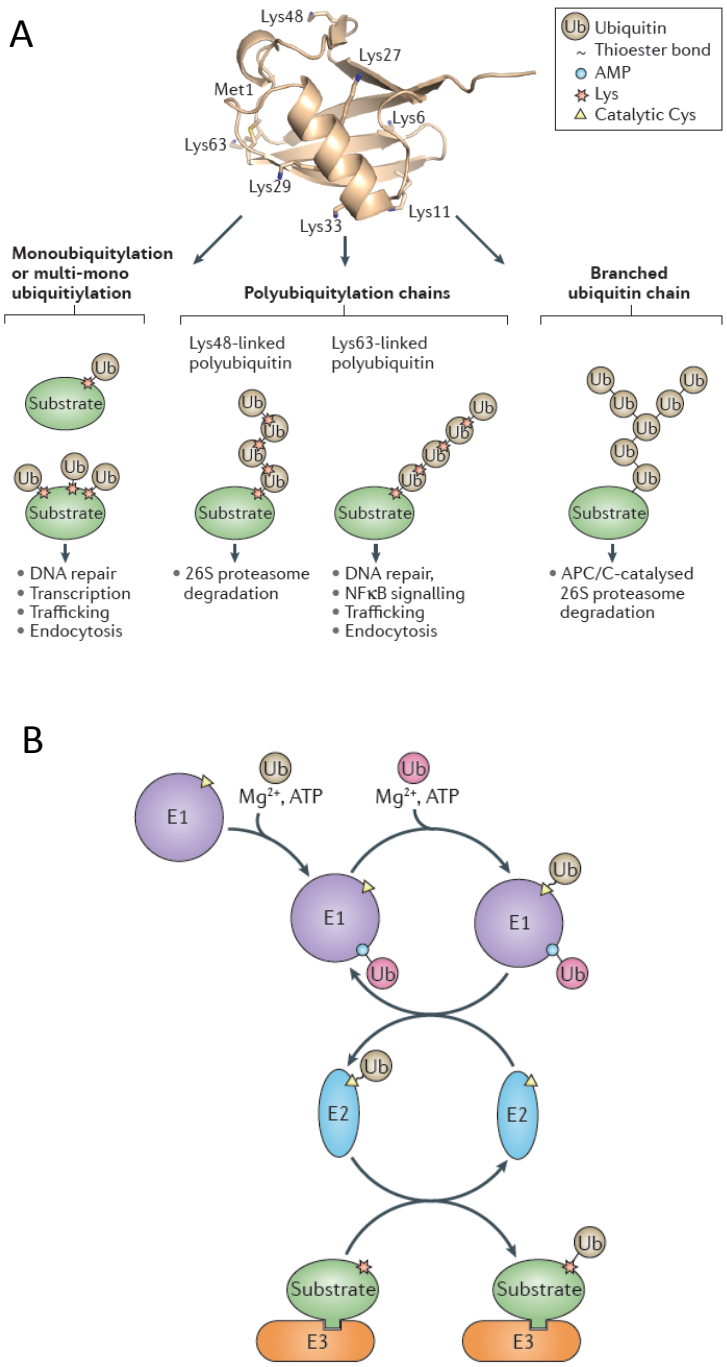

Figure 3: (A) Structure of ubiquitin and different types of ubiquitination. The crystal structure of ubiquitin shows the typical beta(2)-alpha-beta(2). The lysine residues and the first methionine are labeled as they are the site where poly-ubiquitin chains form. Different forms of ubiquitination include mono/multi-mono, poly and branched ubiquitination, each carrying different biological functions. (B) The process of ubiquitination reaction. E1 utilizes ATP to charge ubiquitin to the catalytic cysteine, forming a thioester bond. E1~Ub then transfers the ubiquitin to the catalytic cysteine of E2. With the help of E3, the ubiquitin is transferred from E2 to the lysine of substrate protein(*50*).

Monoubiquitination is the addition of one ubiquitin molecule to one lysine of the substrate protein. Multi-monoubiquitination can also occur in which there is addition of one ubiquitin to multiple lysine residues in the same substrate protein.(Figure 3A)(*50*) Monoubiquitination has been shown to play a role in DNA repair, transcription, trafficking and endocytosis.(*29, 52-55*)

Different from monoubiquitination, polyubiquitination involves the formation of a chain of ubiquitins attached to a single lysine residue of a substrate protein. In ubiquitin, the 7 lysine residues (K6, K11, K27, K29, K33, K48, K63) and the amino terminus provide eight attachment points where ubiquitin molecules can be added. (Figure 3A) (*50, 52*) After monoubiqutination, additional ubiquitins are added to the initial (proximal) ubiquitin to produce a polyubiquitin chain. Depending on which lysine the new ubiquitin is conjugated to, there are numerous forms of polyubiquitin chains. The most common are K48- and K63-polyubiquitination.(*52*)

Ubiquitination conjugation is a complicated process involving multiple steps and enzymes. (Figure 3B) (*50, 51*) There are three types of enzymes: ubiquitin activating enzyme E1, ubiquitin conjugating enzyme E2, and ubiquitin transferase E3. The overall ubiquitination scheme consists of three steps:

1. Activation. The activation of ubiquitin involves one molecule ubiquitin as the substrate, MgATP as the energy source, and E1 ubiquitin activating enzyme as the catalyst. In the human genome, there are only two E1s, but this step is an efficient reaction and very fast.(*56*) First, the E1 binds both ATP and ubiquitin, and catalyzes the acyl-adenylation of the C-terminus of ubiquitin, producing a ubiquitin-adenylate intermediate. The C-terminal di-glycine is a key feature for E1 recognition and further processing. Next, the sulfhydryl

group from the active site cysteine of the same E1 attacks the ubiquitin-adenylate to form a thioester bond, resulting in covalent attachment of ubiquitin to the active site cysteine of the E1 and release of AMP.

2. Conjugation. In this step, activated ubiquitin gets transferred to the active site cysteine on the ubiquitin conjugating enzyme E2. About 35 different E2s have been characterized in the human genome.(*57*) During the conjugation reaction, E2 binds to E1 and the ubiquitin on the active site of E1 undergoes a transthioesterification reaction to switch the ubiquitin to a Cys on the E2.
3. Ligation. In the ligation step, ubiquitin is transferred from the E2 Cys thioester species to the lysine residue of the substrate protein. This is facilitated by participation of E3 ubiquitin ligases which bind the substrate protein and E2~ubiquitin thioester to enable the formation of an isopeptide bond between the C-terminal carboxyl of ubiquitin and the amine group of a lysine sidechain of the substrate. E3s function as the substrate recognition module in the ubiquitination cascade. To ensure specificity, there are more than 600 E3s to target a different set of substrate proteins for ubiquitination.(*58*) The E3s also work together with a particular E2 and other regulators to coordinate the conjugation of specific ubiquitin linkages onto substrates.

The identified E3 ligases can be categorized into three major classes: RING (really interesting new gene), HECT (homologous to E6AP C-terminus) and RBR (RING-between-RING).(*50*) RING E3 ligases catalyze ubiquitination by stimulating the direct transfer of ubiquitin from E2~ubiquitin to substrate. HECT and RBR are different in that they contain a catalytic cysteine which receives ubiquitin from E2~ubiquitin and transfers to substrate protein subsequently. Compared to RING, HECT and RBR are more classical enzymes which are directly involved in the chemical reaction of ubiquitination.

RING E3s, characterized by the presence of a RING domain, are the largest E3 family and contain about 600 members.(*59*) The RING domain is the functional domain in a RING E3 ligase that recruits E2~ubiquitin and facilitates ubiquitin transfer. The structure of a RING domain contains two zinc ions coordinated by cysteines and histidines, which are essential for the correct folding of the domain. With the RING domain as a common feature, the large number of RING E3 family members show great diversity in biochemical and biophysical properties. There are RING E3s that are monomeric, homodimeric, heterodimeric and multi-subunit, and there are also RING E3s that exist as a subunit of a large complex consisting of many protein components.(*50*)

HECT E3s are a family of E3 ligases with 28 members in human. They all contain a HECT domain that uses a cysteine to receive ubiquitin from E2 and transfer to substrate.(*60*) The characteristics of HECT E3s will be discussed in detail in the following sections.

RBR E3 ligases share the structural feature of a RING1-IBR-RING2 domain combination: two RING domains with a IBR domain in between.(*50*) In the human genome, there are 14 known RBR E3 members, among which PARKIN and HHARI have drawn great interest.(*61-63*) RBR E3s, although structurally similar to RING E3s as they both contain the zinc binding RING domains, have distinctive enzyme mechanisms. RBR E3s do not function just as a template that brings E2~ubiquitin and substrate protein together; rather, they contain a catalytic cysteine that forms a thioester intermediate which allows for transfer of ubiquitin to protein substrate.(*62*) In this sense, RBR E3s follow a catalytic mechanism that resembles that of HECT E3. The catalytic cysteine in the RING2 domain receives ubiquitin from E2~ubiquitin that also involves recruitment by RING1 domain, and then transfers ubiquitin to the protein substrate.(*62*)

Structurally like RING E3s and functionally like HECT E3s, RBR E3s are an interesting composite family of ubiquitin ligases.

1.4 Overview of HECT E3 Ubiquitin Ligases

HECT E3 ubiquitin ligases, as introduced above, are a family of 28 members in human.(*50*) In general, they are comprised of an N-terminal substrate-binding domain and a C-terminal HECT domain. Based on different types of N-terminal domains, the HECT E3s can be categorized into three classes: the NEDD4 family (9 members), which contain WW domains that recognize Pro/Tyr motifs in substrate proteins; the HERC family members (6 proteins), which possess RCC1 (regulator of chromosome condensation-1)-like domains (RLD) and include large HERCs (>500 kDa) with multiple RLDs and small HERCs (~100 kDa) with a single RLD; and single HECT E3s (13 members) that have neither WW nor RCC1 domains.(*64*)

The HECT domain is the catalytic domain of HECT E3 ligases and is quite structurally conserved among all HECT family members.(*60*) In general, the HECT domain contains about 350 residues which are divided into a large N-lobe (~240 residues) and a small C-lobe (~110 residues) connected by a hinge loop. (Figure 4A) (*50, 65*) The N-lobe contains the E2 binding region, the protein substrate binding region, and a non-covalent ubiquitin binding site (exosite).(*66-69*) The C-lobe contains the catalytic cysteine which receives and transfers ubiquitin to protein substrates. The hinge loop which is a flexible linker between the N- and C-lobe plays a key role in the conformational dynamics of the HECT domain. (Figure 4A) (*50, 65*) In different orientations of the C-lobe relative to the N-lobe, the HECT domain can adopt two conformations, a closed reversed T-shape and an open L-shape. (Figure 4A, B) (*50, 65*)

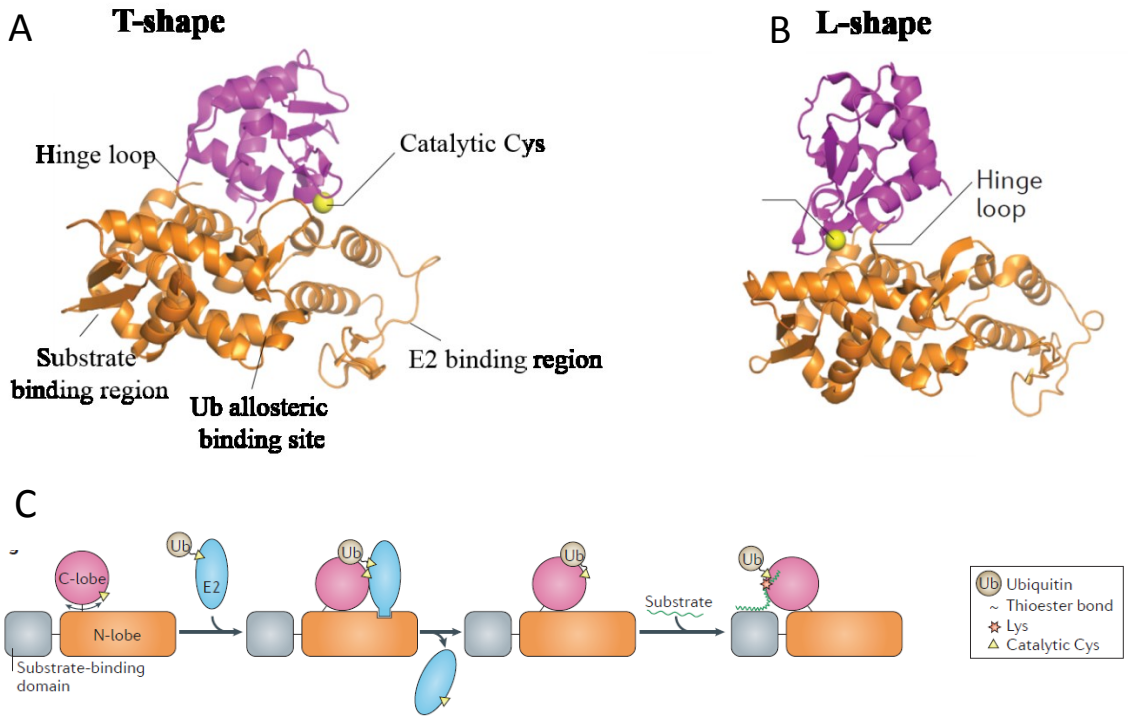

Figure 4: (A) Crystal structure of a HECT domain in the T-shape. HECT domain consists of a large N-lobe (orange) and a C-lobe (magenta), connected by a flexible linker called the hinge loop. The catalytic cysteine is located within the C-lobe, and the N-lobe contains the E2 binding region, the substrate binding region and a ubiquitin allosteric binding site (exosite). (B) The structure of a HECT domain in the L-shape. (C) The catalysis process of a HECT enzyme. The hinge loop is flexible so the HECT domain can freely switch from T to L-shape. When E2~Ub binds to the E2 binding region, the HECT domain stays in the T-shape conformation so the catalytic cysteine is close to the E2 binding region and receives the ubiquitin from E2. Rotation of the C-lobe carrying ubiquitin leads to the L-shape and transfers ubiquitin to the substrate(*50*).

This conformational flexibility allows the C-lobe to receive ubiquitin from the charged E2 protein and transfer it to the protein substrate. Studies have shown that hinge loop truncations or proline mutation disrupt the ubiquitin transferase activity of the HECT domain.(*65*)

The mechanism of HECT E3's catalytic function involves at least four stages: first, recruitment of E2~ubiquitin; second, transthioesterification to the catalytic cysteine in the C-lobe to form a HECT~ubiquitin thioester intermediate; third, transferring ubiquitin to the lysine of a substrate; fourth, adding multiple ubiquitin molecules to form poly-ubiquitin chains. (Figure 4C) (*50*) The E2 binding region at the N-lobe of the HECT domain forms a groove structure comprised of two β-strands and a connecting coil.(*66*) The loop between the α-helix and β-strand at the N-terminus of an E2 interacts with the hydrophobic groove of the E2 binding region within the HECT domain to stabilize the E2-E3 interaction. Hydrophobic residues especially a phenylalanine in the E2 N-terminus is critical and the HECT interacting E2s, such as UbCH7, UbCH5B and UbCH5C, all contain this phenylalanine.(*70*) There are several hydrogen bonds between the ubiquitin and the HECT N- and C-lobe interface that position the C-terminus of ubiquitin in an extended conformation and are proposed to activate the thioester.(*66, 71*) Transfer of ubiquitin from the cysteine of E2 to that of E3 is triggered by the rotation of the hinge loop which changes the position of the E3 cysteine and allows for transthioesterification.(*50*) Subsequently, the ubiquitin is transferred to substrate with a dramatic rotation of the hinge loop which brings the ubiquitin to the substrate binding region on the other side of HECT N-lobe.(*67*)

In addition to the functional motifs such as the E2 binding region, the catalytic cysteine, the hinge loop and substrate binding region, there are two important structural features in the HECT domain including its non-covalent ubiquitin binding region (Figure

4A)(*68, 72-74*) and the last five residues of the C-tail(*71, 75*). The non-covalent binding site, also called the exosite, is located between the E2 binding region and the protein substrate binding region in the N-lobe.(*73*) Distinct from the transferred ubiquitin covalently attached to the catalytic cysteine and located at the interface of the N- and C-lobes, ubiquitin also binds to the exosite non-covalently. The function of the exosite still remains a question. When first discovered in Rsp5 (homolog to NEDD4-1 in yeast) using NMR, the function of the non-covalent ubiquitin binding was thought to limit the length of polyubiquitin chain.(*74*) However, an alternative mechanism was suggested by biochemical and structural studies of SMURF2 and NEDD4-1.(*72, 73*) The crystal structure of HECT~ubiquitin in complex with an additional ubiquitin bound at the exosite showed that the non-covalent ubiquitin might contribute its lysine (K63) as a receiver of the Cys-thioester linked ubiquitin to form polyubiquitin chains.(*73*) Mutation of key interacting residues at the exosite that disrupt the binding of ubiquitin to the exosite resulted in products with shorter polyubiquitin chains.(*73*) However, a recent study using an engineered ubiquitin variant which targets the exosite with high affinity indicated an allosteric activating role of exosite ubiquitin binding.(*69*) In WWP1/WWP2/ITCH, the engineered ubiquitin variants were shown by crystal structures to bind to the exosite just like wild-type, and they dramatically activated the ubiquitin transferase activity of the HECT E3.(*69*) Although it still remains unknown whether non-covalent ubiquitin binding site exists in every member of the HECT E3 family, and what is its exact role for E3 regulation, this site seems to be a promising target for developing small molecules to modulate HECT activity.(*76*)

Another interesting structural feature is the last five residues of the HECT domain. Although the last five residues show some variation among different HECT family members, two residues are highly conserved including a phenylalanine (F-4) and

a terminal acidic residue (E-1).(*71, 75*) Deleting the last five residues or mutating the key residues does not affect the transthioesterification between E2 and E3, but significantly blocks the ubiquitination of substrate, suggesting that these residues are involved in the step for transferring ubiquitin to the lysine of protein substrate.(*67, 71*) In many crystal structures of HECT domains, the last five residues are either deleted to allow crystallization or invisible(*65, 71*), whereas in the structure of a complex involving the Rsp5 WW3-HECT domain, ubiquitin and substrate peptide, which captures the step that ubiquitin is being transferred from HECT to the lysine of substrate, the electron density of F-4 was observed(*67*). The structure depicts the HECT domain in the L-shape conformation such that the C-lobe is rotated into a location near the substrate binding region. F-4 binds to the N-lobe through hydrophobic interaction with another phenylalanine (F505) and a leucine (L506) within the N-lobe at the interface between the N- and C-lobes. Although F-4 mutation to leucine abolishes ubiquitination catalysis, a complementary substitution of L506 to phenylalanine or tryptophan could rescue the activity.(*67*) These results suggest that the role of F-4 is to stabilize the L-shape conformation by anchoring the N- and C-lobe in an orientation which is suitable for ubiquitin transfer to substrate. However, the role of E-1 is uncertain based on current structural studies, where it has not been visualized. It was hypothesized that E-1 might be crucial for positioning or activating the incoming lysine of the ubiquitin acceptor.(*71*) Indirect evidence points to an active site positioning of E-1, since E-1 replacement with a lysine (K-1) leads to ubiquitin conjugation to K-1.(*71*)

Although HECT E3s share a common catalytic domain, the various family members are proposed to have specific substrates and distinct functions.(*64*) They control numerous cellular processes including protein degradation, endocytosis, sorting and trafficking of transmembrane proteins and play important roles in a variety of

physiological and pathological conditions.(*27, 60, 64, 77-84*) E6AP (E6 associated protein), which belongs to the single HECT E3s, was the first HECT E3 identified.(*85*) When associated with E6 protein, the viral oncoprotein expressed by human papilloma virus (HPV), E6AP can target p53 for ubiquitination and proteosomal degradation.(*86*) This is a fundamental mechanism for HPV-mediated oncogenesis. Other important single HECT E3s include EDD, HUWE1 and HACE1 which are involved in cancer and neurodevelopment.(*87-89*) The large HERC protein HERC1 and HERC2 possess phosphatidylinositol-4,5-bisphosphate (PtdIns(4,5)P_2)-dependent guanine nucleotide-releasing factor (GRF) activity(*90*), and are proposed to be involved in membrane protein trafficking, as well as regulate cell size and growth through the mTORC1 pathway(*91*). The small HERC proteins do not have GRF activity and their function has been less studied. The small HERCs are reported to regulate intracellular vesicle transport and are also stated to have roles in spermatogenesis, immune response and other physiological processes.(*92-96*) The NEDD4 family HECT E3s are the most intensively studied HECT enzymes and are the focus of my thesis work, the function of which will be described later.

1.5 Overview of NEDD4 family

The NEDD4 family of HECT E3 ligases are characterized by an N-terminal C2 domain, two to four WW domains and a C-terminal HECT domain.(*50*) The C2 domain is a phospholipid binding domain and can target the E3 to the plasma membrane, endosomes or other proteins.(*97*) The WW domains recognize and bind to PY (Pro/Tyr) motifs in substrate proteins.(*98, 99*) They have a preference for PPxY sequences and can also bind to LPxY and other PY motifs.(*100*) Some WW domains bind to

phosphorylated Ser/Thr, often triggering ubiquitination of phosphorylated proteins.(*101*) The WW domains are small structural units containing about 30 amino acid residues, and the structure usually comprises two to three parallel β-strands.(*99, 102*) Although their sequences and structures are conserved, distinct WW domains show variable affinities for different substrates.(*99*)

The NEDD4 family members play diverse roles in all eukaryotic organisms from yeast to mammals. In yeast, Rsp5 is the only NEDD4 family member and is an essential gene.(*103*) Proposed cellular functions of Rsp5 include chromatin remodeling, regulation of transcription by binding to the large subunit of RNA polymerase II, mitochondrial inheritance, regulation of endocytosis, and sorting of a variety of transmembrane proteins, transporters and receptors.(*103-106*) *Caenorhabditis elegans* WWP1 (ceWWP1) is essential for late stage embryogenesis of these worms.(*107*) ceWWP1 has been shown to target RNA polymerase II for ubiquitination and degradation, as well as LIN-12 to suppress the Notch signaling pathway.(*108, 109*) *Drosophila melanogaster* has three NEDD4 family members including NEDD4, ITCH and SMURF, which also act as suppressors of the Notch pathway.(*110*)

In mammalian cells, there are 9 NEDD4 family members which can be divided into four sub-families: NEDD4-1 and NEDD4-2; SMURF1 and SMURF2; HECW1 and HECW2; WWP1/WWP2/ITCH.(*64*) Each sub-family shares relatively high sequence conservation. The NEDD4 family HECT E3 ligases play diverse roles in regulating transcription by ubiquitinating key transcription factors, leading to proteasomal degradation.(*60, 64*) For example, WWP1 has been suggested to target the transcription factor p53, one of the most important tumor suppressors, for degradation(*111*); WWP2 has been shown to ubiquitinate OCT4, a key transcription factor in embryonic stem cell development and differentiation(*78*). NEDD4 E3 ligases also target many important

signaling proteins for ubiquitination inducing proteasomal degradation or altered trafficking, thus influencing many signal transduction pathways. PTEN, a negative regulator in the PI3K/AKT signaling pathway, is ubiquitinated by WWP2 and NEDD4-1.(*27, 30*) Poly-ubiquitination of PTEN by WWP2 or NEDD4-1 leads to proteasomal degradation of PTEN and activation of downstream AKT signaling, while mono-ubiquitination of PTEN by NEDD4-1 leads to nuclear localization.(*30*) Several transmembrane proteins including growth factor receptors and ion channels have been suggested to be substrates of different NEDD4 E3 ligases. For instance, NEDD4-1 ubiquitinates insulin-like growth factor 1 receptor (IGF1R), epidermal growth factor receptor (EGFR) and fibroblast growth factor receptor (FGFR)(*112-114*); SMURF1 and SMURF2 negatively regulates the TGFβ pathway by ubiquitinating the TGFβ receptor as well as the downstream Smads and TGFβ-responsive transcription factors(*115-117*); ion channels such as epithelial Na^+ channel (ENaC) is targeted by NEDD4-1, NEDD4-2 and WWP2 for degradation.(*118-121*)

Mammalian NEDD4 family members have important roles in numerous physiological processes and are involved in many diseases.(*60, 64, 106*) A number of the NEDD4 family members are identified as vital regulators of development and differentiation.(*106*) WWP2 is highly expressed in embryonic stem cells (ESC) and its level decreases as the stem cell differentiates into different tissues.(*78*) WWP2 targets OCT4 and RNA polymerase II large subunit in ESC for ubiquitination and degradation, and regulation of WWP2 activity could potentially determine the fate of the ESC.(*122, 123*) NEDD4-1, NEDD4-2 and HECW2 have also been shown to regulate the development of neural tissue, intestine and muscle(*124-126*), and SMURF1 and SMURF2 are essential regulators of bone tissue development(*115, 117, 127, 128*). The immune system is regulated by NEDD4 family members as well. ITCH E3 ligase is an

essential molecule for the development and differentiation of regulatory T cells, the knocking out of which leads to defects in T helper 2 (T_H2) cells, increased levels of IL-4, IL-5, IgE and IgG.(*129, 130*) The phenotype of loss of ITCH function includes pruritis and several autoimmunity syndromes. The molecular mechanism of ITCH function includes the observation that ITCH can target JUNB, the transcription factor for IL4 gene expression, for ubiquitination and proteasomal degradation.(*131, 132*) There are a large number of studies that link NEDD4 E3 ligases to cancer.(*60*) Several important cancer related proteins are regulated by NEDD4 E3s including PTEN, p53, and Notch1.(*27, 29, 30, 111, 133*) NEDD4 E3 members are suggested to be oncogenes and can promote the progression of cancer.(*60*) However, accumulating evidence indicates that many NEDD4 E3 ligases, while thought to be oncoproteins, also carry tumor suppressor properties.(*134-136*) These seemingly contradictory functions indicate that the roles of NEDD4 E3s in cancer are complicated and the regulation of NEDD4 E3 under different conditions or in different cell types could can spark distinct biological outputs.

1.6 Regulation of NEDD4 HECT E3 Ligases

Because of their biomedical importance and direct involvement in the catalysis of protein ubiquitination, the enzymatic activities of NEDD4 HECT E3 ligases need to be tightly regulated to ensure normal function and prevent pathogenesis. The C-terminal catalytic HECT domain is autoinhibited through intramolecular interactions with other domains, and can be regulated by posttranslational modifications, dimerization/oligomerization and protein-protein interactions.(*50*)

Most of the intramolecular interactions within NEDD4 HECT E3s are reported to autoinhibit, preventing hyperactivation. The C2 domain has been shown to be the

autoinhibitory domain for Smurf2 and NEDD4-1.(*137, 138*) NMR studies showed that the C2 domain binds to the region near catalytic cysteine in the HECT C-lobe, as well as interfering with the ubiquitin exosite, thus blocking the transthioesterification reaction.(*137, 138*) It has been suggested that WW domains mediate the autoinhibition of NEDD4-2 and ITCH.(*100, 139*) One proposal is that WW domains bind to the LPXY motifs in the HECT domains and inhibit catalytic activity. Competitive binding of substrate proteins containing PPXY motifs to WW domains could release the autoinhibited HECT and activate the enzyme.(*100*) In addition, a proline rich region (PRR) between the C2 domain and the first WW domain was proposed to be an autoinhibitory motif by binding to the HECT domain.(*139*)

The autoinhibited NEDD4 E3 ligases can be activated by different post-translational modifications in a variety of ways. In NEDD4-1, several tyrosine phosphorylation sites have been identified and characterized, including Tyr43 in the C2 domain and Tyr585 in the HECT domain.(*140*) It is proposed that phosphorylation at these two sites could disrupt the autoinhibitory interaction between the C2 domain and the HECT domain, thus activating NEDD4-1 activity.(*140*) ITCH is phosphorylated at Ser199, Ser232 and Thr222 within the PRR, catalyzed by JNK1.(*77, 141*) This phosphorylation event is suggested to lead to a conformational change and activation of ITCH.(*141*) Tyr371, phosphorylated by FYN, in the linker region between WW2 and WW3 domain was proposed to inhibit ITCH activity.(*142*) The Ser444 of NEDD4-2 is a target of AKT1 and SGK1 for phosphorylation upon activation by hormones such as insulin and aldosterone.(*143-145*) Unlike NEDD4-1 or ITCH, which are proposed to be directly activated by phosphorylation events, phospho-NEDD4-2 is suggested to recruit 14-3-3, an accessory protein that facilitates the binding of NEDD4-2 to its substrate ENaC.(*146*) In addition to phosphorylation, NEDD4 HECT E3s are also regulated by

other posttranslational modifications such as arginine methylation which regulates Smurf2 stability(*147*) and lysine neddylation which promotes Smurf2 degradation and increase Smurf1 activity(*148*).

Dimerization/oligomerization has been shown to regulate HECT E3 ligase activity, but the underlying mechanisms still remain elusive and the conclusions are controversial. It was observed that dimerization/oligomerization of WWP2 leads to inhibition of ubiquitin transferase activity through a trans interaction between the C2 domain of one WWP2 and the HECT domain of the other WWP2 molecule.(*149*) NEDD4-1 has also been demonstrated to be regulated by oligomerization. A potential trimerization interface within the HECT domain is blocked by the α1-helix of the HECT domain, and upon ubiquitination of the lysine residue located in the α1-helix, the trimerization interface is exposed and this ubiquitination-dependent trimerization process inhibits the E3 ligase activity of NEDD4-1.(*150*) A recent structural study revealed that HUWE1, another HECT family member, is autoinhibited through dimerization, and disruption of the dimerization interface activates the enzyme.(*151*) However, it still remains elusive and controversial how dimerization/oligomerization regulates the activity of HECT E3 ligases. Although the studies mentioned above indicate inhibitory role of dimerization/oligomerization, contradictory results were observed for E6AP.(*152*) It was found that the active form of E6AP is trimeric.

Intermolecular protein-protein interactions are another regulatory mechanism critical for of NEDD4 HECT E3s. SMAD7 acts as an important activator for Smurf2, which antagonizes the intramolecular interaction between the C2 and HECT domains, relieving autoinhibition.(*137, 153*) SMAD7 also allosterically activates Smurf2 by enhancing the affinity of Smurf2 HECT domain for E2 binding.(*153*) NDFIP1 and NDFIP2 are transmembrane proteins that serve as adaptor proteins for NEDD4 family

members including NEDD4-1, ITCH and WWP2.(*154*) NDFIP1 and NDFIP2 contain three proline rich motifs that bind WW domains of NEDD4 E3s, and NDFIP1 and NDFIP2 can impact the subcellular localization and activity of NEDD4 E3s.(*139*) Smurf1 was demonstrated to interact specifically with casein kinase 2-interacting protein 1 (CKIP1) through its linker region between WW domains, and this interaction was shown to enhance substrate recognition and catalytic activity.(*155*) Protein-protein interactions regulate not only the activity but also the type of NEDD4-mediated ubiquitination. NEDD4-1 regulation by p34 is an example. p34 binds to the WW1 domain of NEDD4-1 and is suggested to augment its ubiquitination activity.(*156*) Overexpression of p34 promotes NEDD4-1-catalyzed polyubiquitination of protein substrate while knocking down of p34 leads to mostly monoubiquitination.(*156*)

1.7 Expressed protein ligation

Expressed protein ligation is a chemical ligation technique that allows for ligation of a synthetic peptide and purified recombinant protein resulting in a semi-synthetic protein.(*157, 158*) There are two major approaches to do expressed protein ligation: C-terminal expressed protein ligation where the protein with C-terminal thioester is ligated with peptide with N-terminal cysteine (Figure 5A)(*158*), and N-terminal expressed protein ligation where the synthetic peptide with C-terminal thioester is ligated with protein that has a N-terminal cysteine (Figure 5B)(*159*).

C-terminal expressed protein ligation is the more classical and widely used approach. This technique introduces a thioester at the C-terminus of the protein taking advantage of intein self-splicing chemistry.(*158*) Inteins are protein domains found in

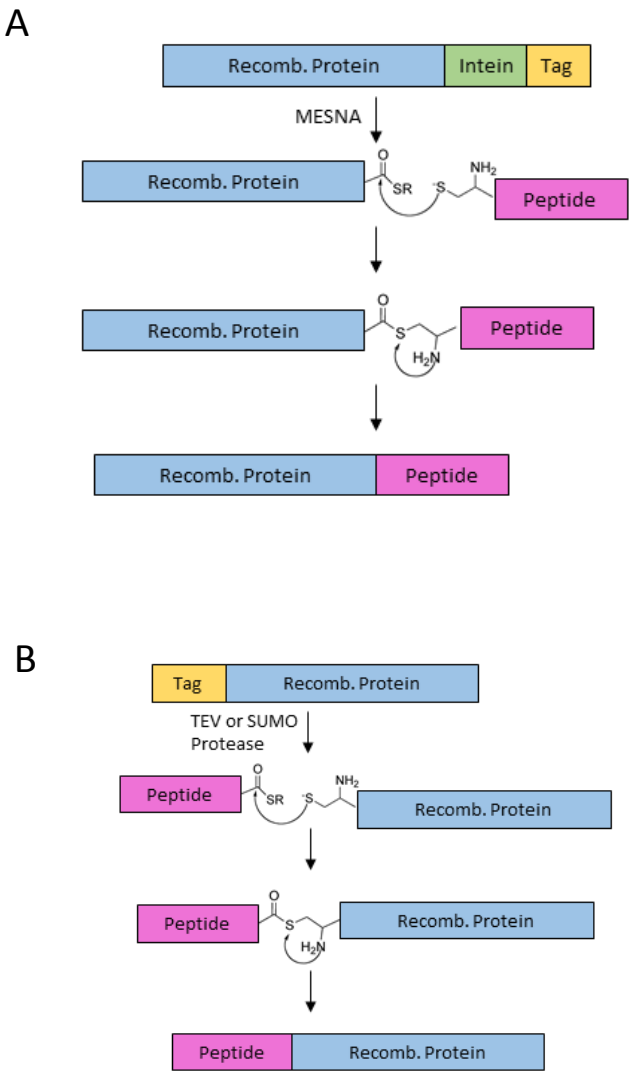

Figure 5: (A) Schematic showing the C-terminal native chemical ligation. (B) Schematic showing the N-terminal native chemical ligation.

bacteria and yeast that can splice themselves out from two flanking polypeptide chains while ligating the two chains together.(*160*) This process is analogous to intron/exon splicing in RNA. The inteins used in expressed protein ligation have been engineered so that they can by trapped in the first step of splicing.(*158*) In this thesis, the technique is utilized to make semi-synthetic PTEN with different C-terminal phosphorylations, as well as unnatural amino acid residues such as benzoylphenylalanine (BPA) and biotinylated lysine for crosslinking studies. In our studies, we employ truncated versions of PTEN fused with intein at the C-terminus, followed by a small chitin binding domain.(*19*) Recombinant fusion protein is purified using chitin resin. The junction site between PTEN and the intein exists in an equilibrium between a native amide bond and an intein catalyzed thioester rearrangement. Using thiol reagent such as mercaptoethanesulfonate (MESNA), the transient thioester bond at C-terminus of PTEN can be trapped, and the intein is cleaved producing PTEN with C-terminal MESNA thioester. The purified PTEN-thioester can subsequently react with the N-terminal cysteine on the peptide. The cysteine on the peptide acts as a nucleophile to displace the MESNA thioester, and the peptide thioester undergoes a rearrangement to yield a native amide bond at the ligation site. In this way, the full-length semisynthetic PTEN is generated containing recombinantly expressed and synthetic parts. The synthetic peptide is naturally incorporated into the PTEN protein which carries site-specific phosphorylation and unnatural amino acids.

While the method mentioned above is efficient for introducing modifications on the C-terminus of the protein, N-terminal expressed protein ligation is an alternative way to ligate a peptide to a recombinant protein.(*159*) The basic concept is similar in that both techniques use the same chemoselective, cysteine-mediated ligation, but for N-terminal expressed protein ligation the thioester is produced in the synthetic peptide.

This thioester synthetic peptide is ligated to a recombinant protein containing an N-terminal Cys. In this thesis, I use the N-terminal expressed protein ligation approach to make a semisynthetic WWP2 construct with tyrosine phosphorylation. The peptide with the C-terminal thioester can be synthesized using Dawson Dbz AM resin(*159*), and the recombinant protein with N-terminal cysteine can be generated using SUMO protease or TEV protease cleavage. The ligation produces a semisynthetic protein with site-specific modification at the N-terminus.

Expressed protein ligation has been a powerful technique to install modifications on the N-terminus and C-terminus of proteins.(*157*) In this thesis work, this technique has been used to site-specifically install posttranslational modifications, as well as unnatural amino acids used for photo-crosslinking and crystallography. Not limited to these, expressed protein ligation can also be applied to introduce any modification that can be incorporated into a synthetic peptide such as fluorescent molecules, isotopic residues and other tags. The great advantage is that it allows for the exact positioning and stoichiometry of the intended modification. Despite many advantages, expressed protein ligation has its limitations. Expressed protein ligation is best suited to study phosphorylation sites located at the N- or C-termini of a protein (or protein domain) of interest, to avoid multi-segment ligation. Fortunately, phosphorylation sites are often near protein termini since they are usually located in flexible regions that tend to be at the ends of proteins or protein domains. In some cases, when flexible modified regions are far from the termini, circular permutation strategies can be employed to analyze PTMs.(*161*) Another potential limitation is the requirement of a cysteine at the ligation junction. Since Cys is one of the least frequently encoded amino acids in proteins(*162*), introduction of a Cys by mutation is commonly required for the convenient use of the technique. Careful controls are needed to ensure that Cys mutation per se is not

perturbing to structure or function. Some groups have developed alternative ligation chemistries to avoid Cys or refined desulfurization reactions to convert Cys to Ala.(*163, 164*) Another concern is that truncation of a protein for expressed protein ligation can disrupt protein stability and this can lead to low yields or even the need for refolding. The gyrase intein can function in the presence of moderate concentrations of denaturant, partly alleviating this problem, but recovering functional protein after removing denaturing agents is often challenging. Despite these limitations, expressed protein ligation is a relatively attractive method for the study of protein posttranslational modifications as evidenced by the many cases where it has been successfully employed.

Chapter 2: Molecular Features of PTEN Regulation by C-terminal Phosphorylation

2.1 Introduction

PTEN is a phosphatidyl 3,4,5-triphosphate (PIP3) lipid phosphatase that is frequently inactivated in cancer by mutation, epigenetic silencing, or post-translational modifications (PTMs) (*7, 8, 20, 165-169*). Loss of PTEN function allows unabated production of PIP3 from PIP2 by PI3-kinases and stimulates the AKT protein kinase signaling pathway and cancer cell proliferation (*8, 170, 171*). Understanding the mechanisms of PTEN regulation is therefore critical to the development of therapeutics that can treat a wide variety of cancers.

PTEN is a ~45 kDa protein composed of an N-terminal PTP-type phosphatase domain, a mid-section phospholipid membrane interacting C2 domain and a 50 residue regulatory tail(*8*). A crystal structure of the core PTEN catalytic-C2 region has revealed intimate interactions between the catalytic and C2 domains but omitted the C-terminal tail, which is considered to be flexible and largely unstructured(*16*). One of the most intensively studied set of PTMs in PTEN is a cluster of four C-terminal phosphorylations at Ser380, Thr382, Thr383, and Ser385(*19, 23, 172, 173*). These phosphorylation events have been suggested to be catalyzed by protein kinases CK2 and/or GSK3β and demonstrated to drive a conformational change that inhibits membrane interactions and reduces catalytic activity(*19, 23, 172, 173*).

Several reports that shed light on the molecular basis for this phospho-dependent regulatory event suggest that the PTEN tail-phosphorylation induces conformational closure involving intramolecular interactions between the tail and the CBR3 loop of PTEN's C2 domain(*19, 173, 174*). However, important aspects of this

structural model remain undetermined. It is not known whether all four tail phosphorylation events are necessary for PTEN's conformational closure or whether specific individual sites are critical for this tertiary structural change. Recently, a mutant form of PTEN, ePTEN, was identified through a genetic screen as a form of PTEN that constitutively binds the membrane, despite C-terminal phosphorylation(*175*). The five mutations in ePTEN, Q17R, R41G, E73D, N262Y, and N329H, are widely spaced throughout the PTEN domains(*175*). It was hypothesized, but not investigated in detail, that these mutations disrupt the phosphorylation-driven conformational change in PTEN(*175*). Other studies on PTEN including H/D exchange experiments have suggested that the catalytic domain and/or the N-terminus may also interact with the phosphorylated tail(*176*).

To help clarify these phospho-PTEN structural issues, we have applied expressed protein ligation(*158*) to generate several semisynthetic phosphorylated forms of PTEN, and we assessed their activity and tail interactions. We demonstrated that there is an approximately proportional relationship between the number of phosphates and degree of conformational closure. In contrast to expectations, tetraphosphorylated ePTEN (4p-ePTEN) showed a closed conformation similar to that of wt 4p-PTEN. However, mutations of a cluster of Lys and Arg residues in the Cα2 loop relaxed phospho-tail interactions with the PTEN body. The incorporation of a benzolyphenylalanine in the C-tail was employed in photocrosslinking experiments and provided direct evidence for a tail-catalytic domain interaction. Here, we describe how this biochemical analysis of a new set of semisynthetic PTENs has led to significant insights into the structural basis for the effects of PTEN tail phosphorylation.

2.2 Methods

2.2.1 Reagents:

Soluble diC6-PIP_3 was purchased from Avanti Polar Lipids (Alabaster, AL). Anti-phospho-PTEN antibody was from abcam (ab131107), and anti-total PTEN antibody was from Santa Cruz (sc-7974). Calf intestinal alkaline phosphatase (CIP) was purchased from New England Biolabs (M0290). MESNA was supplied from Sigma (St. Louis, MO). All canonical Fmoc-amino acids were from EMD (Billerica, MA), whereas Fmoc-L-p-benzoylphenylalanine and Fmoc-L-Lys(biotin)-Wang resin were purchased from Novabiochem and Iris Biotech, respectively. All other reagents were of the highest quality and were purchased from either Sigma or Fisher.

2.2.2 Peptide synthesis:

Peptides were synthesized using the PS3 peptide synthesizer or the Prelude X peptide synthesizer from Protein Technologies (Tuscon, AZ) using conventional Fmoc solid phase peptide synthesis strategies. Synthetic peptides were estimated to be greater than 90% pure after HPLC and their correct structures were confirmed by matrix-assisted laser desorption ionization (MALDI) mass spectrometry. Peptide samples were spotted using the sandwich method with α-cyano-4-hydroxycinnamic acid as the matrix (10 mg/mL CHCA in 50% acetonitrile, 5 mM ammonium citrate). Mass spectra were acquired using the Voyager-DE STR BioSpectrometry Workstation (Applied Biosystems) by averaging 100 shots using a linear detector in either positive (unphosphorylated peptides) or negative ion (phosphorylated peptides) mode.

2.2.3 Generation and purification of semisynthetic PTEN:

Expressed protein ligation was used to generate different semisynthetic phosphorylated PTENs as previously reported by Bolduc et al(*19*). In brief, a C-terminal truncated PTEN (tPTEN: aa1-378) fused to *Mycobacterium xenopi* GyrA intein and chitin-binding domain (tPTEN-intein-CBD) was subcloned into the pFastBac-1 vector and transformed into DH10Bac competent cells, in order to produce a bacmid containing the appropriate PTEN sequence. Site-directed mutants were generated by standard quikchange methods using the primers shown in Table 1. The bacmid containing *t-PTEN-intein-CBD* was then transfected into Sf-21 insect cells to generate the corresponding baculovirus needed for protein expression. High Five insect cells were infected with the baculovirus at a cell density of 1 million/mL and cultured for 48 h at 27°C to express tPTEN-intein-CBD. The final culture was then harvested by centrifugation and the cell pellet lysed with a Dounce homogenizer by 40 strokes in 40 mL of 50 mM HEPES pH 7.5, 250 mM NaCl, 1 mM EDTA, 10% glycerol, and one tablet of complete EDTA-free protease inhibitor cocktail (Roche Diagnostics). The soluble lysate was then incubated with fibrous cellulose (Sigma) for 30 min at 4°C to remove chitinase. Next, t-PTEN-intein-CBD was immobilized by passing it over chitin resin, followed by rigorous washing with 25 mM HEPES pH 7.5, 250 mM NaCl, 1 mM EDTA, 0.1% Triton and 50 mM HEPES pH 7.5, 250 mM NaCl, 1 mM EDTA. Semisynthetic PTEN was then generated by incubating the t-PTEN-intein-CBD-bound chitin resin for 48 – 72 h at room temperature with 50 mM HEPES pH 7.2, 250 mM NaCl, 400 mM MESNA, and 2 mM of the corresponding C-terminal tail peptide. Truncated PTENs were generated by incubating the chitin resin with 50 mM HEPES pH 7.2, 250 mM NaCl, 400 mM MESNA, and 40 mM cysteine for 24 h at room temperature. Following the ligation reaction, semisynthetic PTEN was eluted from the chitin resin in 50 mM Tris pH 8.0, 5

mM NaCl, 5 mM DTT, followed by dialysis with the same buffer to remove unreacted peptide and salt from the ligation reaction. The semisynthetic PTEN was then further purified by FPLC-anion exchange chromatography (MonoQ, GE Healthcare) using a 240 mL linear gradient (0% to 50% Buffer B), whereby Buffer A is the dialysis buffer and Buffer B is 50 mM Tris pH 8.0, 1 M NaCl, 5 mM DTT.

2.2.4 Enzyme activity assay:

Lipid phosphatase activity of PTEN towards the aqueous soluble substrate diC6-PIP3 was measured by monitoring phosphate release using the Malachite Green assay kit (R&D Biosystems) at 620 nm. Initial velocities were measured for a 25 µL reaction containing 50 mM Tris pH 8.0, 10 mM BME, 0.05 mg/mL ovalbumin, and varying concentrations of diC6-PIP3 (20–160 µM). Reactions were initiated with 0.5–20 µg of the corresponding PTEN and reaction rates were measured for 5–10 minutes at 30°C. Reactions were then quenched and inorganic phosphate measured using the Malachite Green assay kit. Background corrections were performed with quenched enzyme. All measurements were performed in duplicate on at least two separate occasions and replicates typically agreed within 20%. The k_{cat}/K_m measurements derived from this data were obtained using the Michaelis-Menten equation or a linear plot when no evidence of saturation was apparent by visual inspection.

2.2.5 Western blotting and alkaline phosphatase sensitivity assay:

Semisynthetic phospho-PTEN forms were subjected to alkaline phosphatase treatment over a period of up to 300 min in 50 mM Tris pH 8.0, 10 mM BME, 1 µM of the

corresponding phospho-PTEN, and 1 μM calf intestinal alkaline phosphatase (NEB). Reaction samples were quenched in SDS-loading dye at 95°C and the fraction of phospho-PTEN remaining was measured by Western blot analysis using an antibody to the PTEN phospho-C-tail cluster (abcam) in combination with a HRP-conjugated anti-rabbit secondary antibody. Western positive bands were detected using Amersham ECL Western blotting detection reagent with Syngene's PXi and quantified by ImageJ image quantification software. Phospho-tail half-liives were calculated using a single exponential decay curve. All measurements were performed at least twice on separate occasions and half-lives from replicates typically agreed within 30%.

2.2.6 UV-induced C-terminal tail crosslinking:

An 18-mer tetraphosphorylated C-terminal tail peptide was synthesized with a photoactivatable *p*-benzoylphenylalanine (Bpa) in the place of Phe392 and an artificial C-terminal lysine that was N^{ε}-biotinylated using conventional Fmoc peptide synthesis strategies and ligated to immobilized t-PTEN-intein-CBD using the methods described above. UV-induced crosslinking was performed with 50 μg of PTEN diluted with 50 mM Tris pH 8.0, 10 mM DTT to ~150 μg/mL. In a quartz reaction chamber with circulating water at 4°C and constant stirring, 4p-PTEN containing Bpa was UV-irradiated at 365 nm with a Blak-Ray C50 UV lamp for 3 h. Next, the UV-irradiated 4p-PTEN was treated with bovine alkaline phosphatase (Sigma) at a final concentration of 1 μM for 2 h at room temperature. The alkaline phosphatase-treated cross-linked PTEN samples were subjected to buffer exchange with 50 mM NH_4HCO_3 followed by reduction with 5 mM tris(2-carboxyethyl)phosphine (TCEP) for 30 min at 60 °C and alkylation with 10 mM 2-chloroacetamide for 30 min at room temperature in the dark. The samples were de-

salted using Protein Desalting Spin Columns and overnight digestion was conducted using trypsin (2% wt/wt) for 16 h at 37 °C. The digests were acidified by the addition of trifluoroacetic acid to 0.1 % final concentration prior to desalting using C18 solid phase extraction. The eluate was dried in a SpeedVac and re-constituted in avidin column loading buffer for enrichment of the biotinylated peptides. Peptides were eluted from the avidin column with 2 mM biotin buffer (100 mM Na_2PO_4 pH 7.0, 150 mM NaCl, 2 mM biotin). The peptide concentration was approximated by UV absorption using a NanoDrop (A_{280nm}) and the samples were re-constituted in a sufficient volume of 0.2% formic acid in water to yield a concentration of 200 fmol/µL prior to LC-MS/MS analysis.

2.2.7 Liquid chromatography-tandem mass spectrometry (LC-MS/MS):

Chromatographic separation was performed using a Dionex Ultimate 3000 RSLCnano system (Thermo Scientific) with a 75 µm x 15 cm Acclaim PepMap100 separating column (Thermo Scientific) protected by a 2 cm guard column (Thermo Scientific). The mobile phase flow rate was 300 nL/min and consisted of 0.1% formic acid in water (A) and 0.1% formic acid, 95% acetonitrile (B). MS analysis was performed using an LTQ Orbitrap Velos Pro mass spectrometer (Thermo Scientific). The spray voltage was set at 2.2 kV. Orbitrap spectra were collected from 400-1800 m/z at a resolution of 30,000 followed by data-dependent HCD MS/MS (at a resolution of 7500, collision energy 35%, activation time 0.1 ms) of the 10 most abundant ions using an isolation width of 2.0 Da. Charge state screening was enabled to reject the generation of MS/MS spectra for unassigned and singly charged precursor ions. A dynamic exclusion time of 40 sec was used to discriminate against previously selected ions.

2.2.8 Data analysis:

Mass spectrometry data from the cross-linked PTEN samples were analyzed using Crossfinder version 1.0 (20,21) with the default parameters. Prior to analysis with Crossfinder, MS/MS data were converted to mzXML files using ProteoWizard.

2.2.9 Crystallography:

A crystallographic form of PTEN (Crystal PTEN) was generated by deleting the N-terminal 7 residues, the C-terminal 51 residues, and the D2 loop within the C2 domain (residues 286-309). Crystal PTEN (200 μM) is mixed with 2 mM 4p-17mer peptide (YpSDpTpTDpSDPENEPFDED), and then screened by hanging drop in 96-well plates for crystallization conditions. PTEN crystals are obtained in 1.6 M sodium/potassium phosphate, pH 6.5, and optimized by varying the salt concentration and pH. The diffraction data was collected at ALS beam line 502 on a DECTRIS Pilatus 6M detector (wavelength 1.0 Å and temperature 100 K). All diffraction data were processed, integrated and scaled with HKL-2000.

The PTEN structure was determined by molecular replacement using the program AMoRe and the published structure of PTEN (PDB ID 1D5R)(*177*) as the initial search model. The model was re-built manually with iterative rounds of Coot and refined using Refmac5 from the CCP4 suite. The final structure was refined to 3.1 Å. All figures were rendered with PyMOL.

2.3 Results

2.3.1 Individual tail phosphorylation effects on PTEN conformation:

To assess the specific effects of the individual Ser/Thr phosphorylations among Ser380, Thr382, Thr383, and Ser385, we employed expressed protein ligation to generate individual semisynthetic phospho-forms of PTEN. In this way, aa1-378 was produced as an intein fusion protein using a baculovirus expression system and then reacted with MESNA to generate the PTEN recombinant fragment C-terminal thioester (Figures 6A and 6B). In addition, we synthesized a series of eight new 25mer N-Cys containing mono-, di-, and tri-phosphorylated C-terminal peptides, along with the unphosphorylated and tetra-phosphorylated peptides prepared previously. These peptides were then chemoselectively ligated individually to the recombinant PTEN thioester with high efficiency (>80%) and then the semisynthetic full-length PTEN proteins purified using anion exchange chromatography to >90% purity (Figure 6C). As shown previously (14), the introduction of Cys379 (in place of Tyr379) and the conditions of ligation are well-tolerated by PTEN regarding its catalytic activity.

We then measured the PIP3 phosphatase activity of these semisynthetic phospho-PTENs using soluble diC6-PIP3 substrate and monitoring inorganic phosphate release using malachite green. As shown in Figure 7 and Table 1, the monophosphorylated forms, p380-PTEN, p382-PTEN, p383-PTEN, and p385-PTEN all showed a modest reduction in catalytic efficiency, with each showing a k_{cat}/K_m approximately 3-fold below that of unphosphorylated PTEN (wt n-PTEN). The three di-phosphorylated PTENs 2p-380/382-PTEN, 2p-382/383-PTEN, and 2p-380/385-PTEN each hydrolyze diC6-PIP3 approximately 6-fold below that of wt n-PTEN. The triphosphorylated PTEN form 3p-380/382/383-PTEN showed approximately a 12-fold reduction in catalytic efficiency compared with wt n-PTEN, and its catalytic efficiency was very similar to that of tetraphosphorylated (wt 4p-PTEN). These data suggest that

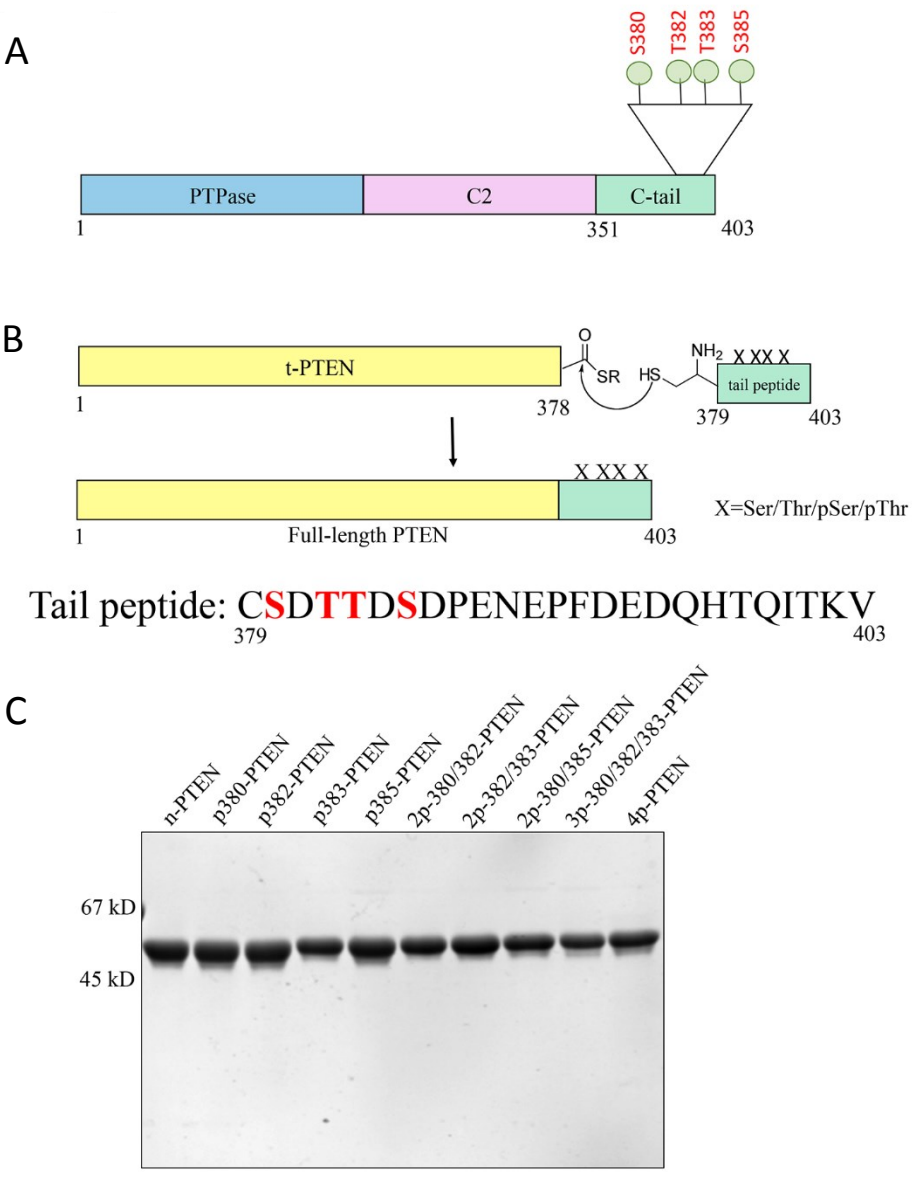

Figure 6: Generation of unmodified, mono-, di-, tri-, and tetra-phosphorylated semisynthetic PTEN proteins. (A) PTEN is composed of a protein tyrosine phosphatase (PTPase) domain, a C2 domain and a regulatory C-terminal tail. The cluster of phosphorylation (S380/T382/T383/S385) is highlighted. (B) C-terminal truncated PTEN (t-PTEN, 1-378) with a thioester at the C-terminus is generated from intein fusion and then treated with mercaptoethanesulfonate (MESNA), and is then ligated to the synthetic peptide containing different combinations of pSer and pThr (mono: p380, p382, p383, p385; di: 2p-380/382, 2p-380/385, 2p-382/383; tri: 3p-380/382/383; tetra 4p-380/382/383/385). X=Ser/Thr/pSer/pThr. (C) Coomassie stained 10% SDS-PAGE gel of the set of differentially phosphorylated semisynthetic PTEN proteins. Ligation of t-PTEN-thioester and the specific peptide proceeds at a constant rate for 48 hours, and the full-length PTEN is further purified by FPLC-anion exchange chromatography using MonoQ column. The final protein is >90% pure. 1. n-PTEN, 2. p380-PTEN, 3. p382-PTEN, 4. p383-PTEN, 5. p385-PTEN, 6. 2p-380/382-PTEN, 7. 2p-382/383-PTEN, 8. 2p-380/385-PTEN, 9. 3p-380/382/383-PTEN, 10. 4p-PTEN.

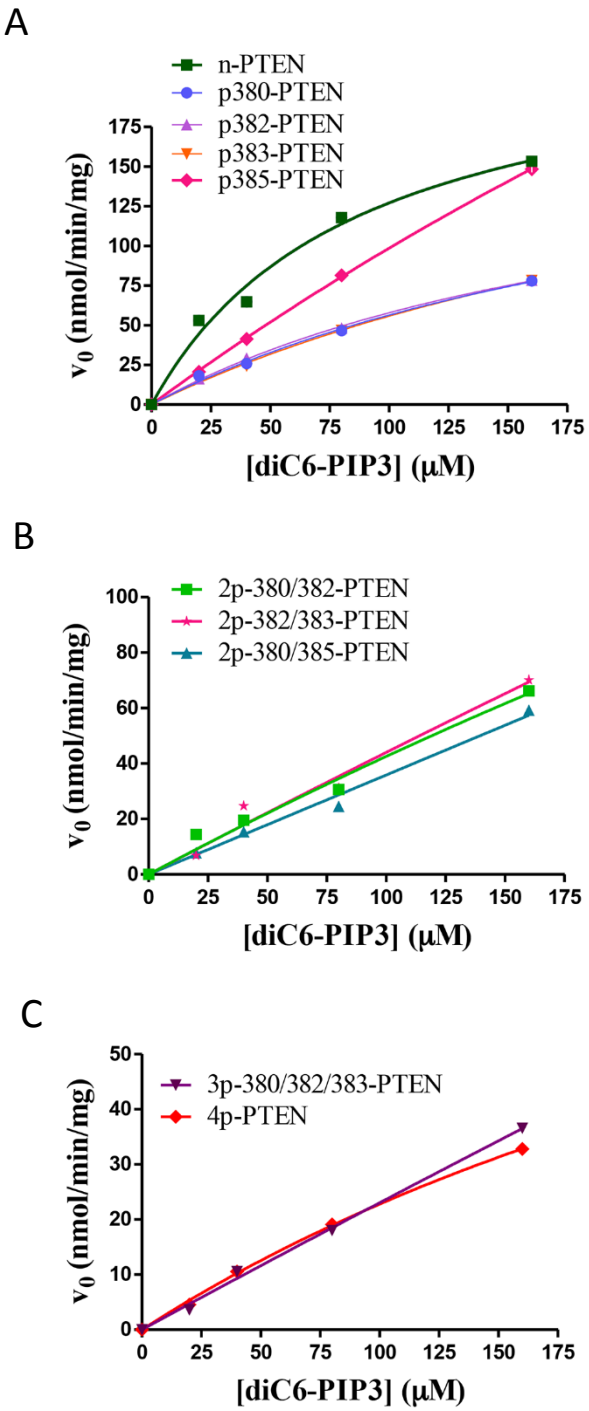

Figure 7: Catalytic activity of the set of differentially phosphorylated semisynthetic PTENs toward a range of diC6-PIP3 substrate concentrations. (A) n-PTEN and mono-phosphorylated PTEN kinetics, (B) di-phosphorylated PTEN kinetics, (C) tri- and tetra-phosphorylated PTEN kinetics (n=2).

Table 1. Catalytic efficiency and tail phosphate reactivity with alkaline phosphatase for different PTENs[1]

Semisynthetic PTENs	PTEN k_{cat}/K_m ($\times 10^2$ $M^{-1}s^{-1}$)	Phospho-tail half-life after alk. phos. treatment $t_{1/2}$ (min)
wt n-PTEN	22 ± 5	ND[2]
p380-PTEN	6 ± 1	3 ± 2
p382-PTEN	7 ± 1	ND[2]
p383-PTEN	6 ± 4	ND[2]
p385-PTEN	9 ± 3	ND[2]
2p-380/382-PTEN	3.1 ± 0.1	6 ± 1
2p-382/383-PTEN	3.4 ± 0.2	ND[2]
2p-380/385-PTEN	2.9 ± 0.2	20 ± 5
3p-380/382/383-PTEN	1.8 ± 0.1	96 ± 13
wt 4p-PTEN	1.7 ± 0.1	104 ± 17
wt t-PTEN	18 ± 5	ND[2]
Cα2D-tPTEN	12 ± 3	ND[2]
Cα2D-4p-PTEN	3.3 ± 0.1	16 ± 5
Cα2A-tPTEN	15 ± 2	ND[2]
Cα2A-4p-PTEN	3.1 ± 0.2	15 ± 2
n-ePTEN	49 ± 23	ND[2]
4p-ePTEN	8 ± 1	141 ± 26
3R/D-4p-PTEN	ND	69 ± 13

[1] Error reported as ± standard error

[2] ND is “not determined”

no single phospho-modification of the Ser/Thr C-terminal cluster is dominant and that each is partially additive in antagonizing catalysis.

To assess the effects of the particular phosphorylation events on PTEN conformation, the mono-, di-, and tri-phosphorylated semisynthetic PTENs were treated with alkaline phosphatase to gauge tail accessibility. As reported previously, natively folded 4p-PTEN versus denatured 4p-PTEN shows resistance to tail phosphate removal catalyzed by the non-specific hydrolase alkaline phosphatase(*19*). Natively folded 4p-PTEN's resistance to alkaline phosphatase is understood to be caused by the masking of the phospho-tail through its intramolecular interactions with the PTEN body. We first determined which of the mono-, di-, and tri-phosphorylated semisynthetic PTENs are recognized by a commercially available phospho-PTEN Ab used in Western blotting. We found that all forms of p380-containing semisynthetic PTEN gave a strong Western blot signal with the anti-phospho-PTEN Ab, but those PTEN forms lacking p380 were not reliably detected (Figure 8A). Thus, we proceeded to analyze the kinetics of alkaline phosphatase-catalyzed dephosphosphorylation of p380-PTEN, 2p-380/382-PTEN, 2p-380/385-PTEN, and 3p-380/382/385-PTEN benchmarked to wt 4p-PTEN standard (Figures 8B and 8C and Table 1). These measurements showed that p380-PTEN was the most rapidly dephosphorylated by alkaline phosphatase ($t_{1/2}$ = 3 min), 30-fold faster than wt 4p-PTEN ($t_{1/2}$ = 104 min), and was followed closely by 2p-380/382-PTEN ($t_{1/2}$ = 6 min), which was ~20-fold faster than wt 4p-PTEN. 2p-380/385-PTEN ($t_{1/2}$ = 20 min) was dephosphorylated by alkaline phosphatase ~5-fold faster than wt 4p-PTEN. The sensitivity of 3p-380/382/385-PTEN ($t_{1/2}$ = 96 min) to alkaline phosphatase was nearly identical to that of wt 4p-PTEN. Taken together, the pattern of alkaline phosphatase sensitivity correlates fairly well with the levels of semisynthetic PTEN catalytic activity,

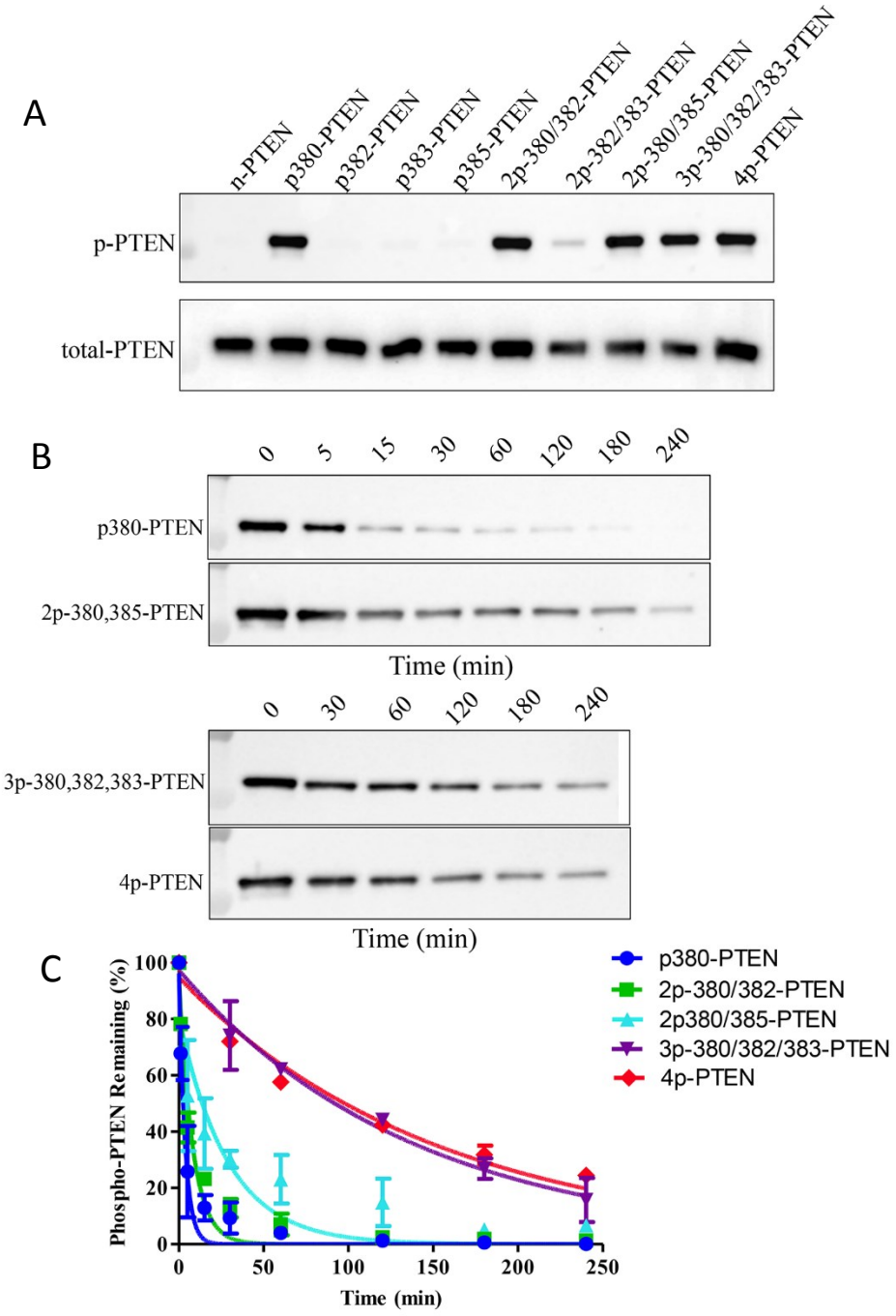

Figure 8: Alkaline phosphatase sensitivity of the set of differentially phosphorylated semisynthetic PTENs. (A) Western blot of the set of differentially phosphorylated semisynthetic PTENs using an anti-phospho-PTEN (S380/T382/T383) antibody. 1. n-PTEN, 2. p380-PTEN, 3. p382-PTEN, 4. p383-PTEN, 5. p385-PTEN, 6. 2p-380/382-PTEN, 7. 2p-382/383-PTEN, 8. 2p380/385-PTEN, 9. 3p-380/382/383-PTEN, 10. 4p-PTEN. (B) Time course of the rate of dephosphorylation of the p380-containing semisynthetic PTENs after alkaline phosphatase treatment analyzed by Western blot. (C) Quantification of the time courses of the Western blot data in Fig. 3B (n=2). Error bars reported as ± standard error.

indicating that the individual phosphorylation events show partial additivity in driving the tail interaction with the PTEN body.

2.3.2 Analysis of mutant semisynthetic 4p-PTENs:

We next combined site-directed mutagenesis along with expressed protein ligation to prepare three semisynthetic 4p-PTEN proteins to investigate the biochemical properties of the ePTEN mutant residues and those of the PTEN Cα2 loop. As previously mentioned, cellular expression of ePTEN indicates that it localizes to the plasma membrane, suggesting that tail phosphorylation may be unable to drive a closed PTEN conformation(*175*). PTEN's Cα2 loop has been implicated in membrane binding and in H/D exchange experiments to participate in PTEN's phospho-tail mediated conformational change(*16, 176*). The 4p-ePTEN mutant containing Q17R, R41G, E73D, N262Y, and N329H was prepared by semisynthesis as described above, as were two 4p-PTEN Cα2 mutants, Cα2D (K327D, K330D, K332D and R335D) and Cα2A (K327A, K330A, K332A, and R335A) to >90% purity (Figure 9). Interestingly both n-ePTEN and 4p-ePTEN had 2-and 5-fold higher diC6-PIP3 phosphatase catalytic efficiencies compared with their wt counterparts (Figure 9 and Table 1). However, the diC6-PIP3 phosphatase catalytic efficiency of 4p-ePTEN was a marked 6-fold lower than that of n-ePTEN (Figure 9B and Table 1) suggesting that tail phosphorylation could drive ePTEN into a closed state. Furthermore, 4p-ePTEN alkaline phosphatase sensitivity showed a slightly (~40%) longer half-life of phospho-tail hydrolysis relative to that of wt 4p-PTEN (Figures 10A and 10B and Table 1). These results suggest that the point mutants of ePTEN do not substantially weaken phospho-tail-PTEN body interactions, and there is an alternative, unidentified explanation for ePTEN membrane localization.

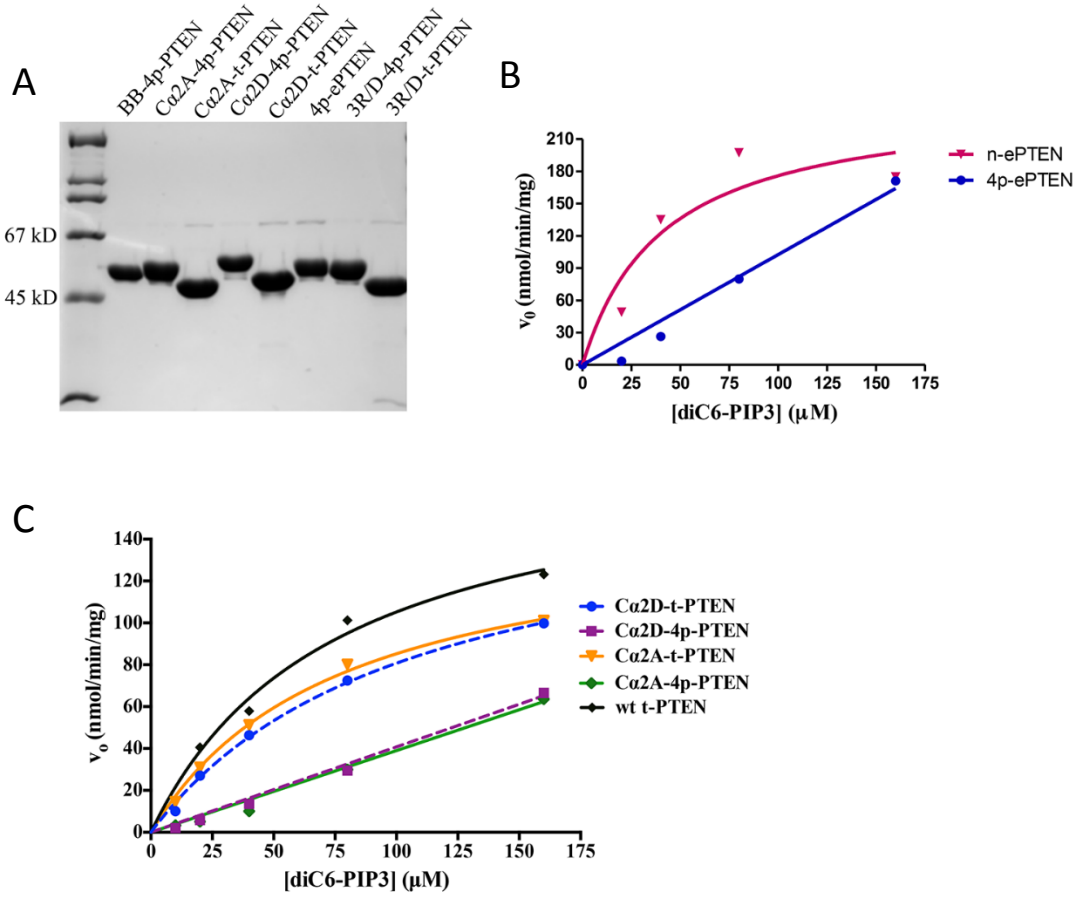

Figure 9: SDSPAGE analysis and catalytic activity of a series of mutant semisynthetic PTENs toward a range of diC6-PIP3 substrate concentrations. (A) Coomassie stained 10% SDS-PAGE gel of semisynthetic PTEN mutants. 1. 2. BB-4p-PTEN, 3. Cα2A-4p-PTEN, 4. Cα2A-t-PTEN, 5. Cα2D-4p-PTEN, 6. Cα2D-t-PTEN, 7. 4p-ePTEN, 8. 3R/D-4p-PTEN, 9. 3R/D-t-PTEN. (B) Catalytic activity of ePTEN forms with diC6-PIP3 (n=2); Q17R, R41G, E73D, N262Y, N329H. (C) Catalytic activity of Cα2 loop mutant PTEN forms with diC6-PIP3; Cα2D = K327D, K330D, K332D, R335D; Cα2A = K327A, K330A, K332A, R335A (n=2).

In contrast, analysis of the 4p-PTEN Cα2 mutants demonstrated that this region participates significantly in phosphorylation-mediated conformational change. Both the Cα2D and Cα2A 4p-PTEN mutants showed increased catalytic efficiencies of diC6-PIP3 hydrolysis relative to that of 4p-PTEN (Figure 9C and Table 1). While still lower than the truncated PTEN Cα2 mutants that lack phospho-tails, the lipid phosphatase activities of these 4p-PTEN Cα2 mutants suggest that replacement of these Lys and Arg residues weakened phospho-tail interactions in phosphorylated PTEN. Furthermore, both Cα2D and Cα2A 4p-PTEN exhibited a marked 6-fold greater sensitivity to alkaline phosphatase-mediated tail dephosphorylation compared with wt 4p-PTEN. The fact that both the Asp and Ala replacements of the Lys/Arg residues in the Cα2 4p-PTEN mutants display similar behaviors is consistent with the possibility that one or more of the Lys/Arg side chains are making important electrostatic interactions with residues in the anionic PTEN tail.

2.3.3 Photo-crosslinking of benzoylphenylalanine containing-4p-PTEN:

To further investigate the structural basis of phospho-tail-body interactions within 4p-PTEN, we pursued a photo-crosslinking strategy. In this regard, Phe392 was replaced with the photo-activatable benzoylphenylalanine (Bpa) and a C-terminal biotin-modified Lys. In this semisynthetic strategy, a 18mer N-Cys peptide (Figure 11A) was used rather than the full-length 25mer tail for synthetic ease and because prior studies have shown the 4p-17mer tail is sufficient to promote high affinity interaction with the core of PTEN(*19*). This Bpa/biotin-modified semisynthetic 4p-PTEN (BB-4p-PTEN) was efficiently produced and appeared greater than 90% pure after anion exchange chromatography (Figure 9A). Irradiation of BB-4p-PTEN was followed by alkaline

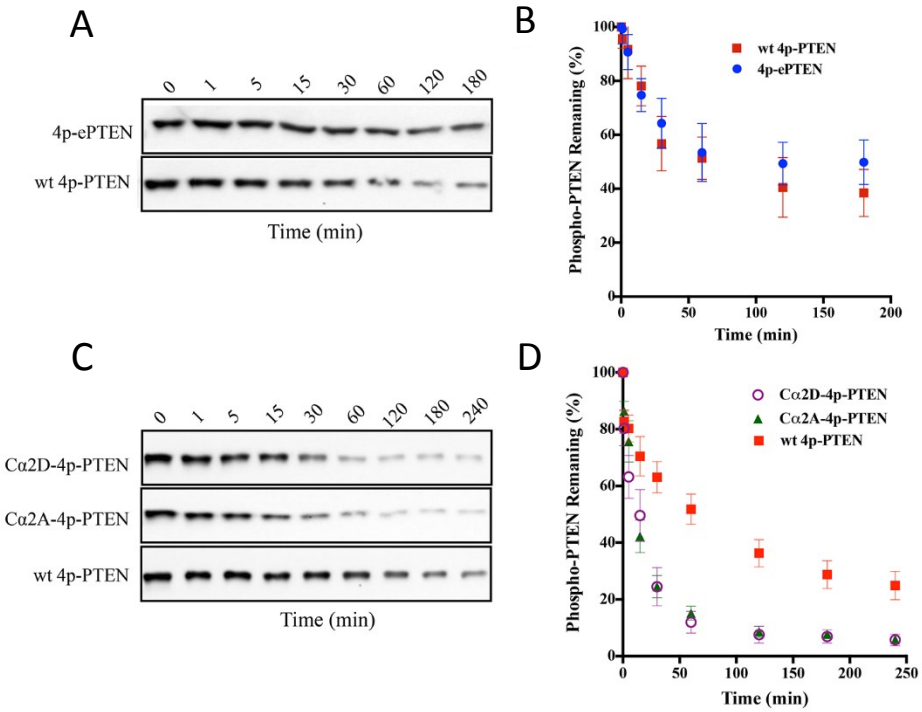

Figure 10**:** Alkaline phosphatase sensitivity of different semisynthetic phospho-PTEN mutants. (A) Western blot of time course from the alkaline phosphatase treated 4p-ePTEN (Q17R, R41G, E73D, N262Y, N329H) and wt 4p-PTEN. (B) Quantification of the alkaline phosphatase assay for 4p-ePTEN and wt 4pPTEN (n=3). (C) Western blot of time course from the alkaline phosphatase treated Cα2D-4p-PTEN (K327D, K330D, K332D, R335D), Cα2A-4p-PTEN (K327A, K330A, K332A, R335A), and wt 4p-PTEN. (D) Quantification of the alkaline phosphatase assay for 4p-Cα2 loop mutants and wt 4p-PTEN (n=6). Error bars reported as ± standard error.

phosphatase treatment (to remove the mass spectrometry electrospray ionization suppressive effects of the phosphates) and trypsinization and avidin treatment to enrich for biotin-containing peptides. These peptides were then subjected to LC-MS/MS and then the data were analyzed using Crossfinder(*178, 179*). This led to the identification of a crosslinked peptide that contained a C-terminal peptide (379-CSDTTDSDPENEP(B)DEDK$_{bio}$-396) attached to an N-terminal peptide (42-LEGVYRNNIDDVVR-55) (Figures 11B and 11C). The assignment of this crosslinked peptide was based on a combination of its intact molecular mass (4090.7 Da) as well as its fragmentation pattern using tandem mass spectrometry, although the site of conjugation to the N-terminal peptide (between Gly45 and Ile50) could not be precisely defined (Figure 11C). This crosslinked peptide was not detected in the absence of UV irradiation. These data thus suggest that the C-tail can access a conformation that places the C-terminal peptide in proximity to the N-terminal catalytic domain segment aa42-55.

To further probe the importance of this interaction, we generated semisynthetic 4p-PTEN containing three point mutations in the vicinity of the three-dimensional surface of the crosslinked N-terminal segment, R41D, R47D, and R74D (3R/D). Even unligated 3R/D-PTEN mutant showed significantly impaired catalytic activity (Figure 12A), as expected from prior studies that have investigated the phosphatase effects of mutating Arg47(*180, 181*). Thus, it was not feasible to use diC6-PIP3 hydrolytic activity to gain insight into the phosphorylation effects of 3R/D-4p-PTEN. To assess the conformation of the 3R/D-4p-PTEN, we relied on alkaline phosphatase sensitivity. In these experiments, we found that 3R/D-4p-PTEN ($t_{1/2}$ = 63 min) showed approximately a 2-fold rate increase in alkaline phosphatase-mediated dephosphorylation compared with 4p-PTEN (Figures 12B and 12C, Table 1). These data support at least a modest

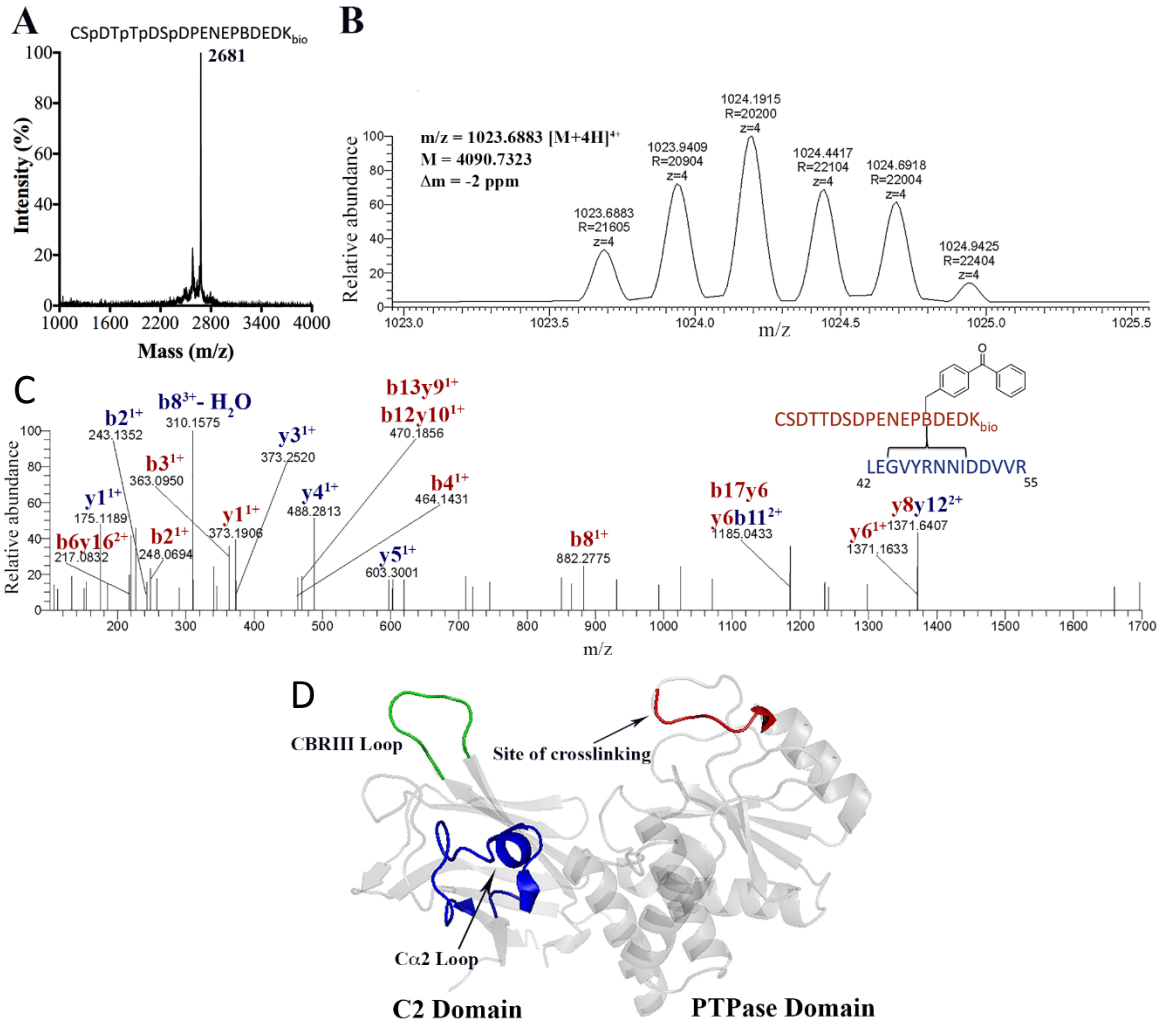

Figure 11: BB-4p-PTEN, photocrosslinking and mass spectrometry analysis. (A) MALDI-TOF MS spectrum of 18mer synthetic peptide containing tetraphosphorylation (Ser380, Thr382, Thr383, Ser385), Bpa at position 392, and a C-terminal biotinylated lysine used for expressed protein ligation. (B) Isotopic distribution of a 4+ charged crosslinked peptide with the reported mass, m/z, and Δm from Crossfinder. (C) High resolution tandem-MS spectrum of the crosslinked peptide. (D) PTEN crystal structure (PDB: 1D5R) highlighting the site of crosslinking and other important areas shown to be involved in phospho-C-tail binding.

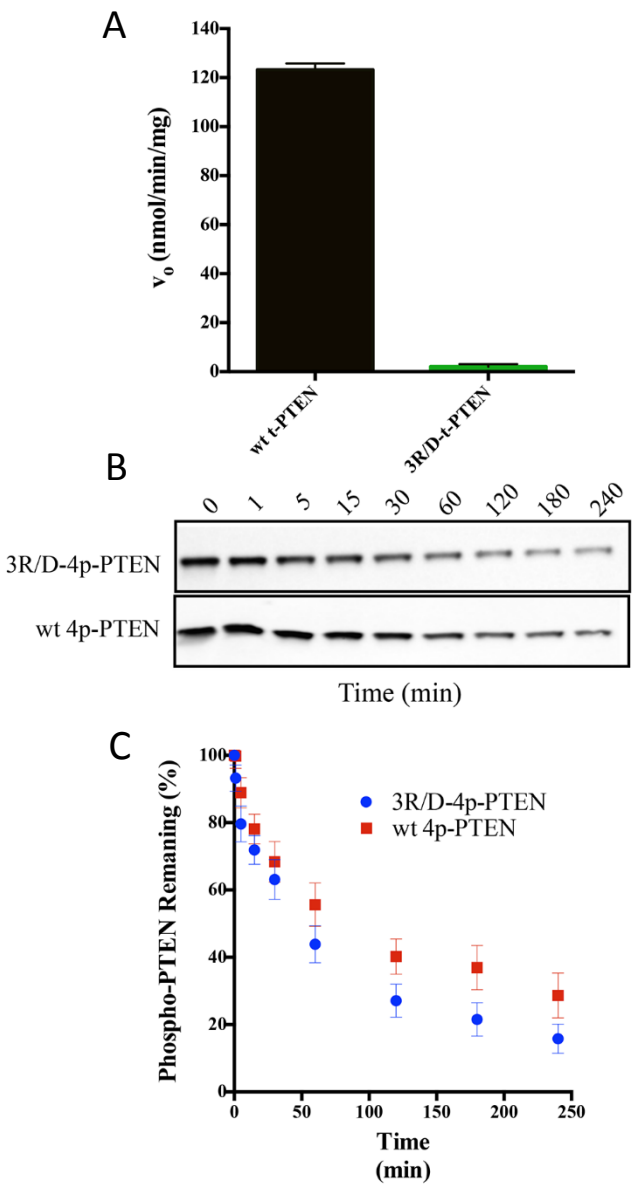

Figure 12: Conformational analysis of the 3R/D PTEN mutant. (A) Catalytic activity of wt t-PTEN (123 ± 4 nmoles/min/mg) compared to 3R/D t-PTEN (<4 nmoles/min/mg) with 160 μM diC6-PIP3 (n=2). (B) Western blot of time course of dephosphorylation of alkaline phosphatase-treated 3R/D-4p-PTEN (R41D, R47D, R74D) and wt 4p-PTEN. (C) Quantification of the alkaline phosphatase assay for 3R/D-4p-PTEN and wt 4pPTEN (n=6). Error bars reported as ± standard error.

contribution of the N-terminal catalytic segment in stabilizing the closed conformation of 4p-PTEN.

2.3.4 Co-crystallization of PTEN with phosphorylated C-tail peptide

To obtain detailed information about how the phosphorylated C-tail inhibits PTEN, we tried to get a high-resolution structure of the phosphorylated form of PTEN. The tetra-phosphorylated PTEN C-tail peptide showed the strongest inhibition of the phosphatase activity of PTEN using soluble PIP3 substrate, indicating a high affinity binding of the phospho-peptide to the protein. Taking advantage of this high affinity binding, we hypothesized that it might be possible to co-crystallize the truncated version of PTEN that was used to solve the crystal structure of partial PTEN in complex with our synthetic tetra-phosphorylated C-tail peptide.

To facilitate the crystallization, we synthesized a peptide lacking the last eight residues of the original C-tail peptide affording the 4p-17mer. The version of PTEN used in crystallization trials deletes the 7 N-terminal amino acid residues, the C-tail residues from 354 to 403, and a D2 loop (286-309). Since this construct was used to solve the crystal structure of PTEN by Pavletich and coworkers, we call it crystal-PTEN.(*16*) We confirmed that the 4p-17mer also inhibits crystal-PTEN's phosphatase activity with high potency, with IC50 about 1 μM (Figure 13A). The mixture of 200 μM crystal-PTEN and 2 mM 4p-17mer peptide with 25 mM DTT are combined with the crystallization screening kit that contains different precipitant and buffer at various concentrations and pH, in the hanging drop vapor diffusion system to screen the optimal conditions.

We got several hits, and optimized them. The first hit was obtained with 1.6 M sodium potassium phosphate at pH 6.5. In this one we got nice crystals and were able to

see X-ray diffraction. The structure was solved using molecular replacement at the resolution of 3.1 Å (Figure 13B). However, in this structure, we did not observe electron density for the C-tail peptide, it was almost identical to the previous known structure of PTEN. Under this condition, the phosphorylated peptide did not bind to PTEN. From this, we learned that the high salt condition could interrupt the binding of phosphorylated C-tail with PTEN which is very sensitive to ionic strength. This observation was further confirmed using PTEN phosphatase activity assays that adding 150 mM NaCl to the assay buffer sharply reduced the potency of 4p-peptide to inhibit PTEN activity (Figure 13C). Thus, in subsequent crystal screening, we focused on low-salt conditions, which we hoped would be more conducive to allowing co-crystallization of PTEN with the phospho-peptide. We got another two hits. The first one involved 100 mM SPG, pH 8.0, and 25% PEG1500. Small crystals were observed. However, crystals in this condition could never been reproduced except using the exact solution from the screening kit. The other hit we got employed 20% PEG3350, 100 mM Bis-Tris Propane, pH7.5, 200 mM sodium potassium tartrate. This condition could be reproduced and partly optimized by changing the concentration of PEG3350, pH and concentration of sodium potassium tartrate. However, after a lot of effort, we were still unable to grow crystals of sufficient size and shape suitable for structural analysis.

2.4 Discussion

The application of protein semisynthesis, mutagenesis, and photocrosslinking has been integrated to refine our understanding of how phosphorylation of a cluster of four C-terminal Ser/Thr residues drives a conformational change in PTEN. Prior to this

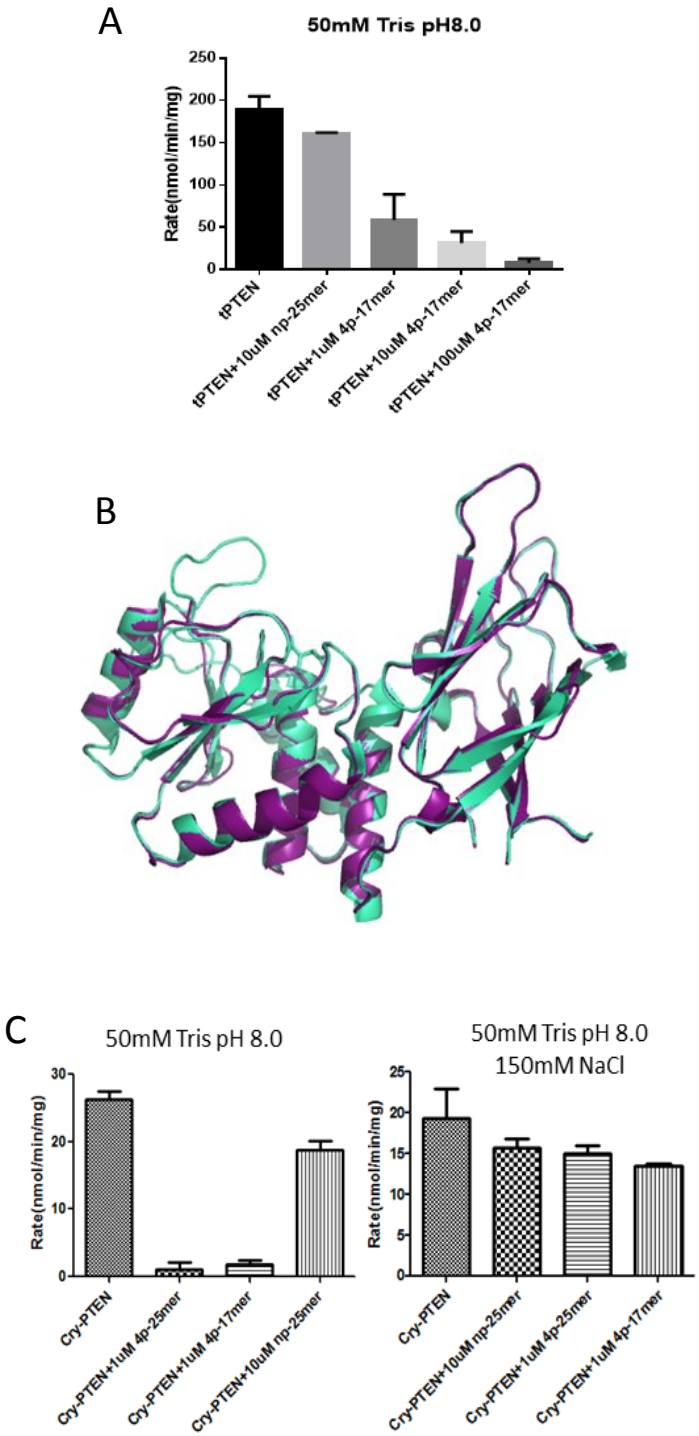

Figure 13: Co-crystallization of crystal-PTEN and phosphorylated C-tail peptide. (A) Malachite Green Assay of crystal-PTEN with different peptides. While 10 uM non-phosphorylated 25mer peptide showed little inhibition, the 4p-25mer, and 4p-17mer which will be used in co-crystallization, showed very potent inhibition of PTEN phosphatase activity. (B) Crystal structure solved by us (purple) superimposed with the published structure of PTEN (green). (C) Malachite Green Assay of crystal-PTEN with different peptides in two different buffers, one with no NaCl, the other with 150 mM NaCl.

work, it was unclear if any single phosphorylation site in PTEN would be predominantly or wholly responsible for inducing the PTEN conformational change and the influence of the three other sites would be negligible. Our data shown here supports the idea that each of the four sites can contribute incrementally to stabilizing the closed PTEN conformation and at least three sites are needed to match the full effects of tetraphosphorylated PTEN. These results imply that the surface of interaction between the phospho-tail and the PTEN body may be rather broad to encompass multiple contact sites with these phosphates. These findings also suggest the concept that a dynamic step-wise degree of PTEN conformational closure may occur by modifying only a subset of the tail Ser/Thr residues, which in turn could give rise to a sliding scale of cellular signaling effects. Our results also highlight that the antibody used here cannot readily distinguish between monophosphorylated p380 and the multiply modified forms that contain p380. This suggests the need for caution in interpreting Western blots and immunocytochemistry data that rely on this reagent for signaling analysis.

Several models have been proposed regarding where the phospho-tail in PTEN contacts the core of the protein(*19, 173, 174*). In the current study, we found additional evidence for key interactions between the PTEN C2 domain and the phospho-tail. Prior studies have shown that the CBR3 loop of the PTEN C2 domain is involved in the phospho-tail interactions(*19*), with an 8-fold enhanced sensitivity to alkaline phosphatase-catalyzed tail dephosphorylation compared with 4p-PTEN. However, while the penta-Lys (260,263,266,267, and 269) to penta-Asp CBR3 loop 4p-PTEN mutant appears to have a relatively open structure, mutation of the penta-Lys motif to penta-Ala is quite similar to wt 4p-PTEN(*19*). Thus, it appears that none of the CBR3 loop Lys residues are making key electrostatic interactions with the phospho-tail, and only when replaced with the negatively charged Asp residues do they prevent conformational

closure, arguing for a more indirect role in stabilizing the closed conformation. In contrast, as shown here the Cα2 Lys/Arg sidechains cannot be substituted functionally by Ala, suggesting that these basic residues are more directly involved in tail phospho-interactions.

Some prior experiments including H/D exchange, mutagenesis, and protease sensitivity have suggested that the catalytic domain of PTEN might also somehow participate in phospho-tail interactions(*19, 173, 176*). Through the use of photo-crosslinking, we find that at least part of the phospho-tail binds to an N-terminal segment in the PTEN catalytic domain. Mutagenesis of this segment is consistent with this region playing a partial role in mediating the conformational closure of phosphorylated PTEN. If we consider the energetic sum of the alkaline phosphatse sensitivity parameters of the N-terminal segment (2-fold), the Ca2 loop (6-fold), and the CBR3 loop (8-fold) mutants reported here and previously, we can more than account for the 25-fold protection measured when comparing folded and unfolded 4p-PTEN. Thus, it is plausible that these three PTEN surfaces are fully responsible for locking the phospho-tail to the PTEN body(*19*). It is perhaps noteworthy that this N-terminal segment as well as the CBR3 loop and the Cα2 loop all have been implicated in PTEN's membrane recruitment(*8, 176, 180, 181*). It is therefore reasonable to postulate that the PTEN phosphate tail acts as a molecular mimic of the phospholipid membrane. These results underscore the very large interaction surface that may govern the 4p-PTEN conformational closure.

The observation that 4p-ePTEN behaves conformationally similarly to wt 4p-PTEN was unexpected, given the dramatic cellular phenotype associated with ePTEN(*175*). We speculate that these ePTEN point mutations may strengthen a specific protein-protein or protein lipid interaction between PTEN and a molecule not yet

identified. Future work will be needed to address these possibilities that could uncover new targets to enhance cellular PTEN functions.

This study also illustrates the power of expressed protein ligation in elucidating how a complex series of post-translational modifications (PTMs) can alter the structure of a protein(*157*). As mass spectrometry has identified hundreds of thousands of PTMs in proteins, it has become daunting to cope with illuminating the structural and functional effects of these PTMs at an individual protein level. The incorporation of four phosphorylations, a benzoylphenylalanine, and a biotin tag site-specifically into a single folded protein of this size would have been difficult to achieve without expressed protein ligation. Expressed protein ligation when coupled with other biochemical, biophysical, and analytical approaches thus offers atomic precision in working through the 21st century challenges of protein science.

Chapter 3: Enzymatic Analysis of PTEN Ubiquitination by WWP2 and NEDD4-1 E3 Ligases

3.1 Introduction

As described in Chapter 2, PTEN loss of function mutations occur commonly in a wide array of human cancers, allowing for the increase in PIP3 levels fueled by PI3-kinases that in turn allosterically activate Akt protein kinase and drive neoplastic growth.(*170, 182-185*) Beyond mutation, PTEN's activity is regulated by other mechanisms including post-translational modification.(*20, 23, 168, 172, 174*) Two types of post-translational modifications occurring on PTEN are phosphorylation and ubiquitination.(*29, 168*) Our study along with others have suggested that a cluster of phosphorylations at residues Ser 380, Thr 382, Thr 383 and Ser 385 can drive an intramolecular interaction with the PTEN C2 domain, resulting in reduced membrane association and catalytic activity.(*19*) Somewhat paradoxically, this phospho-cluster has also been reported to enhance the cellular stability of PTEN.(*20*) However, the evidence of this phosphorylation effect on PTEN stability has been indirect, relying on mutagenesis of the 380-385 cluster to Ala. Moreover, it is unknown if this PTEN instability is related to changes in its cellular localization, altered cellular signaling, or differential ubiquitination.

Three PTEN ubiquityltransferase E3 ligases that have been reported are NEDD4-1, WWP2, and XIAP.(*27, 28, 30*) NEDD4-1 and WWP2 E3 ligases belong to the subset of ubiquityltransferases that have a catalytic HECT domain that operates with E1 and E2 ligases to catalyze ubiquityl transfer to Lys residues on target proteins.(*60, 85*) Unlike the more common RING domain E3 ligases, the HECT domain gets charged by

ubiquitin on a nucleophilic Cys residue to form an intermediate E3-ubiquitin thioester.(*70, 85*) This E3 catalytic intermediate is in turn attacked by substrate Lys residues affording ubiquitylated proteins.(*70*) XIAP is a member of the larger family of RING domain E3 ligases that are Zn-binding proteins and serve as a template facilitating transfer of ubiquitin from the E2 enzyme Cys thioester intermediate to a Lys on a target substrate.(*186, 187*)

In this study, we analyze with purified proteins the NEDD4-1, WWP2, and XIAP catalyzed ubiquitination of PTEN in its unphosphorylated and phosphorylated states. We employed expressed protein ligation(*158*) to generate semisynthetic forms of PTEN that were either tetraphosphorylated on the 380-385 Ser/Thr cluster (4p-PTEN) or unphosphorylated on these residues (n-PTEN). In our hands, XIAP did not catalyze PTEN ubiquitination, whereas both NEDD4-1 and WWP2 showed PTEN ubiquityltransferase activity. Compared with NEDD4-1, we found that WWP2 appears to more rapidly ubiquitylate n-PTEN. NEDD4-1 showed similar ubiquitination kinetics toward both n-PTEN and 4p-PTEN. In contrast, WWP2 showed a marked reduction in its ability to ubiquitylate 4p-PTEN versus n-PTEN. Mass spectrometric analysis suggests that the two E3 ligases possess overlapping but distinct ubiquitination preferences for PTEN Lys specificity. Below we describe these findings and discuss their relevance to PTEN regulation.

3.2 Methods

3.2.1 Reagents:

The pGEX6p-2 WWP2 plasmid for bacterial expression of GST-WWP2 was a gift from Dr. Wenyi Wei at Beth-Israel Deaconess Medical Center. The pFastBac1-His-

NEDD4-1 was described previously.(*30*) Human recombinant XIAP protein was purchased from Sigma Aldrich. Purified wild-type ubiquitin, human ubiquitin-activating enzyme UBE1, and human ubiquitin-conjugating enzyme UbcH5c were prepared as described previously.(*188*) The lysine-free ubiquitin (K0-Ub) and human ubiquitin-conjugating enzyme UbcH7 were purchased from LifeSensors (PA, USA). The Colloidal Blue Staining Kit was purchased from Invitrogen. Anti-PTEN antibody was from Santa Cruz (CA, USA). Apyrase was from New England Biolabs. All other reagents were commercially purchased with the highest quality from either Sigma or Fisher.

3.2.2 Peptide synthesis:

Peptides were synthesized using a PS3 peptide synthesizer from Protein Technologies (Tuscon, AZ) using conventional FMOC peptide synthesis strategies. They were purified by reversed phase HPLC on a C-18 column and the correct structures confirmed by MALDI mass spectrometry.

3.2.3 Expression and Purification of GST-WWP2:

BL-21 Codon Plus cells were transformed with the pGEX6p-2 WWP2 plasmid, and cultured in LB medium at 37 °C to reach the optimal density (OD_{600}=0.6) in a shaker incubator grown on a 1 L scale. GST-WWP2 expression was induced by 0.5 mM IPTG at 16 °C for 20 hours. The cells were resuspended in lysis buffer (25 mM Tris-HCl pH 8.0, 250 mM NaCl, 1 mM PMSF and 1x Roche cocktail protease inhibitors) and were lysed using French Press, and the lysate was loaded on glutathione agarose followed by washing with wash buffer (25 mM Tris-HCl pH 8.0, 250 mM NaCl, 0.1% Triton X-100).

The desired GST-WWP2 was eluted using 25 mM Tris-HCl pH 8.0, 250 mM NaCl containing 50 mM reduced glutathione at pH 8.0. Fractions containing GST-WWP2 were combined and dialyzed against a buffer consisting of 25 mM Tris-HCl pH 7.5, 250 mM NaCl, 1 mM EDTA, 5 mM DTT, and 10% glycerol and the protein was concentrated to 2 to 5 mg/mL and flash frozen. The yield of GST-WWP2 was 0.5 mg/L culture. GST-WWP2 was stored in aliquots at -80˚C after flash freezing.

3.2.4 Expression and Purification of His6-NEDD4-1:

For NEDD4-1, the pFascBac1-His-NEDD4-1 was used to generate Bacmid to infect Sf21 insect cells which produced the baculovirus for NEDD4-1 expression. The Sf9 insect cells were infected with baculovirus and cultured at 27 °C for 48 hours. The cells were then harvested and resuspended in lysis buffer (25 mM HEPES pH 7.5, 250 mM NaCl, 1 mM EDTA, 10% glycerol, 1 mM PMSF, 1x Roche cocktail protease inhibitors). The cells were lysed using a 40 mL homogenizer. The cell lysate from 1 L culture was incubated with 2.5 ml Ni-NTA resin for His-NEDD4-1 binding. After washing with 200 mL wash buffer (25 mM HEPES pH7.5, 250 mM NaCl, 1 mM EDTA, 0.1% Triton X-100), the protein was eluted with a gradient of wash buffer now also containing 80 to 500 mM imidazole. The eluted protein was dialyzed in 25 mM Tris-HCl pH 8.0, 5 mM NaCl, 5 mM DTT overnight. Then His-NEDD4-1 was further purified by FPLC using an anion exchange MonoQ column with the gradient of 5 to 500 mM NaCl added to the dialysis buffer over 240 column volumes. Fractions corresponding to the desired protein were verified by SDS-PAGE, and highly purified fractions were combined. To the combined fractions, 10% glycerol was added and then the protein was concentrated to

5mg/ml. The purified protein was flash frozen, and stored in aliquots at -80 °C. The yield of His-NEDD4-1 is around 5mg/L culture.

3.2.5 In vitro ubiquitination assay:

The *in vitro* ubiquitination reaction was carried out in microcentrifuge tubes in volumes of 20 to 50 µL containing 40 mM Tris-HCl pH 7.5, 50 mM NaCl, 2 mM DTT or 0.5 mM TCEP, 5 mM $MgCl_2$, with 5 mM ATP, 100 µM ubiquitin, 50 nM E1 protein, 1 µM E2 protein, 1 µM E3 protein, and 1 or 10 µM PTEN. The reaction mixture without E1 protein was pre-incubated at 30 °C for 20 minutes and then the reaction was initiated by adding the E1. To quench the reaction, an aliquot of the reaction mixture was mixed with SDS loading dye at different time points and boiled for 5 minutes. The samples were then run out on SDS-PAGE, and stained using a Colloidal Blue Staining Kit following the manufacturer's protocol. In addition, samples were also analyzed using western blotting with an anti-PTEN antibody. The quenched reaction samples containing 50 ng of PTEN were loaded on to 10% SDS-PAGE. The protein was then transferred to nitrocellulose membranes using the iBlot Dry Blotting system (Thermo Fishier). The membranes were blocked with 5% BSA in TBST buffer for 30 minutes, and then incubated with anti-PTEN antibody (1:1000 dilution) at 4 °C overnight. Afterwards, the membranes were washed with TBST and probed with HRP-conjugated anti-mouse secondary antibody at 1:10000 dilution. The bands were detected by chemiluminascence using an ECL western blotting detection kit from GE Healthcare. All assays were repeated on at least two independent occasions with results and replicates showing similar results.

3.2.6 Single-turnover WWP2 ubiquitin transfer assay:

These experiments were based on previously reported methods.(*189*) Reaction mixtures containing 40 mM Tris-HCl pH 7.5, 0.5 mM TCEP, 1 mM $MgCl_2$, 1 mM ATP, 100 µM wild-type ubiquitin, 0.5 µM E1 protein, 5 µM E2 protein, and 2.5 µM WWP2 in a volume of 40 µL were incubated at 30 ℃ for 10 minutes. Then 1 µM apyrase was added to the reaction mixtures, and they were incubated at 30 °C for 1 minute, followed by addition of 1 µM PTEN. The final volume of the reactions was adjusted to 50 µl. Aliquots of the reaction mixture were quenched at different time points after adding PTEN. The samples were analyzed by western blot using an anti-PTEN antibody as described above.

3.2.7 GST-WWP2 pulldown assay of PTEN forms:

Non-phosphorylated or tetra-phosphorylated PTEN (1 µM) was mixed with or without 1 µM GST-WWP2 in 25 mM Tris pH 7.5, 50 mM NaCl, 5 mM DTT, and 10 µL glutathione agarose in a total volume of 100 µL. The mixture was incubated at 4 °C with gentle agitation overnight. Afterwards, the glutathione agarose was washed with 1 mL wash buffer (25 mM HEPES pH 7.5, 250 mM NaCl, 0.1% Triton X-100) three times. 20 µl SDS loading dye was added to the resin, and the mixture was then boiled for 5 minutes. The samples were then analyzed by western blot using an anti-PTEN antibody as described above.

3.2.8 Data analysis:

To quantify the rate of the ubiquitination reaction, the PTEN band was quantified by densitometric analysis using Image J software, and the rate of decrease of unmodified and phosphorylated PTEN (μM/min) was calculated.

3.2.9 Enzymatic digestion:

Approximately 2.5 μg of protein from the PTEN ubiquitination reactions was separated via SDS-PAGE and visualized with coomassie blue staining. Protein bands of interest were excised, cut into 1 × 1 mm pieces and dehydrated with methanol for 5 min. The gel pieces were then washed as follows: 1 x 5 min with 30% methanol/70% water, 2 x 10 min with water, and 3 x 10 min with 100 mM ammonium bicarbonate (NH_4HCO_3)/30% acetonitrile. Gel pieces were dried in a SpeedVac. Protein disulfide bonds were reduced with 10 mM tris(hydroxypropyl)phosphine (TCEP) in 100 mM NH_4HCO_3 for 60 min at 56 °C, followed by alkylation with 55 mM 2-chloroacetamide in 100 mM NH_4HCO_3 for 45 min at room temperature in the dark. The gel pieces were washed with 100 mM NH_4HCO_3 for 15 min and dehydrated with acetonitrile followed by complete drying in a SpeedVac. Gel pieces were rehydrated in trypsin solution (15 ng/μL trypsin in 50 mM NH_4HCO_3) on ice for 45 min. Excess trypsin solution was discarded, replaced with 50 mM NH_4HCO_3 and incubated overnight at 37 °C. Digestion buffer was collected and saved. Peptides were extracted once with 50 mM NH_4HCO_3, once with acetonitrile and twice with 5% formic acid in 50% acetonitrile; each extraction was performed by incubating at 37 °C for 15 min with vortexing. All supernatants were combined and dried in a SpeedVac. The samples were re-constituted in 50 μL AspN reaction buffer (50 mM Tris-HCl, 2.5 mM $ZnSO_4$ pH8) and 12.5 ng/μl AspN was added for overnight digestion at 37 °C. Digestion reactions were stopped by the addition of 50

µl 0.2% trifluoroacetic acid, and the samples were de-salted using C18 STAGE Tips.(*190*) The samples were re-constituted in 0.2% formic acid in water prior to LC-MS/MS analysis, and one-third of each sample was injected.

3.2.10 Liquid chromatography-tandem mass spectrometry (LC-MS/MS):

Chromatographic separation was performed using a Dionex Ultimate 3000 RSLCnano system (Thermo Scientific) with a 75 µm x 15 cm Acclaim PepMap100 separating column (Thermo Scientific) protected by a 2 cm guard column (Thermo Scientific). The mobile phase flow rate was 300 nL/min and consisted of 0.1% formic acid in water (A) and 0.1% formic acid, 95% acetonitrile (B). MS analysis was performed using an LTQ Orbitrap Velos Pro mass spectrometer (Thermo Scientific). The spray voltage was set at 2.2 kV. Orbitrap spectra were collected from 400-1800 m/z at a resolution of 30,000 followed by data-dependent HCD MS/MS (at a resolution of 7500, collision energy 35%, activation time 0.1 ms) of the 10 most abundant ions using an isolation width of 2.0 Da. Charge state screening was enabled to reject the generation of MS/MS spectra for unassigned and singly charged precursor ions. A dynamic exclusion time of 40 sec was used to discriminate against previously selected ions. Data were searched using SEQUEST in Proteome Discoverer v. 1.3 (Thermo Scientific) against a *Homo sapiens* PTEN UniProt database (UniProt accession # P60484). Database search parameters were as follows: enzyme – non-specific (to allow for combined trypsin and AspN cleavage); precursor mass tolerance – 10 ppm; fragment ion tolerance – 0.03 Da; static modification – Cys carbamidomethylation; variable modifications – Met oxidation, Lys ubiquitination and acetylation, and Ser/Thr/Tyr phosphorylation. The data were

filtered using a 1% false discovery rate threshold and a maximum peptide rank of 1. All MS/MS spectra assigned to modified PTEN peptides were manually inspected.

3.3 Results

3.3.1 Ubiquitination of n-PTEN by NEDD4-1, WWP2, and XIAP

For these studies, we prepared 4p-PTEN and n-PTEN using expressed protein ligation as described previously.(*19*) In this method, aa1-378 of PTEN is prepared as a thioester via an intein using a baculovirus expression system, and this is chemoselectively ligated to N-Cys containing synthetic peptides aa379-403 with or without phosphorylations at Ser380, Thr382, Thr383, and Ser385. These are wild-type in sequence except for the presence of a Y379C mutation necessitated by the ligation process which as reported previously does not alter the activity of PTEN.(*19*) These semisynthetic PTEN proteins were shown to be >90% pure (see Figure 14). As shown previously,(*19*) the unligated PTEN forms run just below the ligated forms on SDSPAGE and so the high purity of the semisynthetic PTENs, is achieved after anion exchange chromatography. NEDD4-1 protein was also prepared in a baculovirus expression system and contains an N-terminal His6 tag that was used in Ni resin affinity chromatography for purification (see Figure 14). WWP2 was prepared as a GST-fusion protein using an *E. coli* expression system and purified by glutathione affinity chromatography (see Figure 14). XIAP was obtained from commercial sources as a purified recombinant protein.

Ubiquitination experiments with WWP2 were performed with 50 nM E1 ubiquitin activating enzyme, 1 μM UbcH5c (E2 ligase), 1 μM WWP2 (E3 ligase), 1 μM n-PTEN, 100 μM ubiquitin, and 5 mM MgATP. We monitored the ubiquitination using a

combination of both coomassie stained SDS-PAGE as well as western blots with anti-PTEN Ab. (Figure 15) The reaction mixture's multi-band/streaking pattern readily visualized by both methods was attributed to various levels of ubiquitin and polyubiquitin chain attachment catalyzed by WWP2. There was a clear increase of ubiquitination with time over the course of the reaction and the non-ubiquitylated n-PTEN was largely depleted after 60 min under these conditions (see Figure 15). WWP2, E2, E1, and ATP were each necessary for the reaction to occur as their omission prevented detectable ubiquitination. In the higher molecular weight region of the coomassie stained SDS-PAGE, auto-ubiquitination of WWP2 was also readily detected. (Figure 15A,B). Using a higher concentration of n-PTEN (10 μM) relative to WWP2 (1 μM), perhaps better approximating steady-state conditions, the rate of depletion of n-PTEN was reduced and had a half-life of about 1 h (Figure 15D).

NEDD4-1 (1 μM) was also tested as an E3 ligase with n-PTEN and showed an ability to ubiquitylate PTEN, although at a slower rate relative to that of WWP2 (Figure 16A,B). Given the complexity of the reactions and the wide range of product distributions, it is difficult to precisely quantify the relative rates but monitoring depletion of the unmodified PTEN suggests a ~4-fold difference. In contrast to NEDD4-1 and WWP2, we were unable to detect n-PTEN ubiquitination with XIAP (Figure 16). We are uncertain why XIAP, though undergoing autoubiquitination in our hands, was inactive with PTEN in this assay. However, given the measurable rates with NEDD4-1 and WWP2, we elected not to pursue further experiments with XIAP.

3.3.2 PTEN phosphorylation inhibits WWP2-mediated ubiquitination

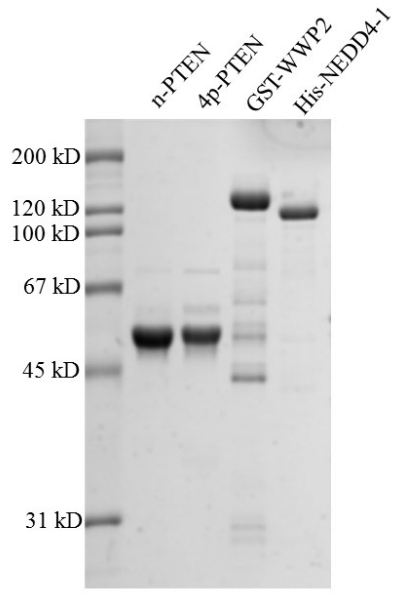

Figure 14: Purified proteins (n-PTEN, 4p-PTEN, WWP2, NEDD4-1) prepared in this study (SDS-PAGE stained with coomassie).

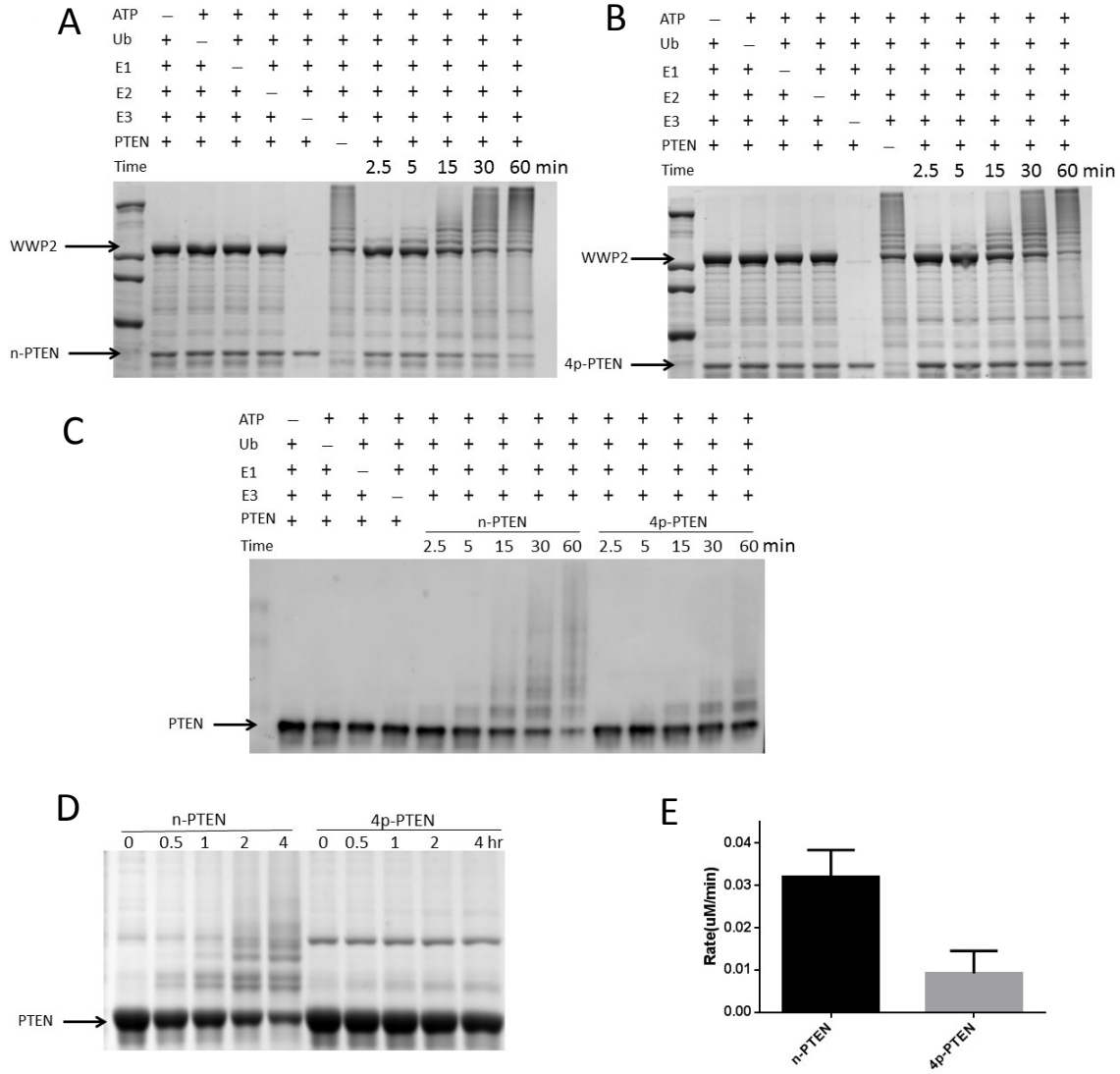

Figure 15: In vitro ubiquitination assay of n-PTEN and 4p-PTEN by WWP2. (A) In vitro ubiquitination assay for n-PTEN. The reaction was carried out in the presence of 5 mM ATP, 100 μM wild-type ubiquitin, 50 nM E1, 1 μM E2 (UbcH5c), 1 μM WWP2, and 1 μM n-PTEN in assay buffer with 40 mM HEPES pH 7.5, 5 mM $MgCl_2$. The reaction was quenched at 2.5, 5, 15, 30, 60 minutes. Negative controls lacking in ATP, ubiquitin, E1, E2, E3 or PTEN were assayed respectively. The samples were resolved by SDS-PAGE, and the gel was stained with colloidal blue. (B) In vitro ubiquitination assay for 4p-PTEN. The reaction was carried out for 4p-PTEN using the same conditions as in Fig. 14A. (C) n-PTEN and 4p-PTEN ubiquitination analyzed by western blotting using anti-PTEN antibody. E2 was added to these experiments but the minus E2 conditions were not shown in this blot. (D) In vitro ubiquitination assay for n-PTEN and 4p-PTEN. The reaction conditions were the same as in Fig. 14A except that 10 μM PTEN was used instead of 1 μM. Ubiquitination of PTEN at time points 0, 0.5, 1, and 2 hours was analyzed by colloidal blue staining. (E) Quantification of the rate of PTEN ubiquitination. The ubiquitination assay carried out in Fig. 14D was quantified by measuring the decrease of non-ubiquitylated PTEN band intensities and calculating the decrease in non-ubiquitylated PTEN protein levels as a function of time over replicates (n=3) with standard error shown.

We then investigated the ubiquitination of 4p-PTEN by WWP2 and NEDD4-1. Whereas, the rate of ubiquitination of 4p-PTEN by NEDD4-1 was similar to that of its reaction with n-PTEN substrate (Figure 16), WWP2 showed a marked reduction in its ubiquitination of 4p-PTEN (Figure 15). In principle, this rate reduction of WWP2 ubiquitination of 4p-PTEN could be caused by an interference with steps up to and including E2's ubiqutyl-transthioesterification loading of E3. This was explored in two ways. First, we examined the WWP2/4p-PTEN reaction in the presence of an alternative E2 enzyme, UbCH7, in place of UbCH5c. We observed that UbCH7 could work in concert with WWP2 to ubiquitylate n-PTEN and 4p-PTEN, but this system showed a similar drop in efficiency with 4p-PTEN substrate relative to that involving UbCH5c (Figure 17A). These results suggest that the differences in WWP2 ubiquitination between 4p-PTEN and n-PTEN are not related to specific interactions between the E2 UbCH5c and E3 WWP2. To examine this further, we performed a single turnover experiment in which WWP2 was charged by the E1 and E2 and then ATP is cleared from the reaction by apyrase-mediated degradation.(*189*) The removal of ATP at this stage prevents recharging of the E3-ubiquityl thioester after it transfers its ubiquitin to PTEN. In this way, one can more specifically monitor the kinetics of the specific step involving the transfer of ubiquitin from WWP2 to PTEN. In this experiment, we showed that n-PTEN is still preferentially ubiquitylated over 4p-PTEN by WWP2 (Figure 17B). These results suggest that the specific enzymatic step that involves transfer of ubiquitin from WWP2 to PTEN is affected by PTEN phosphorylation.

The above observations suggest that the tetraphosphorylation of PTEN may directly disrupt WWP2-mediated ubiquitination of the PTEN protein by weakening the interaction between the WWP2 and PTEN proteins. To assess this possibility, we performed a pull-down experiment in which GST-WWP2 was immobilized on glutathione

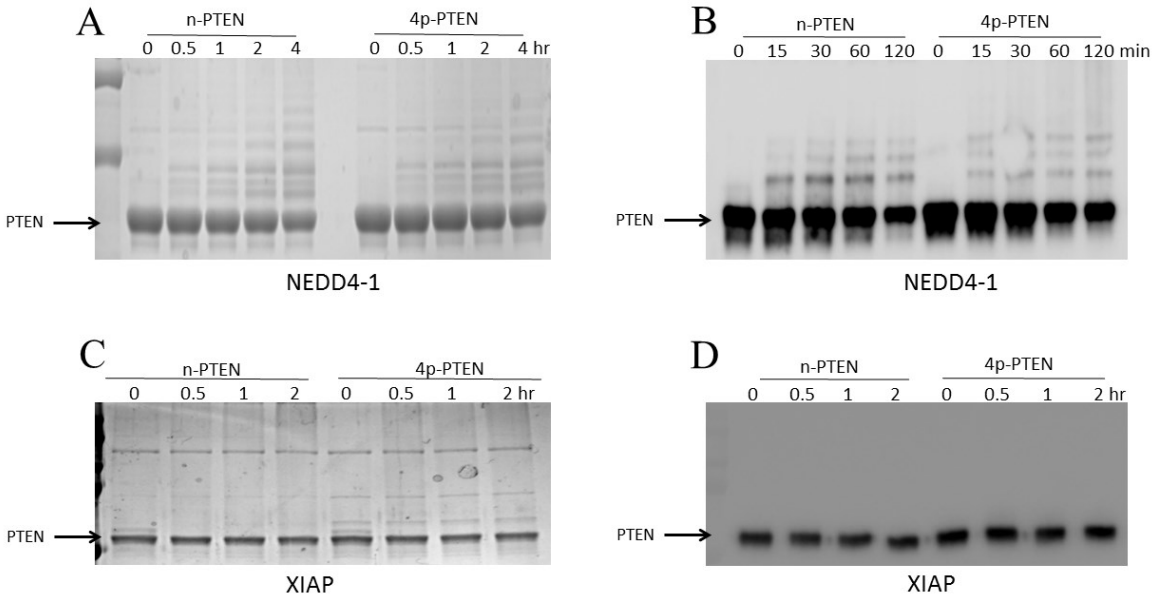

Figure 16: In vitro ubiquitination assay of n-PTEN and 4p-PTEN by NEDD4-1 and XIAP. (A) The reaction for n-PTEN and 4p-PTEN ubiquitination by NEDD4-1 was carried out with 5 mM ATP, 100 μM wild-type ubiquitin, 50 nM E1, 1 μM E2 (UbcH5c), 1 μM NEDD4-1 and 10 μM PTEN, for 0, 0.5, 1, 2, and 4 hours. The samples were analyzed by colloidal blue staining. (B) 1 μM n-PTEN and 4p-PTEN ubiquitination by NEDD4-1 under the same reaction conditions was analyzed by western blotting using anti-PTEN antibody. (C) The ubiquitination of n-PTEN and 4p-PTEN by XIAP was analyzed by colloidal blue staining. The reaction mixture containing 100 μM wild-type ubiquitin, 50 nM E1, 1 μM E2 (UbcH5c), 1 μM XIAP and 1 μM PTEN was quenched at 0, 1, 2, and 4 hours and analyzed by colloidal blue staining. (D) Ubiquitination of n-PTEN and 4p-PTEN under the same condition as in Figure 15C was analyzed by western blotting using anti-PTEN antibody.

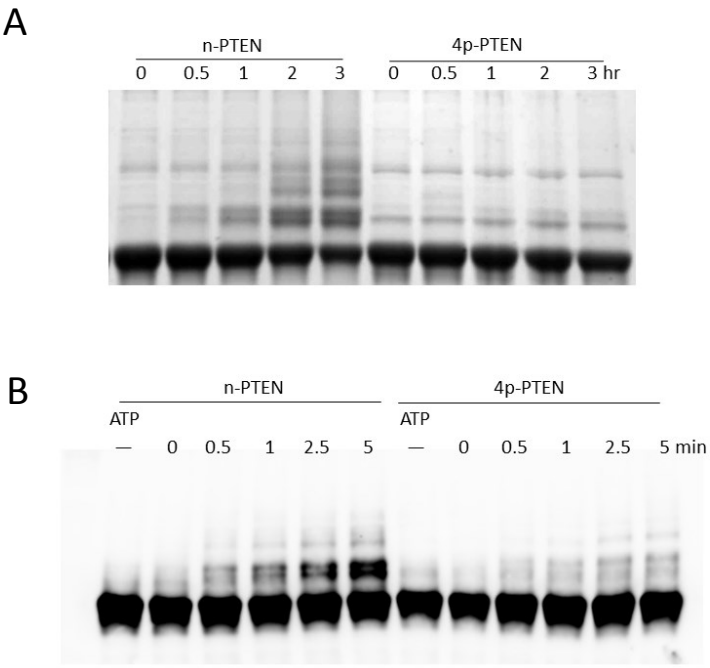

Figure 17: (A) In vitro ubiquitination assay of PTEN by WWP2 using a different E2. The reaction conditions were the same as in Figure 2D except that the E2 was UbcH7 instead of UbcH5c. The samples were analyzed by colloidal blue staining. (B) Single turnover assay to measure ubiquitin transfer from WWP2 to n-PTEN and 4p-PTEN was carried out by charging WWP2 with ubiquitin and then adding PTEN after depletion of ATP using apyrase. The ubiquitination of PTEN was analyzed by western blotting with anti-PTEN antibody.

resin, and these were incubated with either n-PTEN or 4p-PTEN proteins. After washing, the glutathione resin was denatured with SDS and the PTEN was analyzed by western blot using anti-PTEN Ab, revealing that n-PTEN was more efficiently pulled down by WWP2 compared with 4p-PTEN (Figure 18). These findings suggest that tetraphosphorylation of PTEN does indeed reduce its affinity for WWP2 and this likely contributes to 4p-PTEN's diminished ubiquitination by WWP2 compared with n-PTEN.

3.3.3 Site-specificity of WWP2 and NEDD4-1 mediated PTEN ubiquitination

We next analyzed the Lys sites of ubiquitination by WWP2 and NEDD4-1 using mass spectrometry. In these experiments, n-PTEN was exposed to the E3 ligases for 6 h using Lys-free ubiquitin. Although Lys-free ubiquitin compared with natural ubiquitin is less efficiently processed by WWP2 with a rate now similar to NEDD4-1 (Figure 19), its use significantly simplified the analysis since it prevented polyubiquitin chain formation. The reaction mixtures were run out on SDS-PAGE, subjected to in-gel enzymatic digestion and analyzed using liquid chromatography-tandem mass spectrometry (LC-MS/MS). To ensure the maximum sequence coverage of PTEN for these experiments, thereby optimizing the mass spectrometric detection of all the potential PTEN Lys ubiquitination sites, sequential enzymatic digestion was conducted with trypsin followed by AspN. Of the 34 PTEN Lys residues, 29 were covered among the identified peptides from the NEDD4-1 ubiquitination experiment, and 25 were covered among the identified peptides from the WWP2 ubiquitination experiment. The total PTEN sequence coverage was 91.3% and 79.2% for the NEDD4-1 and WWP2 experiments, respectively (Figure 20A). As an indication of the comprehensive PTEN sequence coverage for the NEDD4-1 experiment, all the peptides that were not identified had an average length of four amino

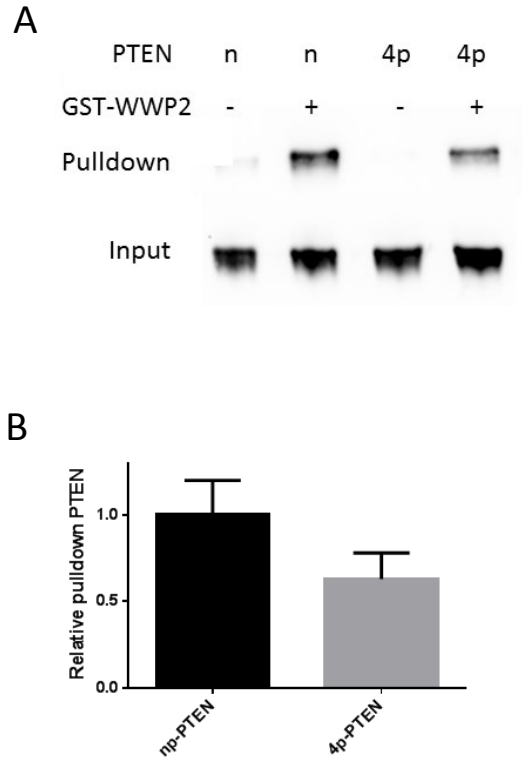

Figure 18: GST pull-down assay of WWP2 and PTEN. (A) 1 μM GST-WWP2 or GST and 1 μM n-PTEN or 4p-PTEN were incubated with glutathione agarose resin overnight. The pull-down of PTEN by WWP2 was analyzed by western blotting using anti-PTEN antibody. (B) Quantification of 4p-PTEN relative to n-PTEN pull-down by WWP2, average over replicates (n=3) with standard error shown.

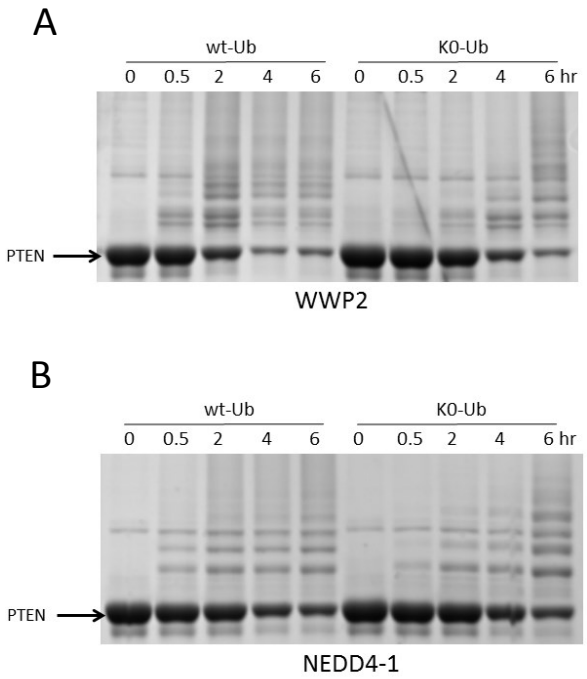

Figure 19: In vitro ubiquitination assay of n-PTEN with wild-type (wt-Ub) or lysine free ubiquitin (K0-Ub). (A) The ubiquitination reaction was carried out in 40 mM Tris-HCl pH 7.5, 5 mM $MgCl_2$, 5 mM ATP, 50 nM E1, 1 μM E2, 1 μM WWP2, 10 μM n-PTEN, with 100 μM wt-Ub or K0-Ub. The reactions were quenched at 0, 0.5, 2, 4, and 6 hours and analyzed by colloidal blue staining, and the reaction with K0-Ub at 6 hours was subject to mass spectrometry analysis. (B) Same in vitro ubiquitination conditions as in Fig. 6A assay using wt-Ub or K0-Ub with NEDD4-1.

acids, which rendered them below the m/z detection range of the mass spectrometer used for this study.

A representative MS/MS spectrum of an ubiquitylated peptide (Ub-Lys322) is shown in Figure 20B. A total of 11 ubiquitination sites were identified in the NEDD4-1 experiment compared to 6 in the WWP2 experiment (Fig. 20A). The PTEN ubiquitination sites that were shared by the two E3 ligases include: Lys6, Lys80, Lys164, Lys237, Lys330, and Lys402. These Lys sites are relatively broadly distributed throughout the PTEN proteins and its major domains, PTPase, C2, and C-terminal regulatory domain (see Figure 6A). It should be noted that of the 5 ubiquitination sites that were identified exclusively in the NEDD4-1 experiment, only 1 of these Lys residues (Lys349) was in a region of PTEN that was not identified in the WWP2 experiment. With the exception of Lys349, each of the peptides containing the putative Lys ubiquitination sites were also identified in their unmodified forms. Of the 6 ubiquitination sites that were identified in common between the NEDD4-1 and WWP2 experiments, only Lys402 appears to be preferentially ubiquitylated by NEDD4-1 as indicated by the greater spectral counts of the peptides containing this ubiquitylated residue (Fig. 20C). The 5 ubiquitin sites only observed with NEDD4-1 included Lys289, Lys322, Lys332, Lys342, and Lys349. Each of these sites occur in the C2 domain. Interestingly, of the 4 known PTEN ubiquitin sites (Lys13, Lys66, Lys80, Lys289) listed in Phosphosite plus (http://www.phosphosite.org/homeAction.action), only Lys289 overlaps with the 11 sites mapped here.

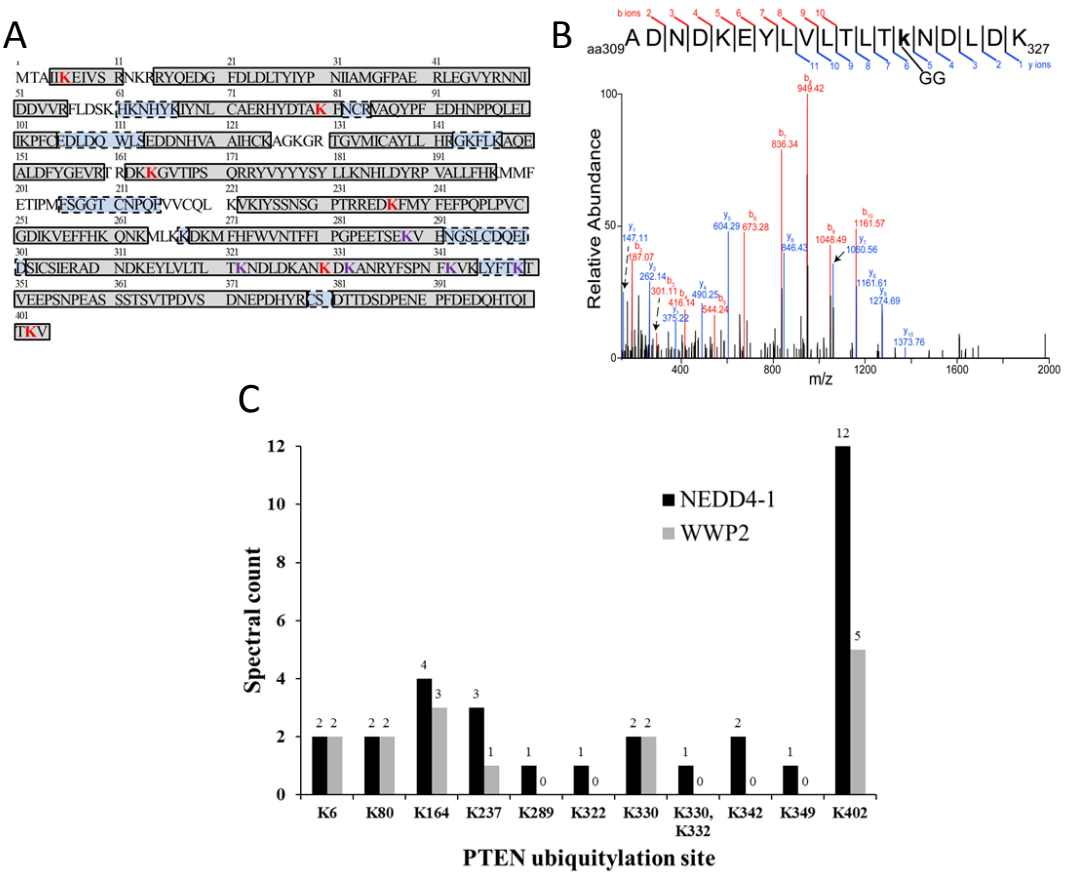

Figure 20: Mass spectrometric identification of n-PTEN. (A) PTEN sequence coverage. Boxed, shaded regions indicate identified peptides. Boxes shaded in gray with solid outlines indicate regions identified in common between the NEDD4-1 and WWP2 experiments. Boxes shaded in blue with dashed outlines indicate regions that were only identified in the NEDD4-1 experiment. Bold, red - identified sites of Lys ubiquitination. Bold, purple – sites of Lys ubiquitination identified only in the NEDD4-1 experiment. (B) Representative MS/MS spectrum of the peptide containing Ub-Lys 322. (C) Relative abundance of PTEN Lys ubiquitination sites based on spectral counts.

3.4 Discussion

Because of PTEN's major role as a tumor suppressor PIP3 phosphatase, understanding how PTEN's cellular stability is controlled may offer new directions for therapeutic intervention. These studies have confirmed the ability of both WWP2 and NEDD4-1 to ubiquitylate PTEN using enzymatic assays with purified proteins, although WWP2 appeared more robust as a PTEN E3 ligase in our hands. We were unable to demonstrate that XIAP serves as a PTEN E3 ligase, but we cannot rule out that other factors in the cell may facilitate it's potential to ubiquitylate PTEN.

We were especially interested in how phosphorylation of PTEN on a cluster of C-terminal Ser/Thr residues 380,383,383, and 385 might influence its potential for ubiquitination, as it had been proposed that this phosphate cluster can increase PTEN's cellular half-life.(*20*) Using tetraphosphorylated PTEN we found that such phosphorylation antagonizes ubiquitination by WWP2 but not NEDD4-1. Coupled with WWP2's greater enzymatic efficiency than NEDD4-1 as a PTEN E3 ligase, these results suggest that WWP2 may be dominant in governing PTEN's cellular degradation when PTEN is non-phosphorylated (Figure 21). Perhaps NEDD4-1's more significant control of PTEN's stability occurs when PTEN exists in its phosphorylated state, although more in vivo experiments will be needed to probe this possibility.

The precise mechanism of how phosphorylation of PTEN inhibits its ubiquitination by WWP2 is uncertain, however, it is improbable that the Ser/Thr phosphates are impeding Lys targeting through proximity-induced obstruction as most of the ubiquitination sites are remote from the C-terminal tail and are spread throughout PTEN. The weakening of the WWP2-PTEN interaction observed by pull-down assays likely contributes to the reduced ubiquitination efficiency. Such weakened interaction could plausibly result from the closed conformation of 4p-PTEN where surfaces of PTEN

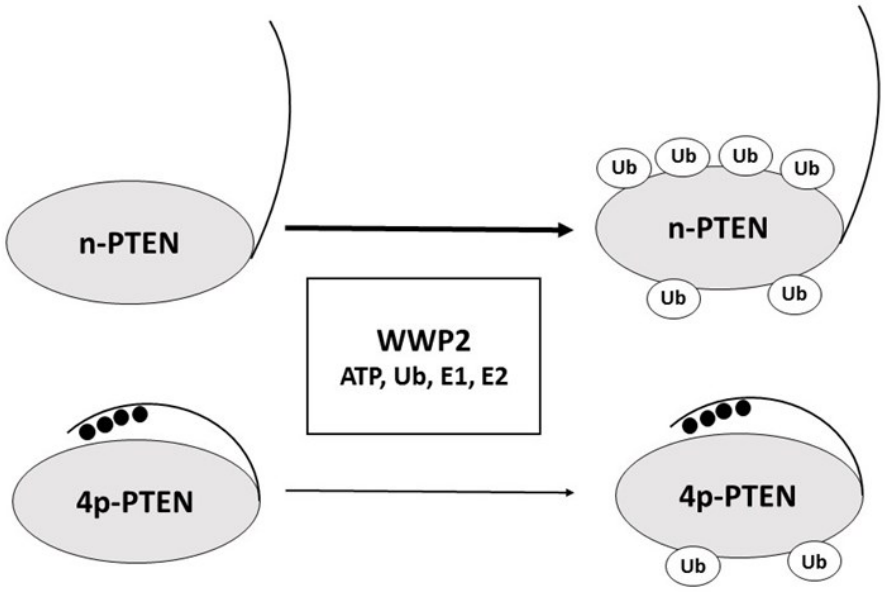

Figure 21: Schematic showing the model how C-tail phosphorylation of PTEN regulates its ubiquitination by WWP2.

interaction would be less available to WWP2 binding.(*19*) Perhaps NEDD4-1 binds to PTEN in a different fashion than WWP2 interacts with PTEN, and is thus less affected by PTEN phosphorylation. Indeed, it has been reported that NEDD4-1 interacts with PTEN in a WW2 motif-independent manner.(*17*) Further evidence for this appears to come from the enhanced targeting of the PTEN C2 domain Lys sites for ubiquitination by NEDD4-1 vs. WWP2.

It is also possible that phosphorylation of PTEN, by virtue of its effects to diminish PTEN membrane binding, may also protect PTEN from membrane associated E3 ligases.(*191*) The combination of cytosolic-nuclear localization of 4p-PTEN and 4p-PTEN's intrinsic resistance to WWP2-catalyzed ubiquitination could synergize to stabilize PTEN in cells. It is not yet clear which of the large number of ubiquitination sites identified here may be most physiologically relevant. It seems likely that the majority of them, if they occur in the cell would help target PTEN toward the proteasome, but if not, they would likely interfere with PTEN's normal enzymatic function.

Prior studies have validated 4p-PTEN's reduced PIP3 phosphatase activity relative to n-PTEN.(*19*) It is therefore somewhat paradoxical that tetraphosphorylation of PTEN, which inhibits its PIP3 phosphatase activity, also promotes a longer cellular half-life for the protein. We speculate that these apparently conflicting properties associated with phosphorylation of PTEN allow for a fine-tuning of signaling that maintain PIP3 levels in a precise range. This regulatory mechanism also can allow for strict kinetic control so that after PTEN is turned on by dephosphorylation and PIP3 levels drop, PTEN can be quickly eliminated by a proteasomal mediated pathway.

Chapter 4: Autoinhibitory Mechanisms for the HECT E3 Ligases

4.1 Introduction

HECT domain ubiquitin transferases (E3 ligases) catalyze the Lys ubiquitination of numerous cellular proteins and are critical for protein homeostasis and cell signaling (*50, 82*). Like all E3 ligases, HECT enzymes are activated by the participation of upstream E1 and E2 enzymes. In contrast to the RING family of E3 ligases which have an indirect role in ubiquitin bond formation, HECT domains have an active site Cys that is charged with ubiquitin by the E2. The HECT thioester intermediate directly ubiquitinates target proteins and itself on Lys residues. Because of their direct role in catalysis, it is presumed that HECT E3 ligases must be held in check to prevent both excessive target ubiquitination as well as self-destruction by autoubiquitination (*50, 192*).

Of the 28 human HECT domain E3 ligases, the most intensively studied comprise the 9 members of the NEDD4 family (Figure 22) (*50, 60, 82*). Members of the NEDD4 family include WWP2, WWP1, ITCH, and NEDD4-1 and these E3 ligases target for destruction key signaling molecules and transcription factors (*50, 79, 81-83*). Abnormal activities of NEDD4 E3 ligases are connected to cancer, immune disorders, and other diseases (*50, 79, 81-83, 192*). The NEDD4 family proteins each contain an N-terminal C2 domain followed by two to four WW domains and culminate in a C-terminal catalytic HECT domain (Figure 22 and Figure 24A) (*50*). The C2 and WW domains have been implicated in substrate selectivity and catalytic regulation of NEDD4 E3 ligases (*100, 137-139, 193*).

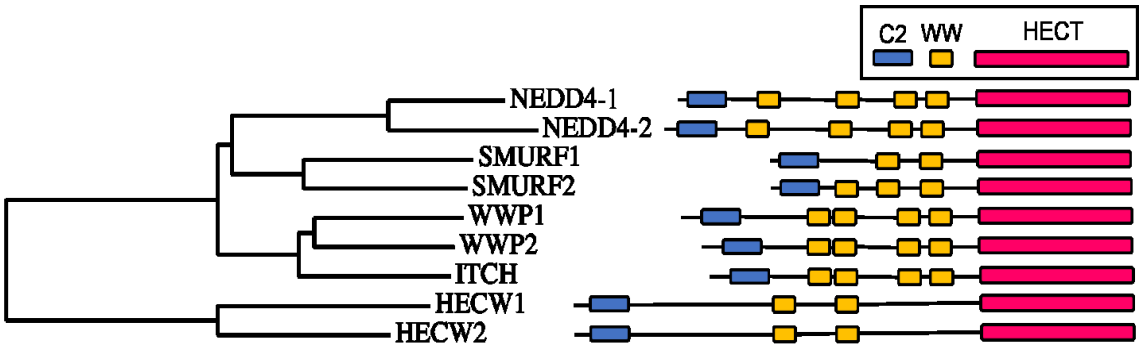

Figure 22: Phylogenetic tree of the NEDD4 HECT E3 ligase family generated using PAM250. These enzymes consist of an N-terminal C2 domain, two to four tandem WW domains, followed by a catalytic HECT domain.

Prior structural studies have revealed that HECT domains contain a larger N-lobe which can interact with E2 proteins and a smaller C-lobe that contains a catalytic Cys residue involved in ubiquitin transfer (*50*). In addition, several HECT family members have been shown to possess an N-lobe ubiquitin binding exosite (*68, 69, 73*). Remote from the ubiquitin substrate binding site in the HECT C-lobe, this exosite has been characterized structurally and shown to engage a distinct ubiquitin molecule in HECTs and this can catalytically activate these E3 ligases (*68, 69, 71-73*). The N- and C-lobes are connected by a hinge loop and the HECT domains have been captured in two conformational states, a ground state T-shape (*65, 73*) and a catalytically proficient L-shape (*67, 73*). The dynamic inter-conversion of the T-shape and L-shape HECT conformations is necessary for turnover, but what governs this transition is uncertain. Interactions with C2 domain, WW domains, and various post-translational modifications have each been proposed to influence HECT domain catalytic activity but biochemical details for this have generally been lacking (*77, 82, 100, 137, 139-142*).

Here we investigate the regulation of WWP2, a NEDD4 family member that has been shown to ubiquitinate and target for removal the key tumor suppressor PTEN and the important stem cell-related transcription factor OCT4 (*27, 78*). WWP2 contains four WW domains (WW1-WW4) and is most closely related to the NEDD4 family members WWP1 and ITCH which have been linked to cancer and immunologic control (*60, 79, 194*). Our studies have revealed an unanticipated autoinhibitory module centrally located in WWP2, WWP1, and ITCH between the WW2 and WW3 domains, and below we describe the mechanism of this regulation and its general significance in the NEDD4 family.

4.2 Methods

4.2.1 Plasmids and reagents

The pGEX6p-2 human WWP2 plasmid was provided by Dr. Wenyi Wei at Beth-Israel Deaconess Medical Center. Human WWP1 cDNA was purchased from Genscript, and subcloned into pGEX6p-2. pGEX-KG containing human ITCH was obtained from Dr. Allan M. Weissman at National Cancer Institute(*195*). Human NEDD4-1 cDNA was provided by Dr. Xuejun Jiang at Sloan-Kattering Mommerial Cancer Center. Mutations and truncations in WWP2, WWP1, and ITCH were introduced by Quik-Change (Agilent) or restriction enzyme based cloning. Purified wild-type ubiquitin, human ubiquitin-activating enzyme UBE1, and human ubiquitin-conjugating enzyme UbcH5c were prepared as described previously (*188*). The Colloidal Blue Staining Kit was purchased from Invitrogen. All other reagents were commercially purchased with the highest quality from either Sigma or Fisher.

4.2.2 Protein expression and purification

BL-21 Codon Plus cells were transformed with the pGEX6p-2 plasmid expressing full-length WWP2, WWP1, ITCH, or the different mutations or truncations, initially as N-terminally modified GST-fusion proteins. The transformed cells were cultured in LB medium at 37 °C to reach the optimal density (OD_{600}=0.6) in a shaker incubator grown on a 1 L scale. Protein expression was induced by 0.25 to 0.5 mM IPTG at 16 °C for 20 hours. The cells were resuspended in 25 mL lysis buffer (25 mM Tris-HCl pH 8.0, 250 mM NaCl, 1 mM phenylmethylsulfonyl fluoride (PMSF) and 1x Roche cocktail protease inhibitors) and were lysed by french press. The cell lysate was loaded on glutathione agarose followed by washing with 25 mM Tris-HCl pH 8.0, 250 mM NaCl, and 0.1%

Triton X-100. The desired GST-tagged protein was eluted using 10 mL 25 mM Tris-HCl pH 8.0, 250 mM NaCl containing 50 mM reduced glutathione at pH 8.0. The eluted fractions were combined and dialyzed against a buffer consisting of 25 mM Tris-HCl pH 8.0, 250 mM NaCl, 10 mM BME, and the protein was treated with PreScission protease at 4 °C overnight to cleave the GST tag. Afterwards, the mixture of GST and cleaved protein was loaded to glutathione agarose again to remove the GST. The protein was concentrated and then loaded on a size exclusion column Superdex 200 (GE Healthcare) with a buffer containing 25 mM Tris-HCl pH 7.5, 150 mM NaCl, 5 mM DTT (dithiothreitol). The corresponding purified fractions assessed by Coomassie stained SDSPAGE were combined and glycerol was added to a final concentration of 10% v/v. The purified protein was concentrated to 1 to 10 mg/mL, flash frozen, and stored at -80ºC.

4.2.3 Peptide synthesis

The 2,3-linker peptides (+/-369-phospho) of sequence (n-TAEYVRNYEQWQSQRNQLQGAMQHFSQRFLYQSS-c) were prepared using the Fmoc solid phase synthesis straetgies with a PS3 peptide synthesizer from Protein Technologies (Tuscon, AZ). The peptides were purified by reversed phase HPLC on a C-18 column using a water:acetonitrile gradient (containing 0.05% trifluoroacetic acid) to >90% and the correct structures confirmed by MALDI mass spectrometry (Figure 23) and amino acid analysis (AAA Service Laboratory Inc.).

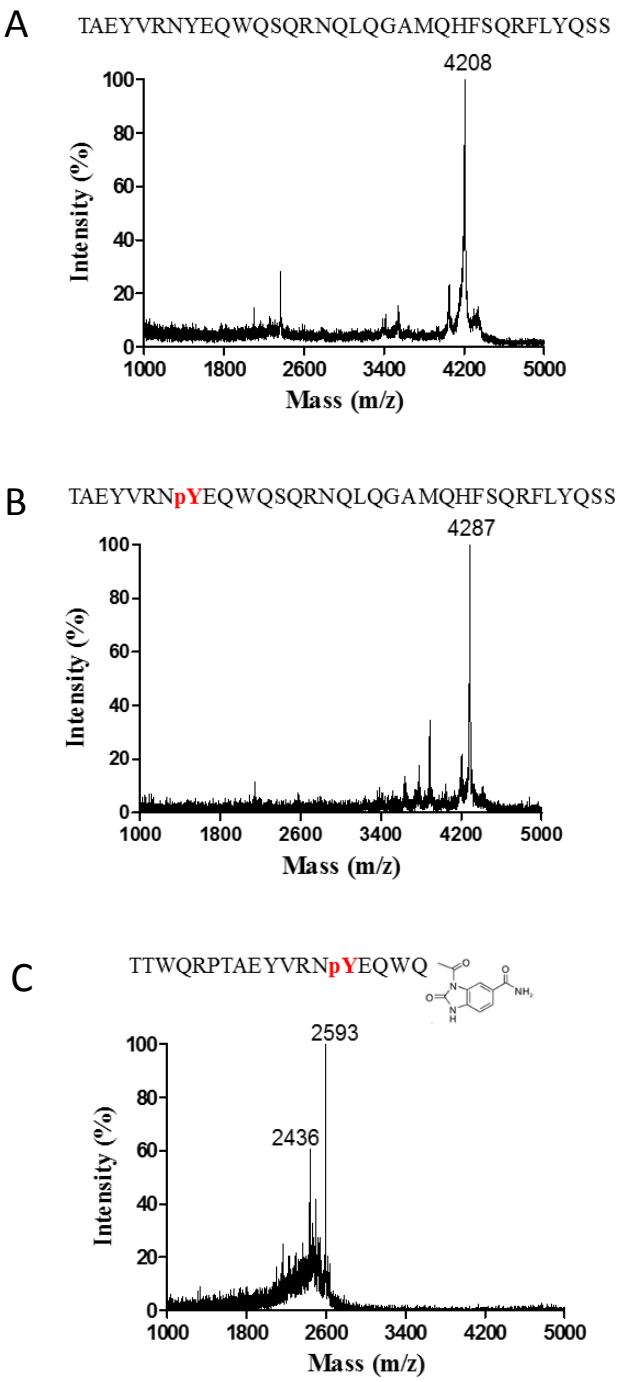

Figure 23: Mass spectrum of peptides used in this study. (A) Mass spectrum of nonphosphorylated 2,3-linker peptide with a C-terminal amide. The calculated mass: m/z 4209. (B) Mass spectrum of Tyr369 phosphorylated 2,3-linker peptide with a C-terminal amide. The calculated mass: m/z 4289. (C) Mass spectrum of Tyr369 phosphorylated 2,3-linker peptide with a C-terminal N-acyl-benzimidazolinone (Dbz) used for protein semisynthesis. The calculated mass: m/z 2594. Note that the m/z 2436 is believed to be mass spec induced fragmentation leading to loss of the Dbz group. However, even this mass is related to Dbz hydrolysis after purification, it will be inert in ligation and not affect protein semisynthesis.

4.2.4 *In vitro* ubiquitination assays

The *in vitro* ubiquitination reactions were carried out in microcentrifuge tubes in final volumes of 20 µL containing 40 mM Tris-HCl pH 7.5, 50 mM NaCl, 0.5 mM TCEP, 5 mM $MgCl_2$, with 5 mM ATP, 100 µM ubiquitin, 50 nM E1 protein, 1 µM E2 protein, 1 µM E3 protein. The reactions were initiated by adding the E1 and carried out at 30 °C. At different time points, the reactions were quenched by mixing 4 µL aliquots of the reaction mixture with SDS loading dye and boiled for 5 minutes. The samples were then run out on SDSPAGE, and stained using a Colloidal Blue Staining Kit following the manufacturer's protocol. The unmodified E3 protein bands at the time points shown in the figures were quantified using ImageJ densitometry and normalized to the zero time points. Note that this quantification method monitors the disappearance of the 'starting material' but does not distinguish among the range of ubiquitinated products formed, and this product distribution pattern varies among different mutants. All assays were performed on at least two independent occasions with replicates showing similar results.

4.2.5 Generation of fluorescein labeled ubiquitin variants (UbF1 and UbF2)

Wild-type human ubiquitin DNA was sub-cloned into pGEX6p-2 and mutated to UbV P2.3 and UbV NL1 (*69*) using Quik-Change. In addition, Ser57 was replaced with Cys by Quik-Change mutagenesis. GST-UbV S57C was expressed by BL21 Codon Plus cells as described for WWP2. The GST-fusion mutant ubiquitin proteins were purified using glutathione agarose and eluted with 50 mM reduced L-glutathione. After cleavage of GST tag by PreScission protease, the proteins were further purified by size exclusion chromatography using Superdex 75 column (GE Healthcare) with PBS buffer. Purified UbV S57C proteins (2 mg) were mixed with 10-fold molar excess of 5-

iodoacetamidofluorescein (Thermo) in PBS buffer containing 5 mM EDTA in 2 mL at room temperature for 4 hours in the dark. The labeled proteins UbF1 and UbF2 were separated from the unreacted reagent by dialysis and size exclusion chromatography using the buffer containing 25 mM HEPES pH 7.3, 150 mM NaCl, 1 mM EDTA, 2 mM DTT, 5% glycerol.

4.2.6 Fluorescence anisotropy

UbF1 and UbF2 protein (100 nM) was mixed with the indicated concentrations of E3 ligase forms in the buffer (25 mM Tris-HCl pH 7.5, 150 mM NaCl, 5 mM DTT, 10% glycerol) and incubated at room temperature for 20 minutes. Steady-state fluorescence anisotropy data were acquired using a FluoroMax-3 spectrofluorimeter (Jobin Yvon Horiba) at 23 °C. The excitation wavelength was set to 495 nm and emission was measured at 520 nm. Each fluorescence anisotropy data point was measured to high accuracy at least three times. The binding curves and K_d values were generated using the quadratic-binding fit with the equation Y= Y0 - [(Y0 - Ymax)/(2*Fixed)] * [b - sqrt(b^2 - 4*X*Fixed)] (b=K_d + X + Fixed, Fixed=0.1). At least two independent replicates were carried out for each data set on independent occasions with K_d values in good agreement (within 30%).

4.2.7 Crystallization

The construct, 2,3-linker-HECT865, used for crystallization, contains residues 369 to 865 whereas aa 399-484, containing the tandem WW3-WW4 domains, has been deleted. Purified 2,3-linker-HECT865 was concentrated to 3 mg/mL in a buffer

containing 25 mM Tris-HCl pH 7.5, 150 mM NaCl, 5 mM DTT. Note that WWP2 residues 866-870 were deleted to facilitate crystallization (*65*). Crystals were grown at 20 °C by vapor diffusion in hanging drops of 1 µL of protein with 2 µL of reservoir solution containing 0.1 M Bis-Tris pH 5.8 to 7.5, 0.2 M $MgCl_2$, 12 to 18% (m/v) PEG3350. Clusters of needle crystals were obtained, and crystal morphology and size were optimized by microseeding.

The WW2-2,3-linker-HECT865 construct contains aa334-865 with the deletion of aa399-484. Freshly-purified WW2-2,3-linker-HECT865 was concentrated to 10 mg/mL in buffer containing 25 mM Tris-HCl pH 7.5, 150 mM NaCl, 5 mM DTT, 5% glycerol. Crystallization trays were set up using the LCP Mosquito robot (TTP Labtech, Inc) with a drop size of 0.3 µL protein with 0.3 µL reservoir solution in 96-well plates in hanging drops. Crystals grew at 20 °C and were monitored automatically using a Rock Imager and Rock maker system (Formulatrix, Inc., USA). Two conditions resulted in single crystals: one condition had 0.1 M potassium thiocyanate, 30% PEG monomethyl ether 2000 as reservoir solution, and the other condition had 0.1 M MMT (DL-malic acid, MES, Tris-base in molar ratio of 1:2:2) pH 6.0, 25% PEG1500 as reservoir. All crystals were cryoprotected in the same solution that they were grown and stored in liquid nitrogen for data collection.

4.2.8 Data Collection and Structural determination

Diffraction data of 2,3-linker-HECT and WW2-2,3-linker-HECT (PEG 1500 precipitant) were collected at ALS beam line 502 on a DECTRIS Pilatus 6M detector (wavelength 1.0 Å and temperature 100 K, Table 2). Diffraction data of WW2-2,3-linker-HECT using PEG MME 2000 as a precipitant were collected using a Rigaku FR-E

SuperBright X-ray generator at a wavelength of 1.5418 Å and recorded on a PILATUS 2M. All diffraction data were processed, integrated and scaled with HKL-2000 (*196*).

The 2,3-linker-HECT structure was determined by molecular replacement using the program AMoRe and the HECT domain of WWP2 (PDB ID 4Y07)(*177*) as the initial search model. The model was re-built manually with iterative rounds of Coot and refined using Refmac5 from the CCP4 suite (*197*). The final structure, PDB ID 5TJQ, was refined to 2.75 Å. Ramachandran plot analysis indicates 4.5 % of outliers, 3.3 % allowed and 92.1 % favored residues. The 2 WW2-2,3-linker-HECT structures were determined by molecular replacement using PDB ID 5TJQ as a template. The initial models were rebuilt and refined as described previously for PDB 5TJQ. The refined structure with disorder the WW2 domain, 5TJ8, has excellent geometry as display by 91.2 % residues in preferred and 4.5 % allowed regions. The refined structure with WW2 domain, PDB ID 5TJ7, has 93.1 % and 3.3 % residues in the preferred and allowed regions respectively. All figures were rendered with PyMOL (*198*).

R.M.S.D. comparison of the new and prior WWP2 and WWP1 HECT domain structures (units in angstroms)

	1ND7	4Y07	5TJQ	5TJ7
5TJQ	1.29	0.73	-	-
5TJ7	1.95	1.06	1.44	-
5TJ8	1.27	0.66	0.95	1.33

4.3 Results

4.3.1 WWP2 E3 ligase activity is autoinhibited

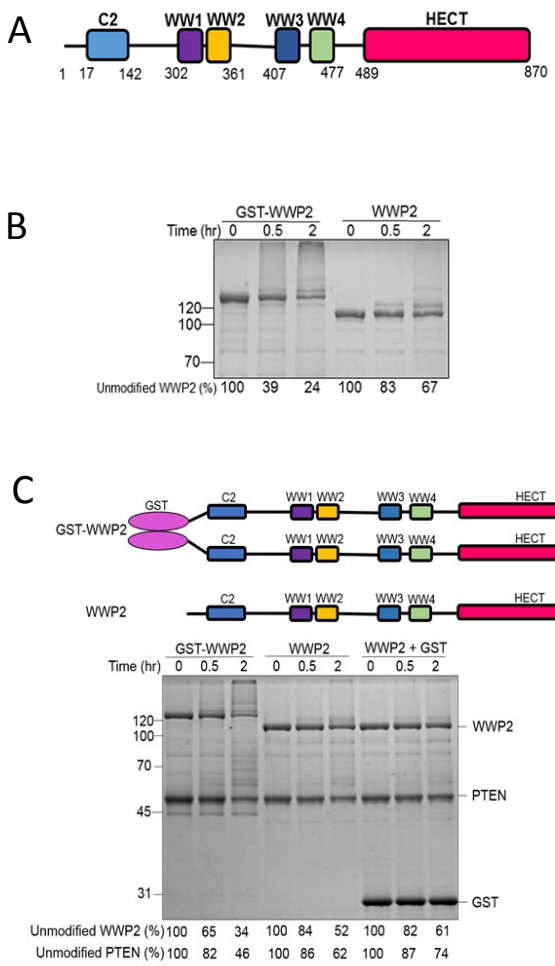

Figure 24: Full-length GST-free WWP2 is autoinhibited. (A) Schematic of WWP2 domains with amino acid residue numbers. (B) Ubiquitination assay of GST tagged WWP2 and GST-free WWP2. The reaction was conducted at 30 °C in the presence of 5 mM $MgCl_2$, 5 mM ATP, 100 μM wild-type ubiquitin, 50 nM E1, 1 μM E2 (UbcH5c), 1 μM E3. The reaction was quenched at 0, 0.5 and 2 hours and samples analyzed by SDSPAGE followed by colloidal blue staining. The activity of WWP2 was determined by the time-dependent depletion of the unmodified E3 ligase band and the appearance of higher MW bands presumed to represent poly-ubiquitination. (C) Ubiquitination assay of full-length WWP2 as GST-WWP2, GST-free WWP2, and WWP2 plus GST as an intermolecular mixture. The reaction was conducted in the presence of 5 mM ATP, 100 μM wild-type ubiquitin, 50 nM E1, 1 μM E2 (UbcH5c), 1 μM GST-WWP2, WWP2 without or with 10 μM GST, and 5 μM PTEN, in assay buffer with 40 mM Tris-HCl pH 7.5, 50 mM NaCl, 0.5 mM TCEP, 5 mM $MgCl_2$. The reaction was quenched at 0, 0.5 and 2 hour time points. The samples were analyzed by SDSPAGE stained with Colloidal blue.

In the course of in vitro analysis of full length WWP2 and ubiquitination of its protein substrate PTEN (*199*), we observed that the fusion protein glutathione S-transferase-WWP2 (GST-WWP2) was a robust catalyst (Figure 24B,C). However, proteolytic removal of the GST reduced WWP2's ubiquitin transferase activity toward PTEN and itself (Figure 24B,C). Addition of GST in trans to GST-free full-length WWP2 failed to restore its activity to the levels observed for the GST-WWP2 fusion (Figure 24C). Size exclusion chromatography of GST-free WWP2 showed that it was largely monomeric (Figure 25A), and this monomeric form showed low ubiquitin transferase activity whereas a small fraction of GST-free full length WWP2 eluted as an oligomeric form which appeared to be much more active (Figure 25B). As GST is an obligate dimer, these results suggest that GST-free WWP2 may be subject to allosteric intramolecular inhibition, partially relieved by self-interaction, although the structural basis for this was unclear.

It has been reported that the C2 domain and the WW domains in HECT E3 ligases (Figure 22 and Figure 24A) may be important for regulating their catalytic activities (*100, 137-139, 193*). To investigate the role of the C2 domain in WWP2, we prepared C2 domain-free WWP2 which showed low activity similar to that of full-length GST-free WWP2 (Figure 26A). We note that these WWP2 results differ from findings in a previous report (*137*). To evaluate the role of the WW domains, we explored the effects of a commercially available canonical WW peptide ligand containing a PPXY motif (WW peptide), and also made mutations in the WW domain-binding LPXY motifs in the WWP2 HECT domain (*100*). Neither WW peptide addition nor LPXY mutation led to altered WWP2 ubiquitin transferase activity (Figure 26B,C), arguing against the importance of WW domain engagement in WWP2 catalytic regulation.

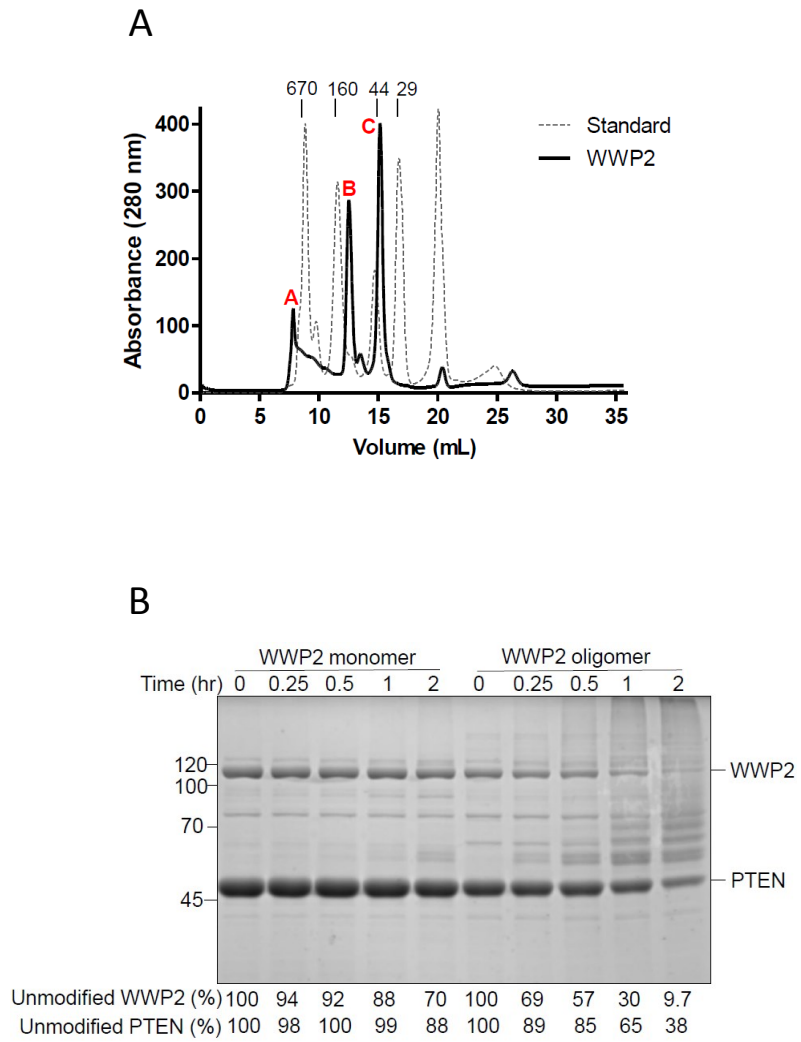

Figure 25: Full-length GST-free WWP2 contains autoinhibited monomer and active aggregate. (A) Size exclusion chromatography of GST-WWP2 after GST cleavage. The purified GST-WWP2 was treated with PreScission protease to cleave the GST tag and then analyzed by FPLC size exclusion chromatography. The dotted line trace represents MW standards corresponding to 670, 160, 44 and 29 kDa. The solid line trace shows the cleaved GST-WWP2: Peak A-WWP2 oligomer (>670 kDa), Peak B-WWP2 momoner (100 kDa), and Peak C-GST dimer (55 kDa). (B) Ubiquitination assay of WWP2 monomer and oligomer. The reaction was carried out in similar conditions as described in Figure 24B, but with 10 μM PTEN, and the reaction was quenched at 0, 0.25, 0.5, 1 and 2-hour time points. All the assays were repeated at least twice (n≥2).

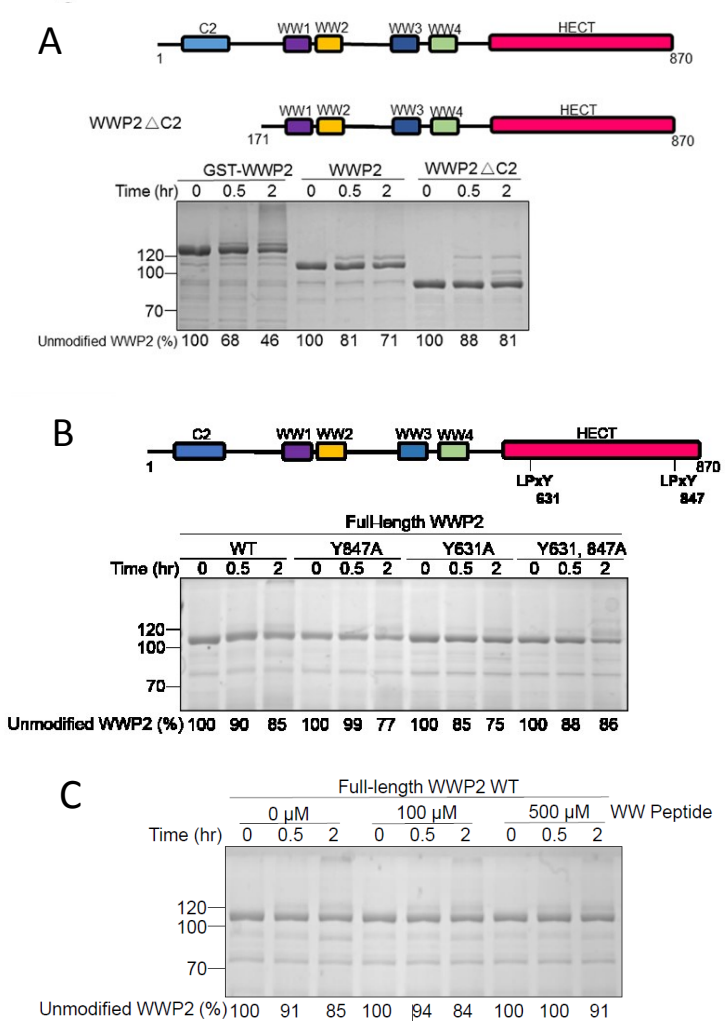

Figure 26: Analysis of C2 domain and WW domain in the auto-regulation of WWP2. (A) Ubiquitination assay of GST-WWP2, Full-length WWP2 (FL-WWP2), and WWP2 △C2. The reaction was conducted in the same condition as Figure 24B, and quenched at the times indicated. (B) Ubiquitination assay of full-length WWP2 containing LPXY motif point mutations. Both the single and double Y to A mutants were generated. (C) Ubiquitination assay of full-length wild-type WWP2 in the presence of the indicated concentrations of PPxY peptide (DPMSSTYIEELGKREVTIPPKYRELLA). The reactions in A and B were carried out as described in Figure 24B.

We next introduced a protease site N-terminal to the WW3 domain in WWP2 (Figure 27A) and determined that the WW3-WW4-HECT protein fragment could partially co-elute with the C2-WW1-WW2 fragment by size exclusion chromatography (Figure 27B,C). This raised the possibility that interactions between the N-terminal and C-terminal components of WWP2 might modulate the activity of intact full-length WWP2. Consistent with this hypothesis, purified recombinant WWP2 HECT domain and WW3-WW4-HECT protein showed robust autoubiquitination activity (Figure 27D). Based on these findings, we suspected that the WW1-WW2 moiety was crucial for enforcing autoinhibition of WWP2. However, intermolecular addition of a purified recombinant WW1-WW2 protein fragment to WW3-WW4-HECT WWP2 did not inhibit the latter's ubiquitin transferase activity (Figure 28).

4.3.2 The WW2-WW3 linker (2,3-linker) as an autoinhibitory module of WWP2

Because of the lack of an apparent role for the C2 or WW domains in WWP2 catalytic regulation, we considered the possibility that the ~30 aa WW2-WW3 linker (2,3-linker), proposed to possess α-helical character by a protein structure prediction algorithm (PSIPRED v3.3), might be critical for autoinhibition of WWP2 enzymatic activity. We tested this possibility in several ways. We prepared purified recombinant 2,3-linker-WW3-WW4-HECT protein and found that it was less active than the linker-free WW3-WW4-HECT WWP2 enzyme form (Figure 29A). In addition, we showed that a synthetic linker peptide (aa362-395) could inhibit WW3-WW4-HECT WWP2 in an intermolecular fashion (Figure 29B). Moreover, genetic deletion of the 2,3-linker from full-length untagged WWP2 profoundly (~100-fold) increased its autoubiquitination activity (Figure 29C, please note the different time scales above the gel).

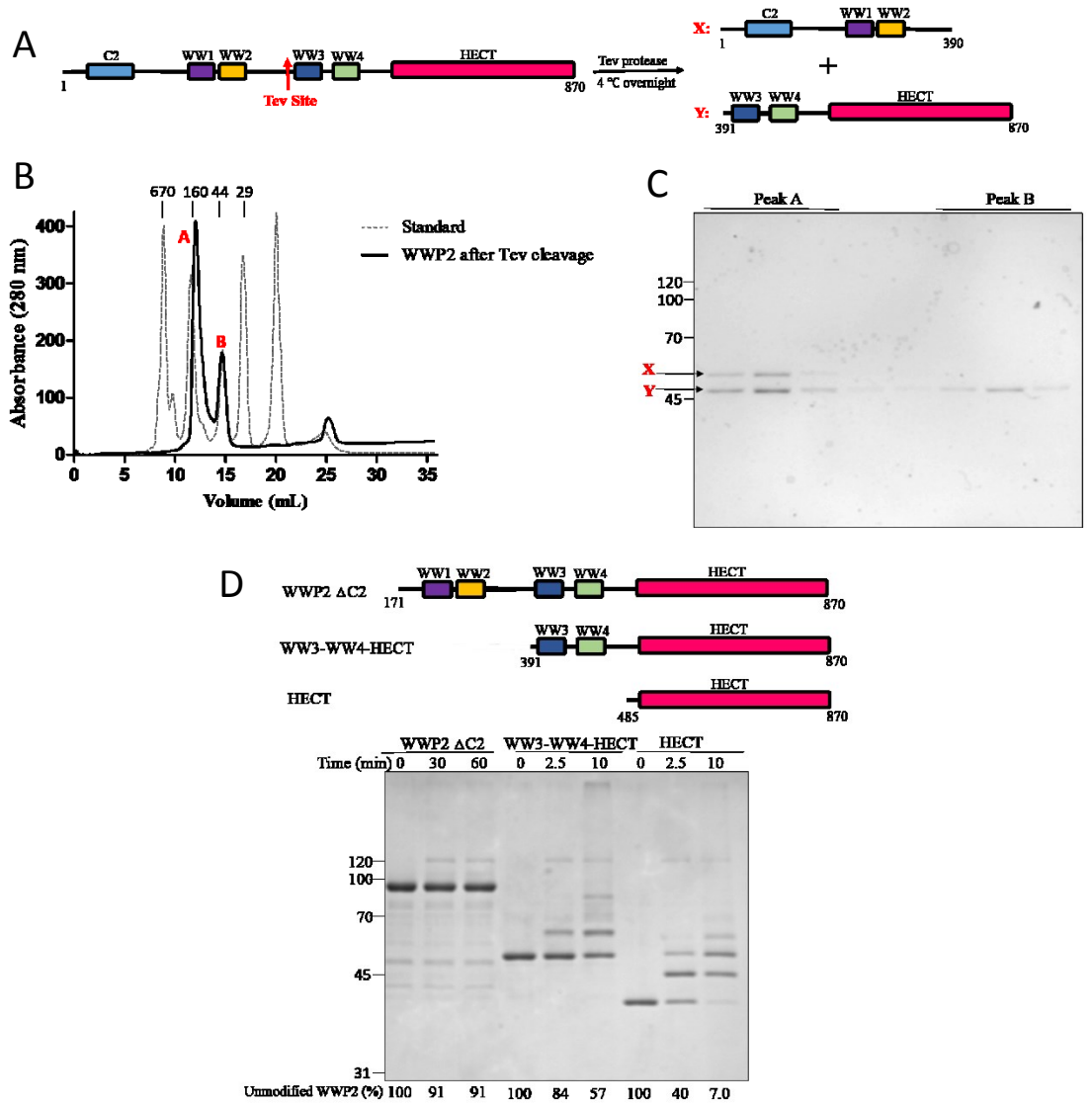

Figure 27: Intramolecular interaction mediates the autoinhibition of WWP2. (A) Schematic diagram showing that a TEV protease cleavage site (ENLYFQ/G) was inserted by mutagenesis between residues Ser395 and Ala396 just N-terminal to the WW3 domain. This purified TEV-site containing WWP2 protein was cleaved by TEV protease into a N-terminal fragment X containing the C2 domain, the WW1 domain, and the WW2 domain and a C-terminal fragment Y containing the WW3 domain, the WW4 domain, and the HECT domain. (B) Size-exclusion chromatogram of the TEV-cleaved WWP2 (solid line trace) superimposed with MW standards (dashed line trace). There were two major peaks Peak A (~100 kDa) and Peak B (~50 kDa). (C) Analysis of the chromatography fractions from D. Fractions corresponding to Peak A and Peak B were analyzed by SDSPAGE and Coomassie staining. Peak A is the heterodimer of fragment X and Y, and Peak B is fragment Y alone. Assignment of the the X fragment band running above the Y fragment band, although paradoxical based on their predicted molecular weights, is based on a recombinant standard of Y (data not shown). (D) Ubiquitination assay of WWP2 △C2, WW3-WW4-HECT, and HECT. Performed as described in Figure 24B and quenched at the times indicated. All the assays were repeated at least twice (n≥2) and showed good reproducibility.

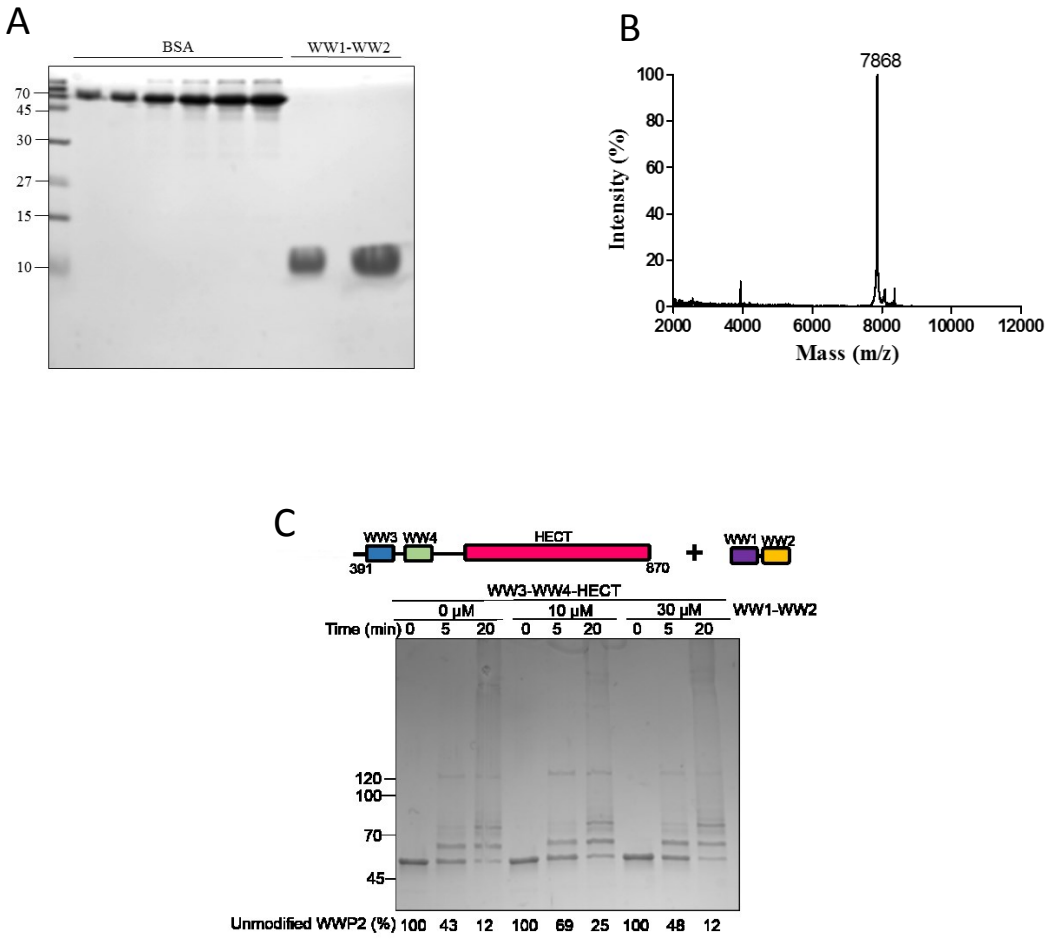

Figure 28: Analysis of WW1-WW2 piece in the auto-regulation of WWP2. (A) Coomassie gel of purified WW1-WW2 protein. (B) Mass spectrum of the purified WW1-WW2 protein. (C) Ubiquitination assay of WW3-WW4-HECT with different concentrations of WW1-WW2. 1, 10 and 30 μM purified recombinant WW1-WW2 was added to the reaction, and the reaction was conducted in similar condition as described in Figure 24B, and quenched at the times indicated.

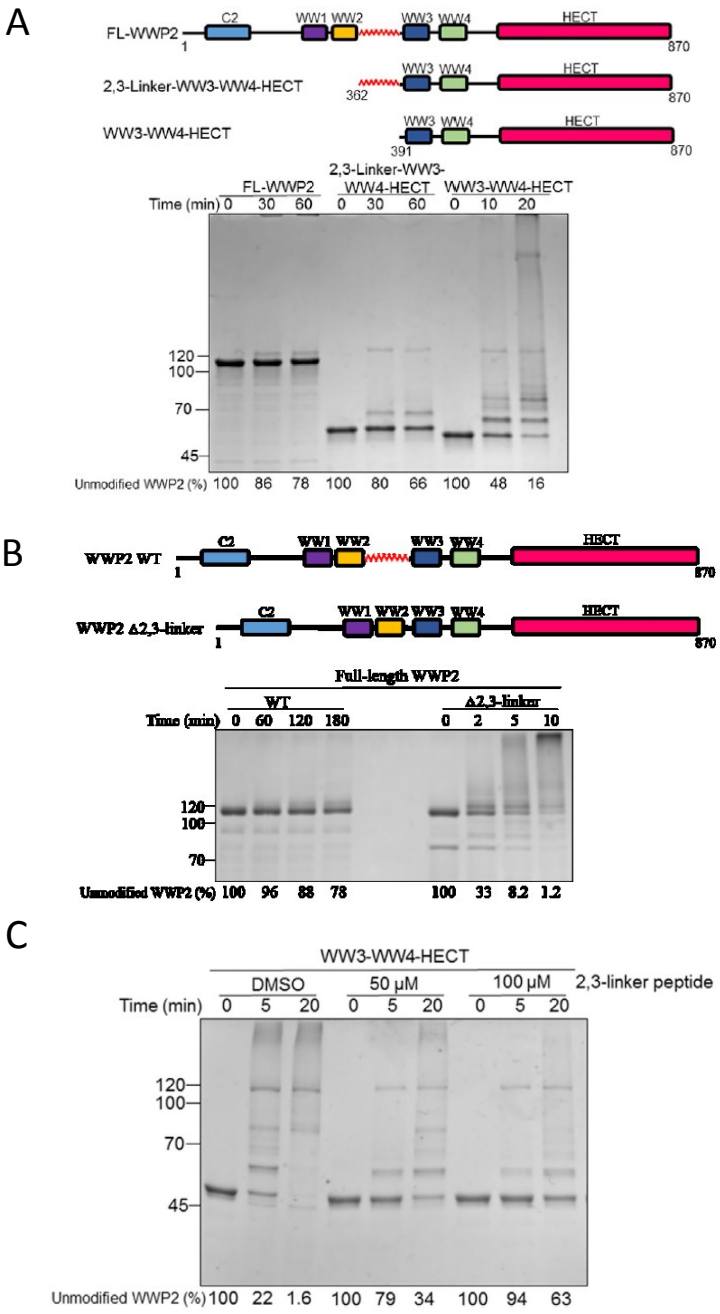

Figure 29: Regulation of WWP2 autoubiquitination activity by WW2-WW3 linker (2,3-linker). (A) Ubiquitination assay of full-length WWP2 (FL-WWP2), 2,3-linker-WW3-WW4-HECT and WW3-WW4-HECT carried out as in Figure 24B. The reaction for FL-WWP2 and 2,3-linker-HECT was quenched at 0, 30 and 60 minutes, and that for WW3-WW4-HECT was quenched at 0, 10 and 20 minutes. (B) Ubiquitination assay of WW3-WW4-HECT in the presence of 2,3-linker peptide (n-TAEYVRNYEQWQSQRNQLQGAMQHFSQRFLYQSS-c) carried out as in Figure 24B with 0, 50 and 100 μM synthetic 2,3-linker peptide. (C) Ubiquitination assay of wild-type WWP2 and WWP2 with 2,3-linker deletion (WWP2 △2,3-linker) carried out as in Figure 24B with quenching at the times indicated.

One possible mechanism for how the 2,3-linker may inhibit WWP2 catalytic activity is by blocking the E2-E3 interaction that is necessary for charging the HECT domain with ubiquitin (*63*). However, the full-length and 2,3-linker-free WWP2 showed a similar ~3-fold stimulation of autoubiquitination activity with a 30-fold increase in E2 concentration (Figure 30A,B) suggesting that the 2,3-linker probably does not modulate the E2-E3 interaction.

4.3.3 Structural basis of WWP2 autoinhibition by the 2,3-linker

To gain greater insight into the molecular basis of the role of the 2,3-linker, we sought to solve the crystal structure of autoinhibited WWP2 construct containing the 2,3-linker. The trials using the constructs WW1-WW2-WW3-WW4-HECT and 2,3-linker-WW3-WW4-HECT did not yield any crystal hits. We considered that the WW3-WW4 piece is not directly involved in the autoinhibition and that it might be flexible which could prohibit crystal formation. Therefore, we generated the WWP2 deletion construct with deletion of the WW3 and WW4 domains, effectively fusing the 2,3-linker directly to the HECT domain. Ubiquitination assay showed this 2,3-linker-HECT construct still displayed autoinhibition (Figure 31A). A brief 96-well plate based screen yielded several crystallization conditions that generated a cluster of needle crystals, indicating that this construct was promising for solving the structure of autoinhibited WWP2. However, optimization by varying the precipitant concentrations and buffer pH did not produce crystals good enough for data collection.

We next went on to try to optimize the construct. Our goal was to to find the shortest construct with the most autoinhibited activity. It is notable that the last five

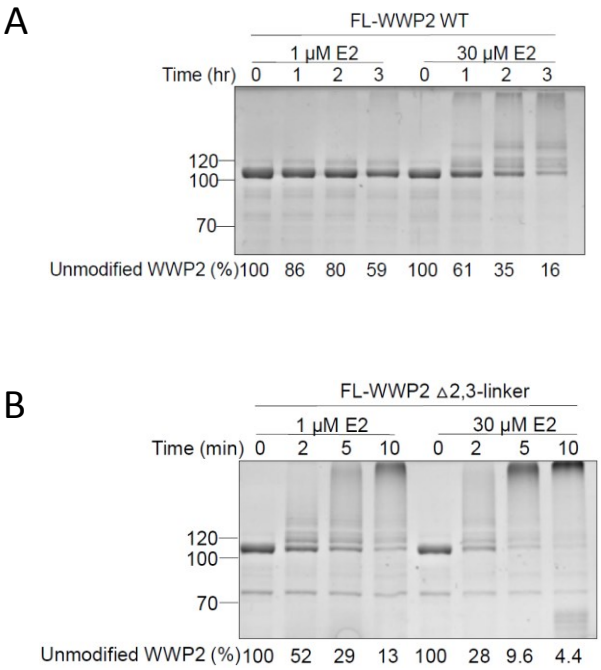

Figure 30: Effect of E2 concentration on the autoubiquitination of WWP2 forms. (A) Ubiquitination assay of wild-type full-length WWP2 (FL-WWP2 WT) with two different concentrations of E2. The ubiquitination assay was carried out in a buffer containing 40 mM Tris-HCl pH 7.5, 50 mM NaCl, 0.5 mM TCEP, 5 mM $MgCl_2$, mixed with 5 mM ATP, 100 μM wild-type ubiquitin, 50 nM E1, 1 μM E3, and 1 μM or 30 μM E2 (UbcH5c). The reaction was quenched at 0, 1, 2, and 3 hours. (B) Ubiquitination assay of full-length WWP2 with 2,3-linker deletion (FL-WWP2 △2,3-linker) with two different concentrations of E2. The reaction was conducted in the same condition as panel A, and quenched at 0, 2, 5, and 10 minutes. Replicate assays were performed on separate occasions (n=2) and showed similar results, with about 3-fold rate enhancements at the high E2 concentrations.

residues of all the constructs used for crystallization needed to be deleted(*177*) while the constructs used for activity assays had to retain a normal C-terminus since is essential for ubiquitin transferase activity(*67, 71, 75*). As an initial step, I optimized the N-terminal part of the construct to delete the redundant residues. The 2,3-linker sequence (TAEYVRNYEQWQSQRNQLQGAMQRFSQRFLYQ, from 362 to 393) was differentially truncated in the 2,3-linker-HECT construct, and the activity was measured. It was found the shortest construct which retained the autoinhibitory activity was the one that started form Y365 (data not shown). The original 2,3-linker-HECT construct contained a 22-amino acid segment between the 2,3-linker and the HECT domain. I then tried to optimize this segment to find the shortest linker. I tested a 16-amino acid segment and a 12-amino acid segment, and it turned out that the 16-amino acid segment-containing construct showed similar activity to that of the original 22-amino acid segment-containing construct, but the 12-amino acid segment-containing construct showed increased autoubiquitination activity (data now shown). Thus, in subsequent screening, we used the construct that started with Y365 and contained a 16-amino acid segment between the 2,3-linker and the HECT domain. The crystals were successfully optimized with this new construct, and we solved the structure (Figure 31B). The X-ray structure of 2,3-linker-HECT WWP2 (Figure 31B) showed the HECT domain in the T-shape conformation, which appeared similar to the known WWP1 and WWP2 HECT domain structures (*65, 177*), but the 2,3-linker was not observed (see Methods for an R.M.S.D. comparison of structures).

To attempt to find the electron density of the 2,3-linker, we employed semi-synthesis to introduce an iodine-phenylalanine, replacing the Y369 in the 2,3-linker-HECT protein, hoping that the heavy atom would show its electron density in the map

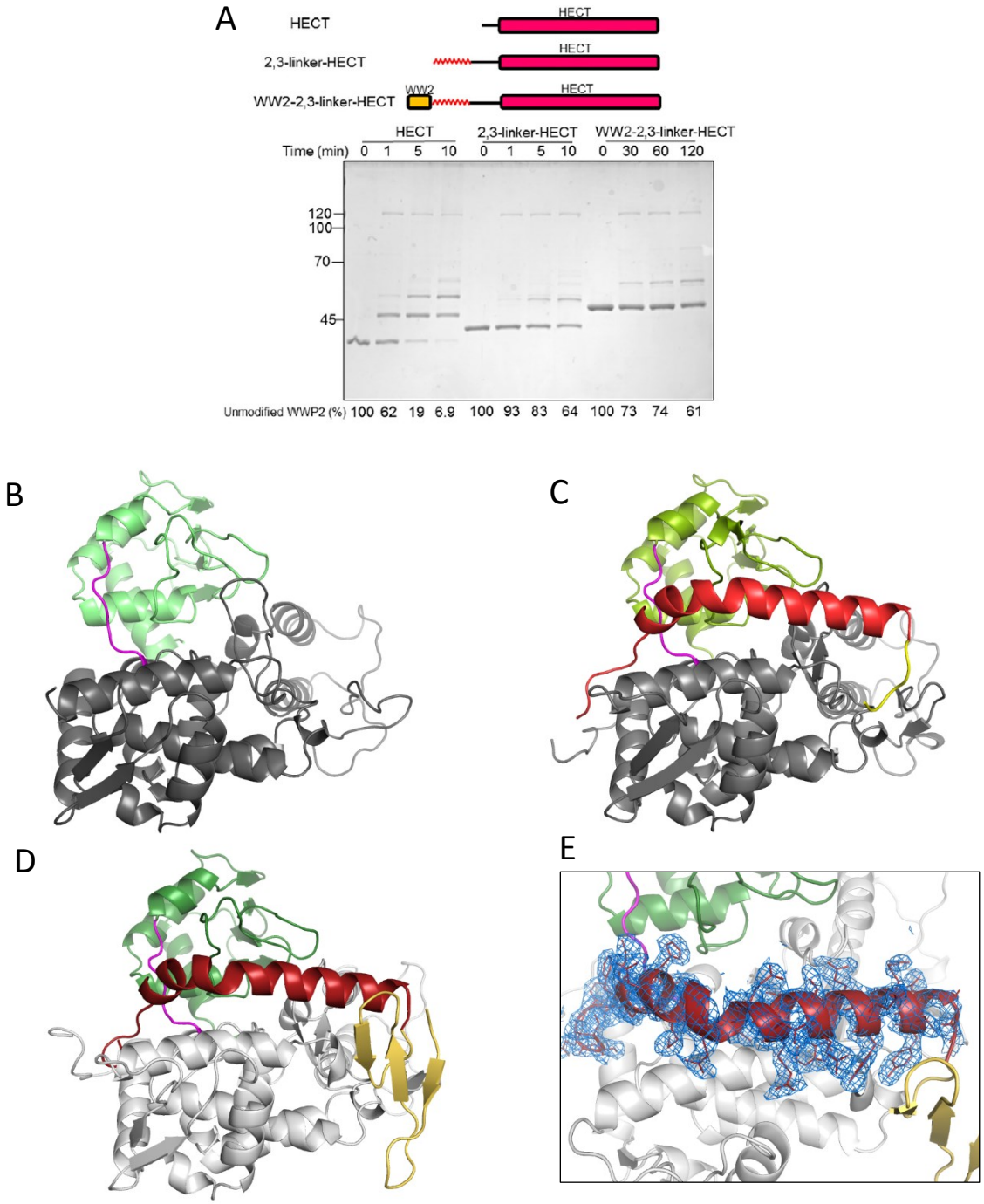

Figure 31: Crystallization of autoinhibited WWP2 HECT domain. (A) Ubiquitination assay of HECT, 2,3-linker-HECT and WW2-2,3-linker-HECT. Ubiquitination assay was conducted in the same conditions as Figure 24B, and the reaction was quenched at 0, 1, 5, and 10 minutes for HECT and 2,3-linker-HECT, and at 0, 30, 60, 120 minutes for WW2-2,3-linker-HECT. (B) Crystal structure of 2,3-linker-HECT showing the HECT domain of WWP2, the N-lobe in dark grey color, the C-lobe in green, and the hinge loop in magenta. (C) Structure of WW2-2,3-linker-HECT crystallized in 0.1 M MMT pH 6.0, 25% PEG1500. The N-lobe of HECT domain is in grey, the C-lobe is in green, the hinge loop in magenta, the 2,3-linker in red, and the C-terminal six residues of the WW2 domain in yellow. (D) Structure of WW2-2,3-linker-HECT crystallized in 0.1 M potassium thiocyanate, 30% PEG monomethyl ether 2000. The N-lobe of HECT domain is in silver, the C-lobe in green, the hinge loop in magenta, the 2,3-linker in red, and the WW2 domain in yellow. (E) Electron density map of 2,3-linker is shown as blue color

Table 2 Data collection and refinement statistics

	2,3-linker-HECT PDB ID 5TJQ	WW2-2,3-linker-HECT PDB ID 5TJ7	WW2-2,3-linker-HECT PDB ID 5TJ8
Data collection			
Space group	$P2_12_12_1$	P1	$P2_12_12_1$
Cell dimensions			
a, *b*, *c* (Å)	61.0, 62.5, 102.3	72.0, 73.9, 82.3	44.2, 89.2, 111.4
a, b, g (°)	90.0, 90.0, 90.0	89.9, 89.6, 90.0	90.0, 90.0, 90.0
Resolution (Å)	50.00-2.75 (2.80-2.75)	50.00-2.60(2.64-2.60)	50.00-2.20 (2.24-2.20)
R_{sym} or R_{merge}	0.052 (0.42)	0.04 (0.10)	0.07 (0.26)
I / sI	28.77(2.19)	21.95 (6.42)	31.45 (2.85)
Completeness (%)	99.1 (98.6)	90.2 (55.1)	92.5 (65.2)
Redundancy	6.0 (5.2)	2.1 (1.8)	5.3 (2.5)
Unique Reflections	10,662	47,023	21,431
Total # Reflections	63,445	90,187	111,903
Refinement			
Resolution (Å)	53.39-2.75	50.00-2.60	69.68-2.30
No. reflections	10,094	44,712	18,436
R_{work} / R_{free}	0.22 (0.34)/0.31 (0.37)	0.21 (0.28)/0.28 (0.39)	0.21 (0.31)/0.31 (0.40)
No. atoms			
Protein	3,093	14,925	3,525 (416 aa)
Ligand/ion	-	3	1
Water	11	996	56
B-factors			
Protein	88	24	69
Ligand/ion	-	-	59
Water	62	36	56
R.m.s. deviations			
Bond lengths (Å)	0.011	0.013	0.013
Bond angles (°)	0.003	0.008	0.002

which we hypothesized could highlight the location of 2,3-linker. Unfortunately, we were still unable to find the electron density of the iodine or the 2,3-linker.

We found that although the 2,3-linker-HECT construct showed reduced autoubiquitination activity relative to the isolated HECT domain, inclusion of the WW2 domain in a WW2-2,3-linker-HECT construct further intensified autoinhibition, with activity comparable to full-length WWP2 (Figure 31A, please note the different time scales above the gel). The crystallization of WW2-2,3-linker-HECT construct was successful, and we determined the X-ray crystal structures (Figure 31C,D) at 2.8 and 2.3 Å resolution, respectively (Table 2). The structures of two crystal forms of WW2-2,3-linker-HECT WWP2 were determined. In one, the complete WW2 domain and 2,3-linker was observed (Figure 31D), and in the other, only the C-terminal 6 residues of the WW2 domain could be resolved, but the rest of the structures including the 2,3-linker and HECT domains were nearly identical (Figure 31C).

The fold of the WW2 domain shows a characteristic three-stranded β-sheet, and interestingly, its interaction with the HECT domain is mediated by its C-terminal 6 residues, especially Trp358 (Figure 32A), which is mutated in cancer (*200*). Indeed we found that the WWP2 W358L cancer mutant is more active than wt WWP2 (Figure 32B). The 2,3-linker forms a 26-residue α-helix that makes extensive interactions with the N-lobe and C-lobe of the WWP2 HECT T-shape conformation (Figure 31B,C,D,E and Figure 33A,D). The helix displays a unique bent conformation and wraps around the HECT domain with buried surface area of 1150 A^2. The N-terminal residues of the 2,3-linker and the WW2 domain occupy a site in the HECT N-lobe that is the proposed allosteric binding exosite for non-covalently bound ubiquitin (Figure 33B) (*69, 73*). Therefore, in the 2,3-linker bound WWP2 form, it appears that the 2,3-linker would obstruct ubiquitin's ability to bind to this exosite, negating ubiquitin's ability to stimulate

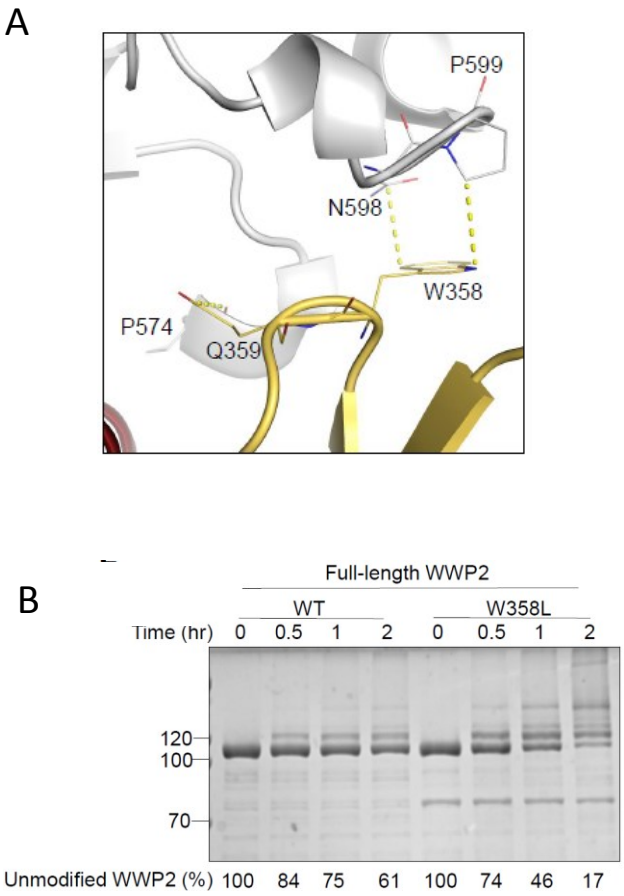

Figure 32: Interaction between the C-terminal six residues of the WW2 domain and the HECT domain in WWP2, and analysis of Trp358 mutation. (A) Zoom-in structure of the C-terminus of WW2 domain illustrating that Trp358 forms pi-stacking/hydrophobic interactions with the side chains of Asn598 and Pro599, and Gln359 makes a hydrogen bond with the main chain of Pro574. (B) Ubiquitination activity of WWP2 cancer mutant W358L compared with wt WWP2, performed as described in Figure 24B (n=2, similar results on separate occasions).

WWP2 activity. The C-terminal residues of the 2,3-linker are engaged with the hinge-loop that tethers the WWP2 HECT domain N- and C-lobes (Figure 33D and 33E) (*65*). This 2,3-linker-hinge interaction appears to restrain the flexibility of the C-lobe which is necessary for ubiquitin transferase activity (*65*), locking WWP2 in the T-shape, as the L-shape conformation would be incompatible with such linker engagement.

The autoinhibited WWP2 structure predicts that the affinity of ubiquitin binding to the WWP2 exosite (*69, 73*) in the 2,3-linker-HECT or the WW2-2,3-linker-HECT constructs would be reduced relative to that of the isolated WWP2 HECT domain. To investigate this, we prepared a ubiquitin variant (UbF1) engineered to have high affinity for the WWP2 exosite (*69*) and also tagged with fluorescein via Cys alkylation, introduced at a ubiquitin surface residue (Ser57) that is remote from its E3 binding surface (Figure 34). Using a fluorescence anisotropy assay, we found that UbF1 had a K_d of 0.23 μM for the isolated HECT domain, 0.93 μM for 2,3-linker-HECT and 20 μM for WW2-2,3-linker-HECT (Figure 33C). This progressive loss of affinity for allosteric ubiquitin by these WWP2 forms correlates well with the different catalytic activities of these three proteins (Figure 31A) and is consistent with the distinct X-ray crystal structures of the isolated WWP2 HECT domain and autoinhibited WWP2. In addition, we investigated the conserved hinge residues Met752 and Gln753 that appear to make close contacts with the WWP2 2,3-linker amino acids 389-RFLY-392. It is notable that M752T and Q753L WWP2 point mutations have been found in cancer (*201, 202*). The WWP2 double mutant M752A/Q753A and the single mutant WWP2 M752T both showed considerably increased WWP2 autoubiquitination activity relative to wt WWP2 (Figure 33F). These mutagenesis results validate the structural model and indicate how cancer mutations can activate WWP2.

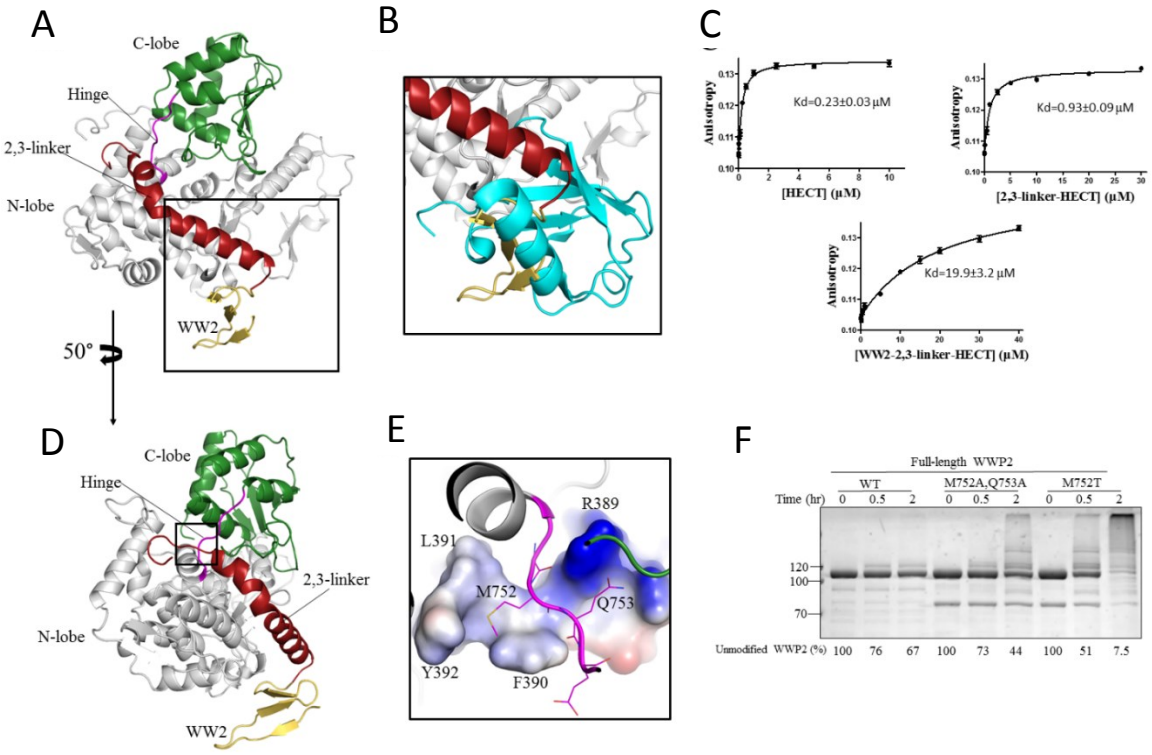

Figure 33: Structural mechanisms for 2,3-linker mediated autoinhibition of WWP2. (A) Overall structure of WW2-2,3-linker-HECT with the HECT domain in an inactive (inverse T-shape) conformation. The WW2 domain is in yellow, the 2,3-linker is in red, the N-lobe of HECT domain is in silver, the C-lobe of HECT domain is in green, and the hinge loop between N and C-lobe is in magenta. (B) A blow-up of the region highlighted with a square in Figure 33A showing the ubiquitin-binding exosite in the HECT domain. The structure of the WWP2 WW2-2,3-linker-HECT protein is superimposed with the structure of the WWP1 HECT-UbV P2.3-UbvH7 complex (5HPT). The ubiquitin-binding exosite in the HECT domain is occupied by the N-terminus of the 2,3-linker and the WW2 domain. (C) Affinity of fluorescein-labeled UbV P2.3 (UbF1) for WWP2 forms HECT, 2,3-linker-HECT, and WW2-2,3-linker-HECT, respectively measured by fluorescence anisotropy. K_d values were obtained using quadratic fits and shown +/-SEM (n=2). (D) 2,3-linker interacts with the hinge region in WWP2. WW2-2,3-linker-HECT structure visualized by rotating by 50° relative to the orientation in Figure 33A. From this perspective, the structure of the WW2 domain consisting of three beta strands is clear. The hinge which connects the N- and C-lobes of the HECT domain is boxed. (E) A blow-up of the boxed region in Figure 33D illustrates the interaction between the hinge (magenta, sticks) and the C-terminal section of the 2,3-linker (electrostatic surface). Met752 and Gln753 from the hinge loop are shown to be anchored by the residues from the 2,3-linker. (F) Ubiquitination assays of wild-type full-length WWP2 and the hinge loop mutants M752A, Q753A and M752T. The reactions were performed as in Figure 24B. All the assays were repeated at least twice (n≥2) and showed good reproducibility.

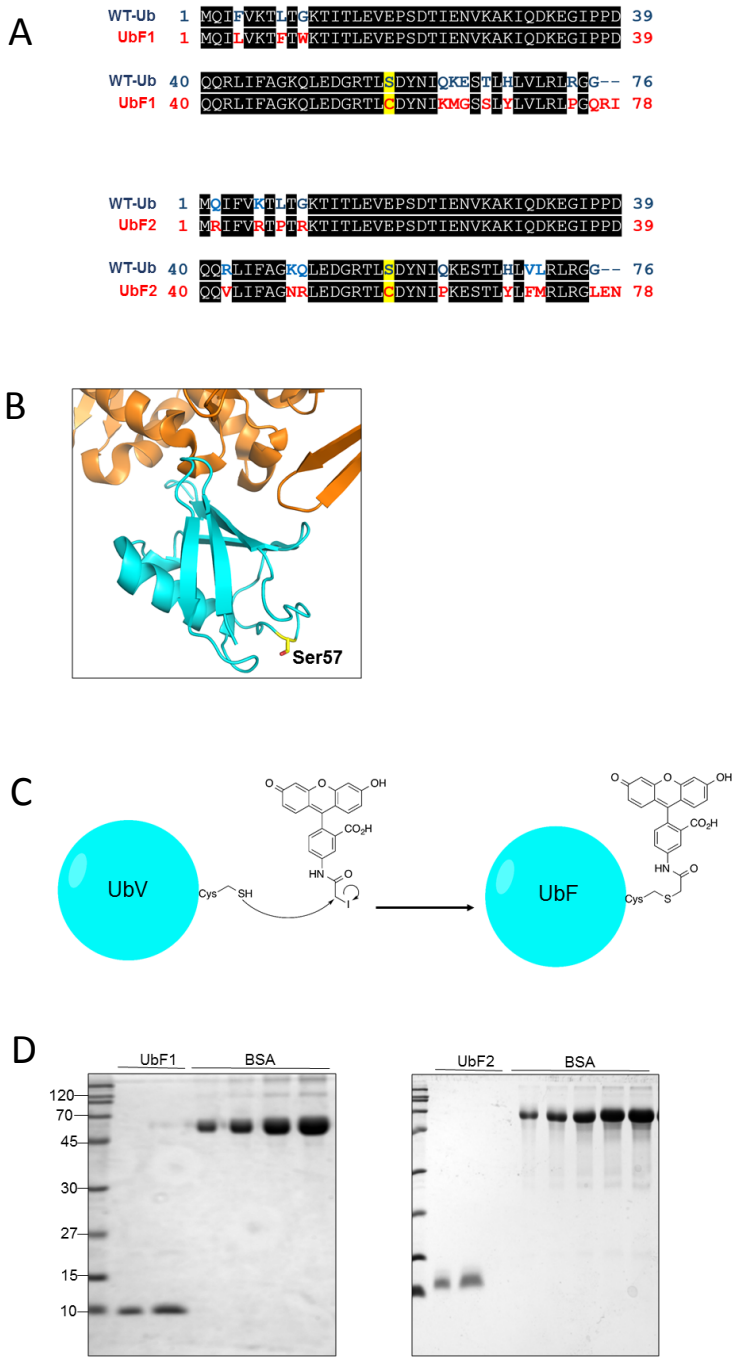

Figure 34: Generation of fluorescein-labeled ubiquitin variant (UbF). (A) Sequence alignment of wild-type ubiquitin (WT-Ub) and ubiquitin variant (UbF1 and UbF2). The mutations: F4L, L8F, G10W, Q62K, K63M, E64G, T66S, H68Y, R74P and G76Q, and two extra residues at the C-terminus R77, I78 are introduced to make UbF1; Q2R, K6R, L8P, G10R, R42V, K48N, Q49R, Q62P, H68Y, V70F, L71M, G76L, and extra E77, N78 are introduced for UbF2. A S57C mutation is also performed to enable fluorescein labeling by cysteine alkylation. (B) Structure of UbF bound to the HECT domain of WWP1 (pdb accession: 5HPT). Ser57 was chosen to be mutated to cysteine for labeling because it is located in a flexible loop distant from the interface of UbF and HECT. (C) Schematic of the reaction showing labeling of the cysteine side-chain by reacting with 5-iodoacetamidofluorescein and generating UbF. (D) Coomassie gel of the purified UbF1 and UbF2.

4.3.4 Autoinhibitory mechanisms for other NEDD4 family members

Given the high degree of sequence conservation of the 2,3-linker of WWP2 with that in WWP1 and ITCH (Figure 35A,B), we speculated that deletion of this linker would have a similar effect on these closely related E3 ligases. Indeed, deletion of the 2,3-linker from WWP1 and ITCH sharply increased their autoubiquitination activity as compared to the full-length proteins (Figure 35C,D). These experiments indicate the functional conservation of the 2,3-linker as a key negative regulator among these highly homologous E3 ligases.

Like WWP2, NEDD4-1 also contains four WW domains (Figure 22 and Figure 36A). In comparison to WWP2, WWP1, and ITCH, however, NEDD4-1 shows no apparent sequence conservation of its WW2-WW3 linker with that of the WWP2, WWP1, and ITCH proteins, nor is it predicted to be α-helical (PSIPRED v3.3). Indeed, autoubiquitination activity of WW2-WW3 linker deleted NEDD4-1 showed nearly identical activity compared to full-length intact NEDD4-1 (Figure 36B). However, we hypothesized that a different segment of NEDD4-1 might play an analogous autoinhibitory role in NEDD4-1. We therefore analyzed the predicted secondary structure of the domain linker segments within NEDD4-1 focusing on predicted α-helical regions. In this regard, the stretch of amino acids C-terminal to the WW1 domain (aa225-244) was selected as a potential regulatory motif based on its projected high probability as an α-helix (PSIPRED v3.3) and an established Thr phosphorylation (Thr229, Figure 36A) (*203, 204*).

We generated NEDD4-1 containing this partial linker deletion (1,2-linker-deleted NEDD4-1) and showed that 1,2-linker deleted NEDD4-1 showed enhanced autoubiquitination activity relative to wt enzyme (Figure 36B,C). In addition, T229E

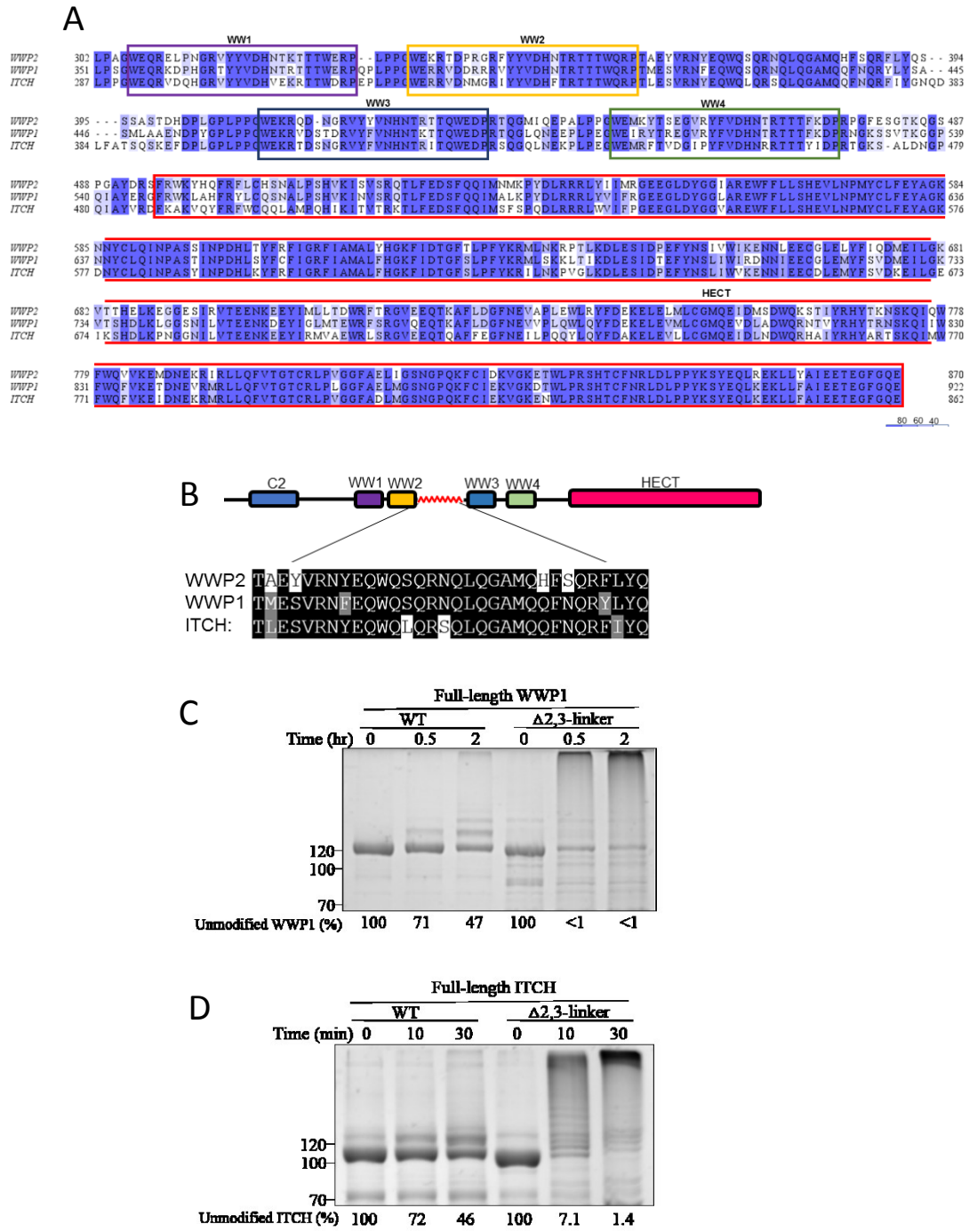

Figure 35: Sequence information for selected HECT E3 ligase regions and regulation of WWP1/ITCH by 2,3-linker. (A) Sequence alignment of WWP2/WWP1/ITCH WW1-WW2-WW3-WW4-HECT sections showing the sequence identity. (B) Schematic diagram showing the architecture of WWP2, WWP1, and ITCH E3 ligases and the sequence alignment of the 2,3-linker region. WWP2, WWP1, and ITCH showed high sequence identity in the 2,3-linker region. Ubiquitination assay of (C) wild-type WWP1 and WWP1 with 2,3-linker deletion (WWP2 △2,3-linker) and (D) wild-type ITCH and ITCH with 2,3-linker deletion (ITCH △2,3-linker) were carried out as in Figure 24B with quenching at the times indicated.

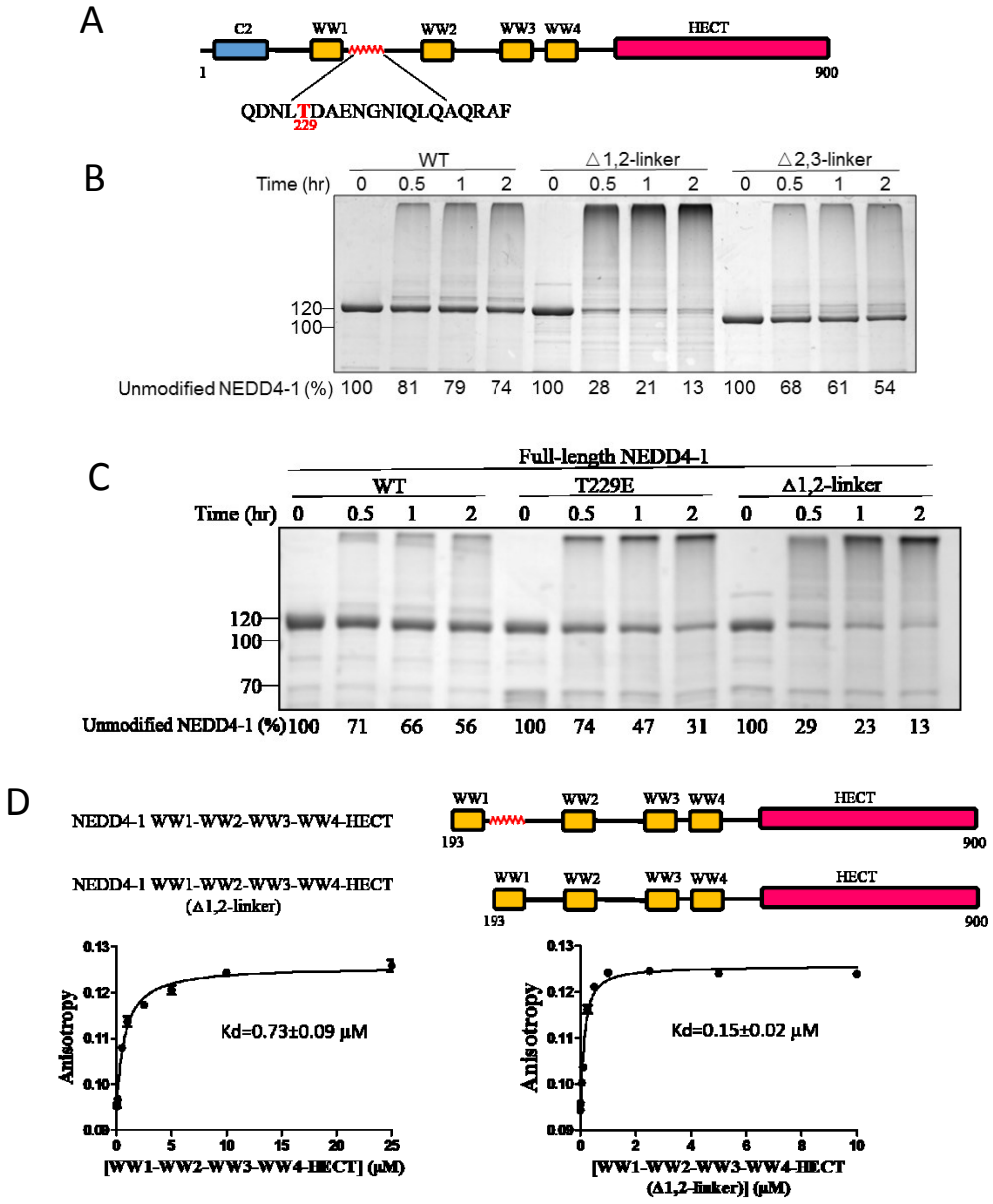

Figure 36: Autoinhibition of NEDD4-1. (A) Ubiquitination assay of wild-type NEDD4-1 and the △1,2-linker and △2,3-linker forms. The assay was carried out in same condition as Figure 24B, and quenched at time points indicated. (B) Schematic diagram showing the architecture of NEDD4-1. The predicted helix sequence (225-QDNLTDAENGNIQLQAQRAF-244) right after the WW1 domain is shown, with the threonine (T229) highlighted in red. (C) Ubiquitination assay of wild-type NEDD4-1, T229E NEDD4-1 and NEDD4-1 with 1,2-linker deletion (WWP2 △1,2-linker). (D) Fluorescence anisotropy assay for UbF2 with NEDD4-1 WW1-WW2-WW3-WW4-HECT and WW1-WW2-WW3-WW4-HECT with WW1,2-linker deletion. Two replicates for this assay were done with similar K_d values.

NEDD4-1 showed activity intermediate between 1,2-linker deleted and wt NEDD4-1 (Figure 36C). We also prepared a fluorescent ubiquitin variant (UbF2, Figure 34) selective for the NEDD4-1 exosite (*69*) and showed that it bound a 1,2-linker deleted form of NEDD4-1 ~5-fold more avidly than the corresponding NEDD4-1 with an intact 1,2-linker (Figure 36D). These findings suggest that the regulatory linker module present in WWP2, WWP1, and ITCH is likely to be represented in NEDD4-1 and perhaps other HECT family members in diverse locations.

4.4 Discussion

Prior studies have suggested WW domain, C2 domain, and post-translational modification mediated autoinhibitory mechanisms for NEDD4 family HECT enzymes (*50, 82, 100, 137, 139, 142*). The experiments in our study have identified an unanticipated mechanism of regulation of HECT domain E3. The centrally located WWP2 2,3-linker is highly conserved in the WWP1 and ITCH E3 ligases so it was unsurprising that WWP2, WWP1, and ITCH are similarly autoinhibited by this regulatory module. It seems likely that an analogous autoinhibitory mechanism will extend to other HECT E3 ligases, given that NEDD4-1 which is a more weakly related enzyme to WWP2 shows similar behavior with deletion of a predicted linker helical module. Future work will be needed to investigate this possibility across the range of HECT family members. The form of regulation uncovered for WWP2, WWP1, ITCH, and NEDD4-1 is somewhat reminiscent of many proteases which exist as inactive pro-enzymes that are turned on by proteolytic removal of an autoinhibitory peptide segment (*205*), as well as the majority of protein tyrosine kinases that possess autoinhibitory loops that are stimulated by autophosphorylation (*206*). The comparison to proteases is perhaps most relevant since

premature activation of proteases can lead to self-destruction prior to performing their necessary cellular jobs akin to what was observed for Δlinker WWP2.

The crystal structure solved here greatly advanced our understanding of the molecular mechanism of linker mediated autoinhibition of HECT E3 ligases which involves locking the hinge loop and blocking ubiquitin exosite. While the hinge loop as a key regulatory structure of HECT is consistent with many previous studies(*65, 67*), the role of the exosite is more controversial. The results from several groups support the theory that the noncovalent ubiquitin adopted by the exosite serves as the acceptor of the ubiquitin at the active site, facilitating formation of poly-ubiquitin chains.(*68, 72, 73*) Recent studies indicate that the ubiquitin binding at exosite activates the ubiquitin transferase activity.(*69, 76*) Our study further supports the latter hypothesis. However, the mechanism of how the exosite ubiquitin binding could activate the HECT enzymatic activity remains elusive. One possible mechanism is that ubiquitin binding to the exosite leads to a conformational change, which enhances the flexibility of hinge loop or facilitates the ubiquitin transfer between E2, E3 and substrates, allosterically activating the HECT domain. It is also possible that the exosite plays distinct roles among different HECT E3 ligases. Further systematic and mechanistic studies are necessary to clarify the role of the exosite. Based on our structural study and others(*76*), the exosite seems to be a promising target for drug development that can regulate the activity of HECT E3 ligases.

Although this study reveals the importance of the 2,3-linker in the catalytic regulation of WWP2, WWP1, and ITCH E3 ligases, it is likely that the C2 domain and WW domains participate in significant ways in impacting WWP2, WWP1, and ITCH functions including cellular localization or protein substrate targeting. It has previously been reported that the C2 domain autoinhibits WWP2 (*137*) which we did not observe

here. However, the C2 domain likely still contributes to the autoinhibition of the SMURF2 and NEDD4-1 HECT ligases as proposed previously (*137, 138*). The role of the WW1-WW2 linker in NEDD4-1 appears to play a related role to the WW2-WW3 linker in WWP2, although it appears not as quantitatively impactful to autoinhibition of NEDD4-1. Perhaps in the case of NEDD4-1, the C2 domain and WW1-WW2 linker synergize to autoinhibit NEDD4-1 catalytic activity. Future work should investigate the presumed complex interplay between the multiple mechanisms of regulating NEDD4 family functions in normal and pathologic states to optimize the potential of therapeutic interventions for cancer and other diseases.

Chapter 5: Molecular Mechanism of Activation of Autoinhibited HECT E3 Ligases

5.1 Introduction

As discussed in Chapter 4, we demonstrated a new autoinhibitory mechanism for the HECT E3 ligase family beyond the previously proposed C2 and WW domain models. These autoinhibitory mechanisms ensure that the HECT enzymes are maintained in a relatively inactive state so that they only become activated in response to critical signaling events. It is therefore important to understand how these HECT E3 ligases are activated and regulated under physiologic conditions in the cell.

One mechanism for the activation of autoinhibited HECT E3 ligases is the disruption of an intramolecular conformation by post-translational modifications which releases the HECT domain from its interactions with autoinhibitory domains. A previously reported example is that the tyrosine phosphorylation on the C2 domain and the HECT domain of NEDD4-1 leads to activation of ubiquitin transferase activity(*140*), which is proposed to relieve the autoinhibitory interaction between C2 domain and HECT domain(*140*). Another proposed mechanism of activation involves the competitive binding of substrates to the autoinhibitory domain, displacing it from binding the HECT domain(*100*). This is believed to happen in WW domain-mediated autoinhibition. The WW domains bind to the HECT domain through a weak WW-LPXY motif interaction, and in the presence of a substrate containing the PPXY motif, phosphorylated Ser/Thr and other high affinity structural features, the WW domain bound to the HECT domain could be replaced by protein substrates, leading to activation of the HECT E3 ligases(*100*).

Since we discovered the linker as the autoinhibitory element which is not a canonical domain within HECT E3 ligases, it was interesting to investigate how the linker

mediated autoinhibition is regulated. It is notable that within the sequence of the WWP2 linker, there are two conserved tyrosine residues that have been shown to be phosphorylated according to previous studies(*142, 207, 208*). Here, we report that the two tyrosine phosphorylation sites within the linker could stimulate the HECT E3's enzyme activity, and structural and biochemical characterization indicates that these two phosphorylation sites employ different mechanisms for activation of the E3. We also investigate the functional effects of tyrosine phosphorylation of WWP2 in the cell using mutagenesis.

5.2 Methods

5.2.1 Plasmids and reagents

OCT4 cDNA was from Dr. Izpisua Belmonte from Barcelona, Spain (*209*), and subcloned into pcDNA3.1 plasmid. Mutations and truncations in WWP2 were introduced by Quik-Change (Agilent). Purified wild-type ubiquitin, human ubiquitin-activating enzyme UBE1, and human ubiquitin-conjugating enzyme UbcH5c were prepared as described previously (*188*). The Colloidal Blue Staining Kit was purchased from Invitrogen. Anti-PTEN, anti-β-actin and anti-MYC antibodies were from Santa Cruz (CA, USA). Anti-OCT4 antibody was from Bethyl Laboratories (USA). Anti-NEDD4-2, anti-AKT, anti-pAKT308 and anti-pAKT473 were from Cell Signaling Technologies (USA). Anti-ITCH antibody was from BD Biosciences (USA). Anti-phosphorylated tyrosine antibody (4G10) and the Dawson Dbz resin was from EMD Millipore (Germany). All other reagents were commercially purchased with the highest quality from either Sigma or Fisher.

5.2.2 Protein expression and purification

BL-21 Codon Plus cells were transformed with the pGEX6p-2 plasmid expressing full-length WWP2 or the different mutations or truncations, initially as N-terminally modified GST-fusion proteins. The transformed cells were cultured in LB medium at 37 °C to reach the optimal density (OD_{600}=0.6) in a shaker incubator grown on a 1 L scale. Protein expression was induced by 0.25 to 0.5 mM IPTG at 16 °C for 20 hours. The cells were resuspended in 25 mL lysis buffer (25 mM Tris-HCl pH 8.0, 250 mM NaCl, 1 mM phenylmethylsulfonyl fluoride (PMSF) and 1x Roche cocktail protease inhibitors) and were lysed by french press. The cell lysate was loaded on glutathione agarose followed by washing with 25 mM Tris-HCl pH 8.0, 250 mM NaCl, and 0.1% Triton X-100. The desired GST-tagged protein was eluted using 10 mL 25 mM Tris-HCl pH 8.0, 250 mM NaCl containing 50 mM reduced glutathione at pH 8.0. The eluted fractions were combined and dialyzed against a buffer consisting of 25 mM Tris-HCl pH 8.0, 250 mM NaCl, 10 mM BME, and the protein was treated with PreScission protease at 4 °C overnight to cleave the GST tag. Afterwards, the mixture of GST and cleaved protein was loaded to glutathione agarose again to remove the GST. The protein was concentrated and then loaded on a size exclusion column Superdex 200 (GE Healthcare) with a buffer containing 25 mM Tris-HCl pH 7.5, 150 mM NaCl, 5 mM DTT (dithiothreitol). The corresponding purified fractions assessed by Coomassie stained SDSPAGE were combined and glycerol was added to a final concentration of 10% v/v. The purified protein was concentrated to 1 to 10 mg/mL, flash frozen, and stored at -80ºC.

5.2.3 Peptide synthesis

The C-terminal thioester in n-TTWQRPTAEYVRNpYEQWQ-c was generated using the Dawson's Dbz resin (*159*). The peptide was synthesized manually using Fmoc solid phase synthesis. After assembling this peptide on the Dbz resin, the mixture was treated with p-nitrophenyl chloroformate and DIPEA to form C-terminal N-acyl-benzimidazolinone (Dbz) followed by trifluoroacetic acid cleavage. The peptides were purified by reversed phase HPLC on a C-18 column using a water:acetonitrile gradient (containing 0.05% trifluoroacetic acid) to >90% and the correct structures confirmed by MALDI mass spectrometry (Figure 23) and amino acid analysis (AAA Service Laboratory Inc.).

5.2.4 WWP2 semisynthesis

To enable its ligation to the C-terminal thioester of the synthetic peptide n-TTWQRPTAEYVRNpYEQWQ-c, the recombinant WWP2 protein fragment (aa 374-870) was generated containing an N-terminal Cys (S374C). As there was no Cys in a practical location for semisynthesis, we elected to perform a conservative replacement of a Cys for Ser374. Using QuikChange (Agilent) mutagenesis, the construct pGEX6p-2 2,3-linker-WW3-WW4-HECT was modified to have a TEV protease site N-terminal to Cys374. The protein was expressed and purified in a similar way to other protein but using TEV protease instead of PreScission protease. During the FPLC purification step, the buffer used was 25 mM Tris-HCl pH 8.0, 150 mM NaCl, 1 mM TCEP (tricarboxyethyl-phosphine), to avoid DTT or BME (beta-mercaptoethanol). For the ligation reaction, about 1 mg of purified protein was mixed with 2 mM peptide in the buffer containing 75 mM HEPES pH 7.4, 400 mM MESNA, 1 mM TCEP, 10% glycerol in 1 mL. The ligation reaction was allowed to proceed at room temperature for 24 hours,

followed by dialysis against buffer with 25 mM Tris-HCl pH7.5, 5 mM NaCl, 5 mM DTT, 10% glycerol. The protein was then further purified by anion exchange chromatography using MonoQ column. The fractions containing purified semisynthetic pY369-2,3-linker-WW3-WW4-HECT (aa356-870) were combined and concentrated to about 1 mg/mL.

5.2.5 *In vitro* ubiquitination assays

The *in vitro* ubiquitination reactions were carried out in microcentrifuge tubes in final volumes of 20 µL containing 40 mM Tris-HCl pH 7.5, 50 mM NaCl, 0.5 mM TCEP, 5 mM $MgCl_2$, with 5 mM ATP, 100 M ubiquitin, 50 nM E1 protein, 1 µM E2 protein, 1 µM E3 protein. The reactions were initiated by adding the E1 and carried out at 30 °C. At different time points, the reactions were quenched by mixing 4 µL aliquots of the reaction mixture with SDS loading dye and boiled for 5 minutes. The samples were then run out on SDSPAGE, and stained using a Colloidal Blue Staining Kit following the manufacturer's protocol. The unmodified E3 protein bands at the time points shown in the figures were quantified using ImageJ densitometry and normalized to the zero time points. Note that this quantification method monitors the disappearance of the 'starting material' but does not distinguish among the range of ubiquitinated products formed, and this product distribution pattern varies among different mutants. All assays were performed on at least two independent occasions with replicates showing similar results.

5.2.6 Cell culture and Western blotting

HeLa cells were seeded in 6-well plate, and transfected with 0.6 µg pcDNA3.1 PTEN C124S (note that catalytically defective C124S PTEN was used because wt PTEN was toxic to cells under these conditions) and 0.3 µg pcDNA3.1 Myc-WWP2 using

Lipofectamine 3000 (Invitrogen) when the cell confluency reached 70-90%. For OCT4, the cells were transfected with 0.4 μg pcDNA3.1 OCT4, 0.5 μg pRK HA-ubiquitin, and 0.6 μg pcDNA3.1 Myc-WWP2. 24 hours after transfection, the cells were lysed using RIPA buffer containing 1 mM PMSF and 1x Roche cocktail protease inhibitor. The lysate was mixed with SDS loading dye and boiled for 5 minutes. 30 μg of total protein (BCA assay) was subjected to SDSPAGE, and transferred to a nitrocellulose membrane using an iBlot dry blotting system (Thermo Fishier). The membranes were blocked with 5% BSA in TBST buffer for one hour, and then incubated with anti-PTEN antibody (1:50 dilution) or anti-OCT4 antibody (1:500 dilution), anti-Myc antibody (1:100 dilution), and anti-actin antibody (1:8000 dilution) at 4 °C overnight. Afterwards, the membranes were washed with TBST and probed with HRP-conjugated anti-mouse secondary antibody at 1:5000 dilution. The bands were detected by chemiluminescence using an ECL western blotting detection kit from GE Healthcare. All assays were repeated on at least two independent occasions with results and replicates showing similar results.

5.2.7 Fluorescence microscopy

To image fluorescent protein localizations in growing cells, HeLa cells were plated on eight-well chambered coverglasses (Lab-Tek, Thermo Scientific, Nunc), and when they reached 50% confluency, the cells were transfected with 50 ng pcDNA3.1 GFP-WWP2 using lipofectamine 3000. Cells were also co-transfected with 5 μL of BacMam 2.0 expressing RFP tagged Lamp-1 (Thermo Fishier) as a lysosome marker. After 24 hours, cells were imaged with a 40×/1.3 oil objective on a Zeiss Observer.Z1 inverted microscope. Images were acquired with GFP and RFP (where applicable) illumination using AxioVision software. These experiments were performed on 3

independent occasions and replicates gave consistent results. Classification of protein distribution across cells shown in Figure 41 was based on visual inspection from the combined replicates and based on examining at least 8 regions from the slides per WWP2 construct.

5.2.8 CRISPR knockout of WWP2 in SHSY5Y cells

We designed the guide RNA using the gene editing tools at benchling.com. Two guide RNA sequences were selected with relatively high on-target and off-target scores, targeting Exon 2 (TCTGCCAGCTCTAGCCGGGC) and Exon 3 (ACCTCGAATTAACTCCTACG). The constructs pSpCas9(BB)-2A-Puro-v2 carrying guide RNA sequence together with sgRNA and Cas9 protein were cloned following the protocol by Ran FA, et. al.(*210*) SHSY5Y neuroblastoma cells in 6-well plates with 70-90% confluency were transfected with the two plasmids (0.75 µg each) using Lipofectamine 3000. 24 hours after transfection, cells were incubated with 1 µg/mL puromycin for 48 hours. Then the cells were seeded into 96-well plates using serial dilutions for the selection of single clones. After three weeks, the single clones were expanded and tested for WWP2 knockout using western blot.

5.3 Results

5.3.1 Activation of WWP2 by 2,3-linker tyrosine phosphorylation

We considered how the linker interactions in WWP2 might be regulated under physiological conditions. Interestingly, there are two tyrosine phosphorylation sites, Tyr369 and Tyr392, which have been mapped previously by mass spectrometry to the

linker region of WWP2 and are mostly conserved in WWP1 and ITCH (Figure 37A) (*142, 207, 208*). We hypothesized that phosphorylation at one or both of these sites could influence WWP2 catalysis by disrupting interactions between the 2,3-linker and the HECT domain. Consistent with this, a pTyr369 containing synthetic 2,3-linker peptide was shown to be less potent as a WWP2 HECT domain inhibitor compared with the unmodified peptide (Figure 37B). To gain further insight into the role of pTyr369, we used protein semisynthesis (*158*) in the context of 2,3-linkerL-WW3-WW4-HECT WWP2 (aa 356-870) to site-specifically install a pTyr residue at this position. In this method, a synthetic peptide (aa 356-373) containing pTyr369 and a C-terminal thioester (*159*) is chemoselectively ligated to an N-Cys containing WWP2 recombinant fragment (Figure 38B,C) (*157*). This ligation strategy introduces a Cys in place of Ser374, which was shown to be non-perturbing for WWP2 catalysis (Figure 38A). The extended linker, 2,3-linkerL, was selected for semisynthetic WWP2 construction since it incorporates the C-terminal residues of the WW2 domain that contribute to autoinhibition (Figure 31C,D and Figure 32A).

As expected, pTyr369-2,3-linkerL-WW3-WW4-HECT WWP2 was observed to have markedly enhanced autoubiquitination activity compared with non-phosphorylated control (Figure 38D). Although Glu is typically of limited reliability as a mimic of pTyr (*157*), analysis of the autoinhibited WWP2 crystal structure suggested that Glu replacement of Tyr369 or Tyr392 could be similarly disruptive as tyrosine phosphorylation to the linker-HECT interactions. Replacement of either Tyr369 or Tyr392 with Glu as the single or double mutants in recombinant full-length WWP2 stimulated its autoubiquitination activity, although these Y/E mutants were still less active than full 2,3-linker deletion (Figure 39A). In addition to stimulating WWP2 autoubiquitination activity, Y369E and Y392E also showed enhanced ubiquitin transferase activity toward PTEN

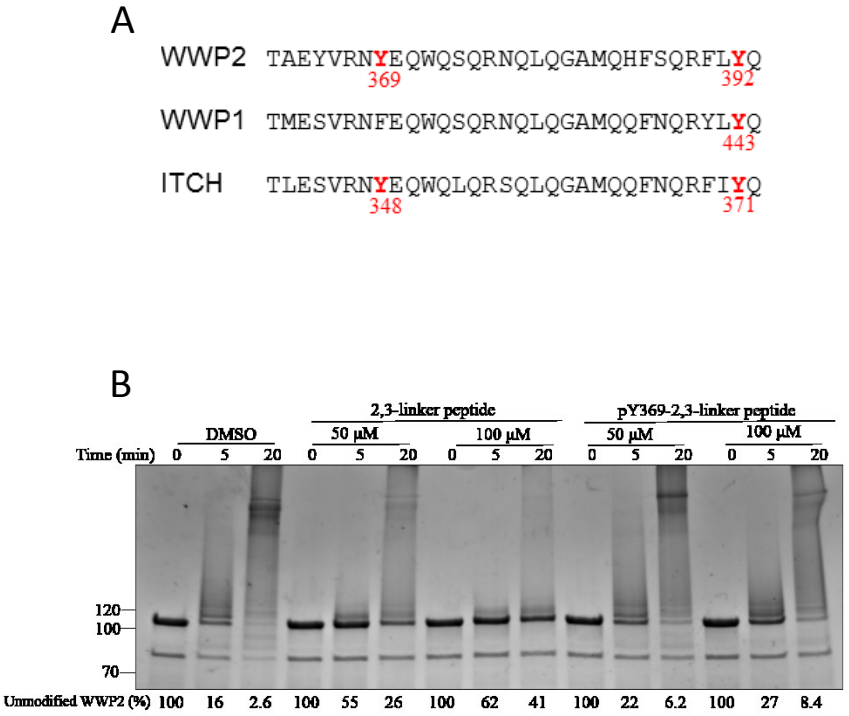

Figure 37: Conserved Tyrosine phosphorylation sites in the WWP2 2,3-linkers and E3 ligase regulation, and their potential role to disrupt the autoinhibition. (A) Known tyrosine phosphorylation sites in 2,3-linker region of WWP2/WWP1/ITCH from phosphositeplus.com. (B) Ubiquitination assays of WWP2 △2,3-linker with different concentrations of 2,3-linker peptide with or without Tyr369 phosphorylation. Unphosphorylated 0, 50 and 100 μM 2,3-linker peptide with natural sequence (2,3-linker peptide) or with phosphorylated Tyr369 (pY369-2,3-linker peptide) was added to the reaction, and the reaction was quenched at the indicated times.

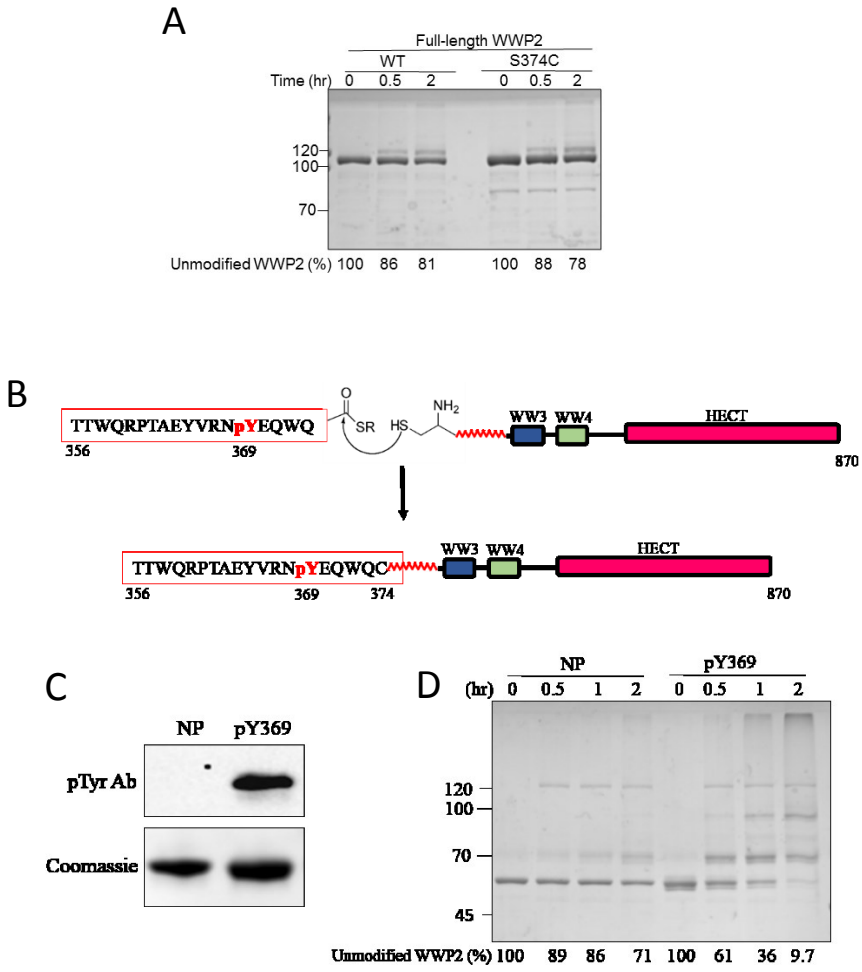

Figure 38: Activation of WWP2 autoinhibition by Tyrosine 369 phosphorylation revealed by N-terminal expressed protein ligation. (A) Ubiquitination assay of wild-type or S374C mutant WWP2. Ser374 was mutated to cysteine for N-terminal native chemical ligation. Here the full-length recombinant WWP2 S374C mutant was assayed and its activity compared to wt WWP2. The reaction was performed as described in Figure 24B, and quenched at the indicated times. (B) Schematic diagram showing the strategy for semisynthesis of pY369-2,3-linkerL-WW3-WW4-HECT using so-called 'native chemical ligation.' The peptide (n-TTWQRPTAEYVRNpYEQWQ-c) with a C-terminal thioester was reacted with the purified recombinant WWP2 protein fragment aa374-870 possessing an N-terminal Cys S374C generating pY369-2,3-linkerL-WW3-WW4-HECT protein (aa356-870). (C) Western blot of the non-phosphorylated (NP) and phosphorylated (pY369) 2,3-linkerL-WW3-WW4-HECT proteins using anti-phosphorylated tyrosine antibody (4G10). (D) Ubiquitination assays of non-phosphorylated (NP) and phosphorylated (pY369) 2,3-linkerL-WW3-WW4-HECT. The reaction was conducted as described in Figure 24B, and quenched at the times indicated.

using both coomassie staining and western blot (Figure 39B,C). In contrast, a tyrosine to phenylalanine mutation at Tyr369 or Tyr392 showed no appreciable effect (Figure 39D,E). The crystal structure of WWP2 (Figure 40A,B,D) showed that Tyr369 contributes to the ubiquitin-binding exosite while Tyr392 sits on the hinge, indicating different roles for these two phospho-modifications. We tested the mechanistic impact of pTyr369 and pTyr392 on WWP2 by measuring the binding affinities of UbF1 for WW2-2,3-linker-HECT Y369E and WW2-2,3-linker-HECT Y392E. These measurements showed that WW2-2,3-linker-HECT Y369E (UbF1 K_d of 0.86 μM) was much more available to ubiquitin binding at its exosite relative to WW2-2,3-linker-HECT Y392E (UbF1 K_d of 5.8 μM) as predicted by the crystal structures (Figure 40). These results establish distinct mechanisms of activation by the 2,3-linker tyrosine phosphorylation modifications at each end of the 2,3-linker.

5.3.2 Cellular analysis of the role of the 2,3-linker in WWP2 regulation

Investigation of the cellular properties of WWP2 2,3-linker mutants using HeLa cell transfections showed that Myc-tagged full-length WWP2 containing a 2,3-linker deletion (ΔLinker) generated less WWP2 detectable by western blot than the wt WWP2 protein (Figure 41A,B). We hypothesized that such reduced WWP2 detection could be related to highly autoubiquitinated ΔLinker WWP2, which might be degraded or sequestered. Consistent with these possibilities, ΔLinker WWP2 carrying a catalytically inactivating (C838S) mutation restored wild type WWP2 levels on western blot presumably because the autoubiquitination was eliminated (Figure 41A,B).

Live cell imaging demonstrated that GFP-tagged full-length ΔLinker WWP2 was co-localized with LAMP-1, the lysosomal marker, rather than showing the diffuse

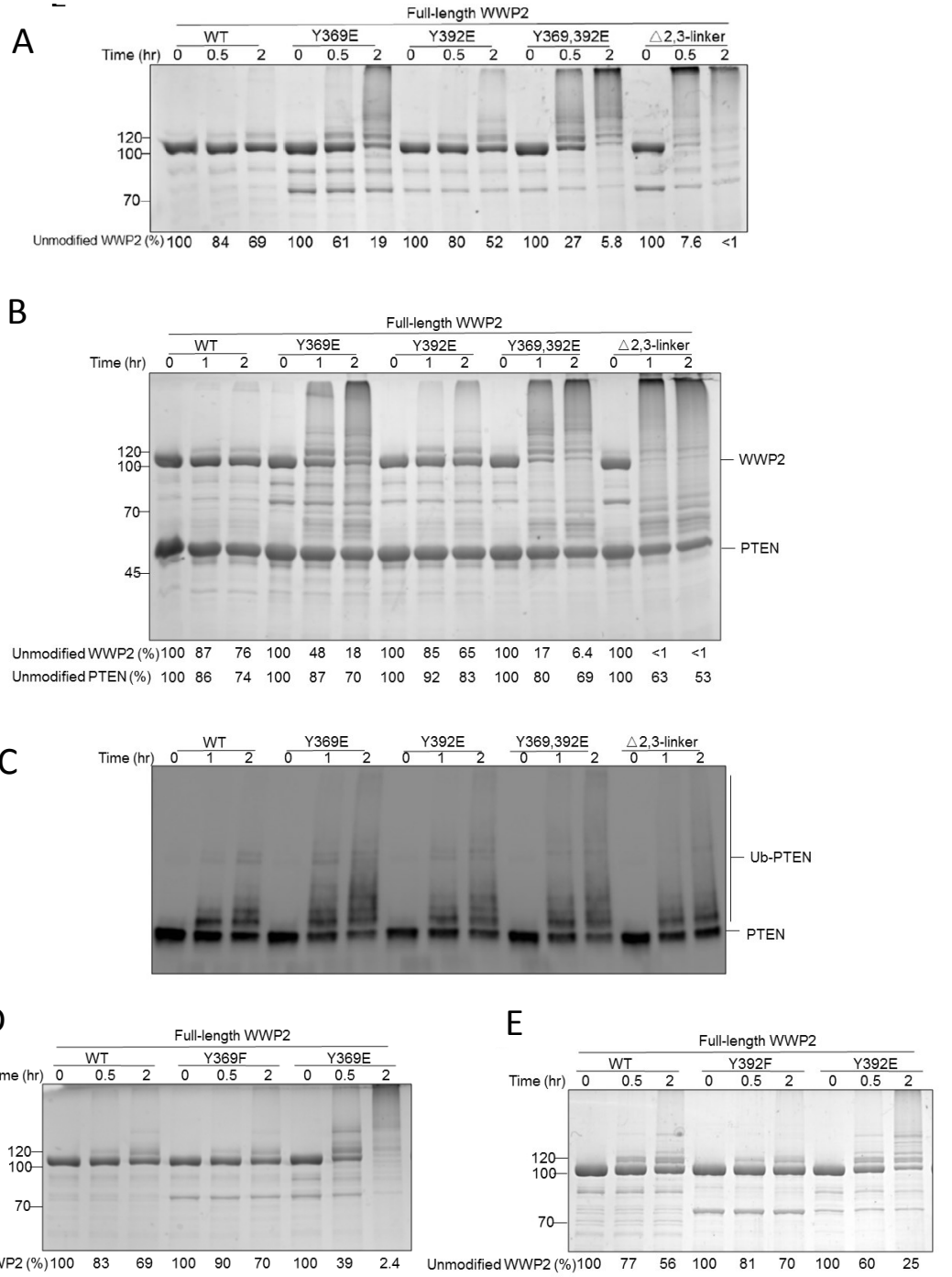

Figure 39: Tyrosine to glutamate mutation activates WWP2 E3 ligase activity. (A) Ubiquitination assays of full-length wt WWP2 and the tyrosine to glutamate mutant forms (Y369E, Y392E, and Y369,392E). The reaction was carried out as described in Figure 24B and quenched at the times indicated. (C) Ubiquitination assays of full-length wt WWP2 and the tyrosine to glutamate mutant forms (Y369E, Y392E, and Y369, 392E) and the 2,3-linker deleted form using PTEN as substrate. The reaction was carried out as described in Figure 24B with 5 μM PTEN, and quenched at the times indicated. (D) Immunoblot analysis of the ubiquitination assay in Figure 39C using PTEN antibody. (E) Ubiquitination assay of wt full-length WWP2 and the Y369E and Y369F mutant forms. The assay was carried out as described in Figure 24B, and the reaction was quenched at 0, 0.5 and 2 hours. (F) Ubiquitination assay of wt full-length WWP2 and the Y392E and Y392F mutant forms done in the same way as Figure 39E.

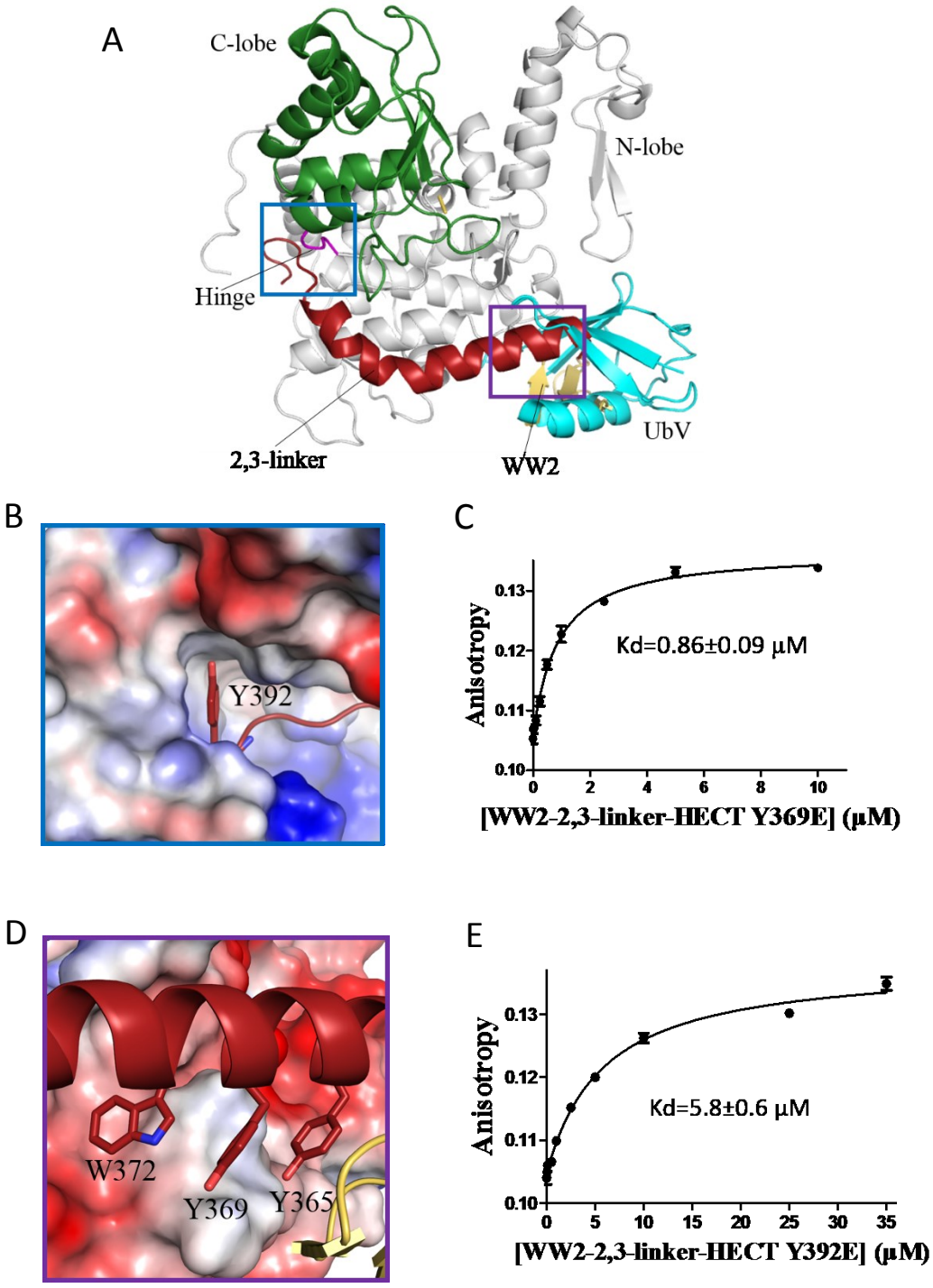

Figure 40: Structural mechanism for the Y369 and Y392 phosphorylation mediated activation of WWP2. (A) Overall structure of the WW2-2,3-linker-HECT protein superimposed with the UbV P2.3 structure. Local environments of Tyr369 (purple) and Tyr392 (blue) are highlighted by squares. (B) Zoom-in structure in the vicinity of Tyr369. Tyr369 (red, stick) appears to make pi-stacking interactions with the sidechains of Tyr365 and Trp372 near the N-terminus of the 2,3-linker helix (red, cartoon). The HECT domain is shown as electrostatic surface (blue, red, and white). (C) Fluorescence anisotropy binding of UbF1 to WW2-2,3-linker-HECT Y369E. (D) Zoom-in structure in the vicinity of Tyr392. (E) Fluorescence anisotropy binding of UbF1 to WW2-2,3-linker-HECT Y392E. All the assays were repeated at least twice (n≥2) and shown good reproducibility.

distribution observed for wt GFP-WWP2 (Figure 41C). This is compatible with previous findings that polyubiquitinated (K63) proteins can be targeted to lysosomes (*80, 211*). Experiments with C838S ΔLinker GFP-WWP2 revealed a wild-type WWP2-like cellular distribution, indicating a catalytic dependence for lysosomal localization of ΔLinker WWP2 (Figure 41C). These results highlight that unrestrained autoubiquitination activity could derail the E3 ligase from executing its normal functions. To test this idea, we performed co-transfections of WWP2 forms with the WWP2 substrate PTEN. In this experiment, it was found that wt full-length WWP2 reduced cellular PTEN protein, whereas ΔLinker WWP2 did not. The PTEN effects were reciprocal to WWP2 expression levels (Figure 42A,B) implying that uncontrolled, hyperactive WWP2 is disabled from targeting substrates because of self-destruction.

We also investigated the potential impact of WWP2 tyrosine phosphorylation in a cellular context with PTEN by transfecting HeLa cells with Myc-tagged full-length WWP2 Y369E and Y369F. Y369E, Y369F, and wt WWP2 showed similar expression by western blot under these conditions (Figure 43A,B), suggesting that Y369E was more catalytically restrained than ΔLinker WWP2 which is consistent with the in vitro assays (Figure 39B). However, Y369E WWP2 transfection more powerfully reduced PTEN and OCT4 level than either wt or Y369F WWP2 (Figure 43A,B,C,D). To confirm that this PTEN protein level change is due to reduced protein stability, we treated transfected HeLa cells with cycloheximide (CHX) to block protein biosynthesis. These experiments showed that for up to 6 hours after CHX treatment, the WWP2 protein forms are fairly stable, but the PTEN level in Y369E WWP2 transfected cells showed significantly faster degradation than that in wt or Y369F WWP2 transfected cells (Figure 43E,F). The transfection of Myc-tagged full-length Y392E and Y392F WWP2 forms showed similar results with those of the corresponding Y369 mutant WWP2s (Figure 44A,B). Taken

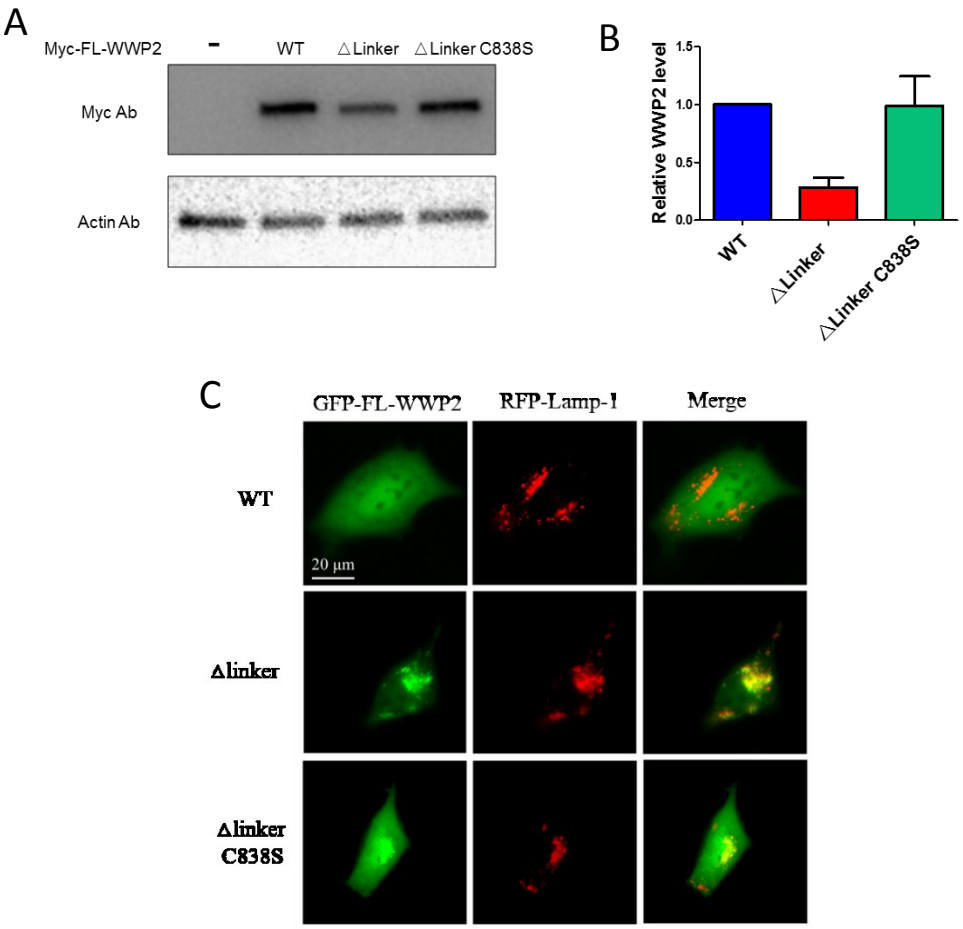

Figure 41: Expression and localization of WWP2 △2,3-linker in Hela cells. (A) Western blot analysis of WWP2 WT, WWP2 △2,3-linker, WWP2 △2,3-linker C838S in HeLa cells. HeLa cells were transfected with plasmids expressing N-terminally Myc-tagged full-length WWP2 forms: wild-type (WT), 2,3-linker deleted (△linker), and 2,3-linker deleted/C838S (△linker, C838S) for 24 hours, lysed, and analyzed by western blot using anti-Myc antibody and anti-actin antibody. (B) Quantification of WWP2 expression level. WWP2 and actin bands were quantified by densitometric analysis using Image J software. Relative WWP2 protein level was calculated by normalization with actin as loading control. (n=5, SEM shown). (C) Live-cell fluorescence analysis of WWP2 localization in HeLa cells. HeLa cells were transfected with plasmids expressing N-terminally GFP-tagged full-length WWP2 forms: WT, △2,3-linker, and △2,3-linker/C838S, and co-transfected with BamMam 2.0 (lysosome marker RFP-tagged LAMP-1) for 24 hours and then imaged. The GFP and RFP signals were analyzed and merged to show the localization of different WWP2s. Shown are representative cells from WT (appearance of 40 out of 44 cells examined), △2,3-linker (appearance of 41 out of 52 cells examined), and △2,3-linker/C838S (appearance of 30 out of 35 cells examined).

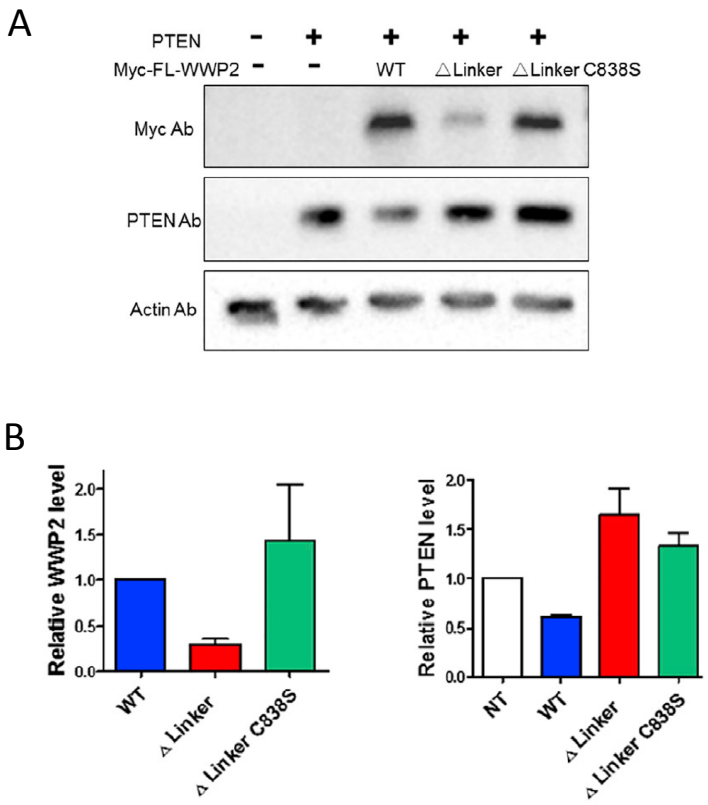

Figure 42: Activity of WWP2 △2,3-linker on PTEN substrate in Hela cells. (A) Western blot analysis of WWP2 WT, WWP2 △2,3-linker, WWP2 △2,3-linker C838S in HeLa cells. HeLa cells were transfected with plasmids expressing N-terminally Myc-tagged full-length WWP2 forms: wild-type (WT), 2,3-linker deleted (△linker), and 2,3-linker deleted/C838S (△linker, C838S), and co-transfected with catalytically impaired PTEN (C124S) for 24 hours, lysed, and analyzed by western blot using anti-Myc antibody anti-PTEN antibody and anti-actin antibody. (B) Quantification of WWP2 and PTEN expression level. WWP2, PTEN and actin bands were quantified by densitometric analysis using Image J software. Relative WWP2 and PTEN protein level was calculated by normalization with actin as loading control. (n=3, SEM shown)

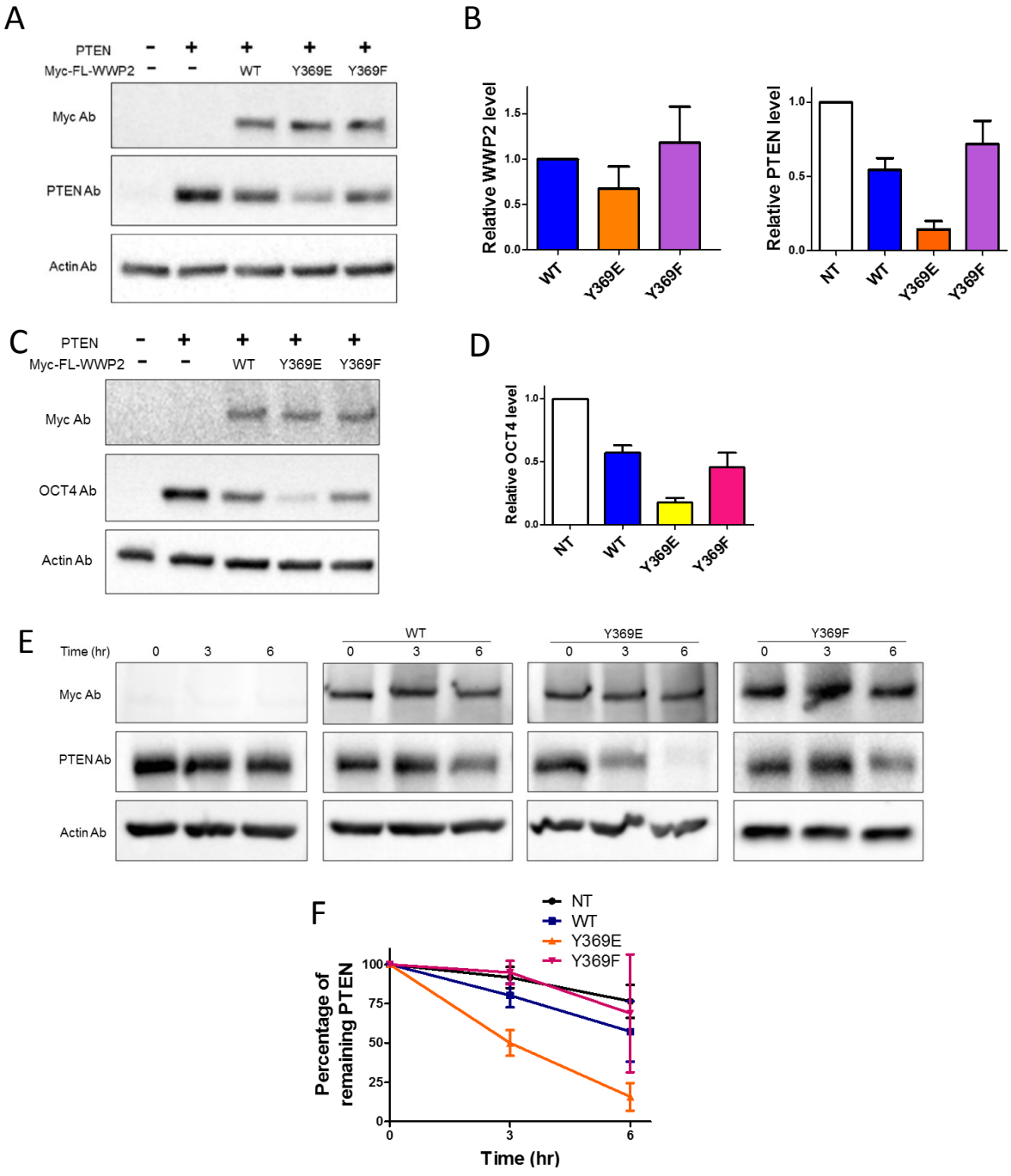

Figure 43: Tyrosine 369 phosphorylation regulates WWP2 activity on PTEN and OCT4 substrates. (A) Western blot analysis of PTEN levels in HeLa cells transfected with N-terminally Myc-tagged WWP2 forms and co-transfected with PTEN (C124S). After 24 hours, cells were lysed and analyzed by western blot using anti-Myc, anti-PTEN and anti-actin antibodies. (B) Densitometry analysis of WWP2 and PTEN levels of data in Figure 43A. (n=4, SEM shown). (C) Western blot analysis of OCT4 levels in HeLa cells co-transfected with Myc-tagged WWP2 forms, HA-ubiquitin and OCT4. After 24 hours, transfected cells were lysed and analyzed by western blot using anti-Myc, anti-OCT4 and anti-actin antibodies. (D) Densitometry analysis of OCT4 levels. (n=3, SEM shown). (E) HeLa cells transiently expressing PTEN were co-transfected without or with Myc-tagged wild-type WWP2, Y369E WWP2, or Y369F WWP2. 24 hours post-transfection, cells were treated with cycloheximide (CHX) for 0, 3, and 6 hours, lysed and analyzed by western blot. (n=3) (F) Densitometry quantification of the protein level change of PTEN after cycloheximide treatment in Figure 43E.

together, these results imply that 2,3-linker WWP2 phosphorylation has the potential to enhance WWP2-mediated protein substrate ubiquitination in cells.

5.3.3 Genome-editing of WWP2 in SHSY5Y cells

The cellular studies above were dependent on transfection and overexpression, the results of which could be misleading. To gain further insights into the regulation of WWP2 in the cell, we employed the CRISPR/Cas9 based genome-editing technique to delete WWP2 in a cancer cell line.

We first tested the expression level of endogenous WWP2 and PTEN in different cell lines. As indicated by the western blot results (Figure 45A), among HEK293, HeLa, SHSY5Y and PC3, SHSY5Y has the highest expression of both WWP2 and PTEN. We thererfore chose the SHSY5Y neuroblastoma cell line to do the following CRISPR experiments.

Among 35 clones tested, there were at least five with undetectable WWP2 expression (Figure 45B). Interestingly, for the knockout cells, there appeared a lower band detected by WWP2 antibody. We speculate that it is the transcript variant of WWP2 which does not contain the first five exons and the translational product is a truncated WWP2 without C2 domain. This WWP2 transcript variant has been reported to be involved in cell cycle regulation(*212*). Our result indicates that the expression of the truncated transcript variant increased after the knockout of full-length WWP2, probably through a compensation mechanism. Since the NEDD4 family members are closely related, we wondered whether the knockout of WWP2 would lead to increase of other NEDD4 E3s. As hypothesized, the protein level of NEDD4-1, NEDD4-2 and ITCH was

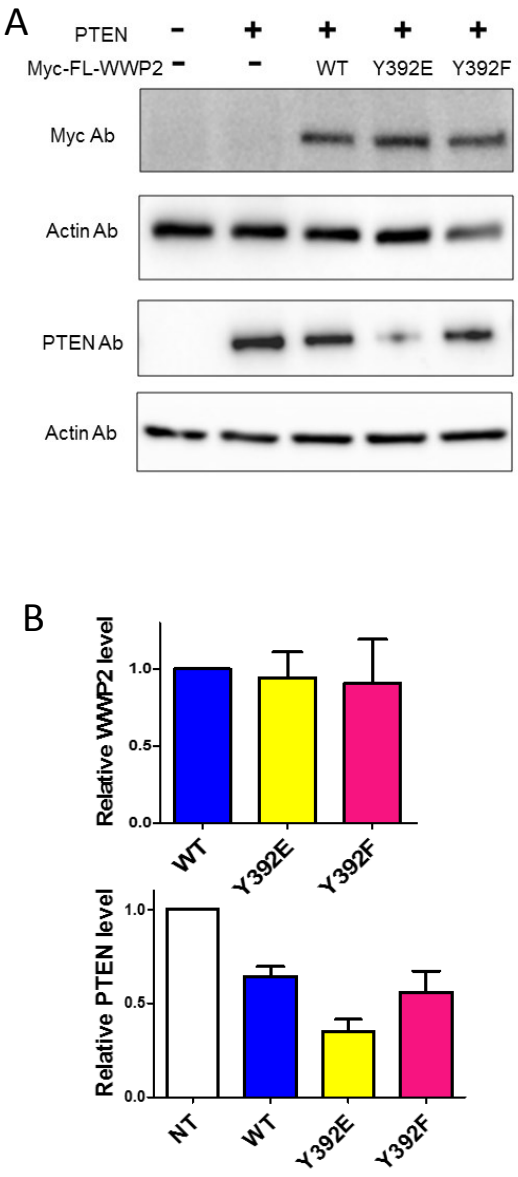

Figure 44: Tyrosine 392 phosphorylation regulates WWP2 activity on PTEN substrate. (A) Western blot analysis of PTEN levels in HeLa cells transfected with N-terminally Myc-tagged WWP2 forms and co-transfected with PTEN (C124S). After 24 hours, cells were lysed and analyzed by western blot using anti-Myc, anti-PTEN and anti-actin antibodies. (B) Densitometry analysis of WWP2 and PTEN levels. (n=4, SEM shown).

elevated compared to wild-type (Figure 45C). It remains to be investigated whether this increase is due to transcriptional activation or because other NEDD4 members are the substrates of WWP2. We also found that PTEN, as the canonical substrate of WWP2, was increased after WWP2 knockout. Increased PTEN typically leads to inactivation of the AKT signaling pathway, and indeed we also detected decreased AKT308 and AKT473 phosphorylation (Figure 45C).

At the time of writing this thesis, the ongoing work is focused on making the Y369E mutation in WWP2 gene in SHSY5Y cells using CRISPR. The goal is to introduce the mutation to mimic phosphorylation and generate endogenous WWP2 with activated ubiquitin transferase activity. With this model, we will be able to interrogate the biological roles of WWP2 phosphorylation and activation.

5.4 Discussion

Although the precise signaling mechanisms remain to be elucidated, tyrosine phosphorylation of the 2,3-linker in WWP2 was shown to be a potential mechanism to relieve autoinhibition. That tyrosine phosphorylation takes place within an α-helical segment is notable, since tyrosine kinases generally bind substrate motifs in extended conformations (*213*). We assume that when the linker dissociates from its intramolecular interactions with the HECT domain it would be flexible and can adopt a conformation suitable for kinase recognition. We found that the two different tyrosine phosphorylation sites confer distinct mechanisms to relieve autoinhibition (Figure 46). When the N-terminus of the 2,3-linker is phosphorylated, allosteric activation by ubiquitin is enabled (Figure 46). When the C-terminus of the 2,3-linker is phosphorylated, destabilization of the T-shape conformation is proposed to be facilitated (Figure 46). It is

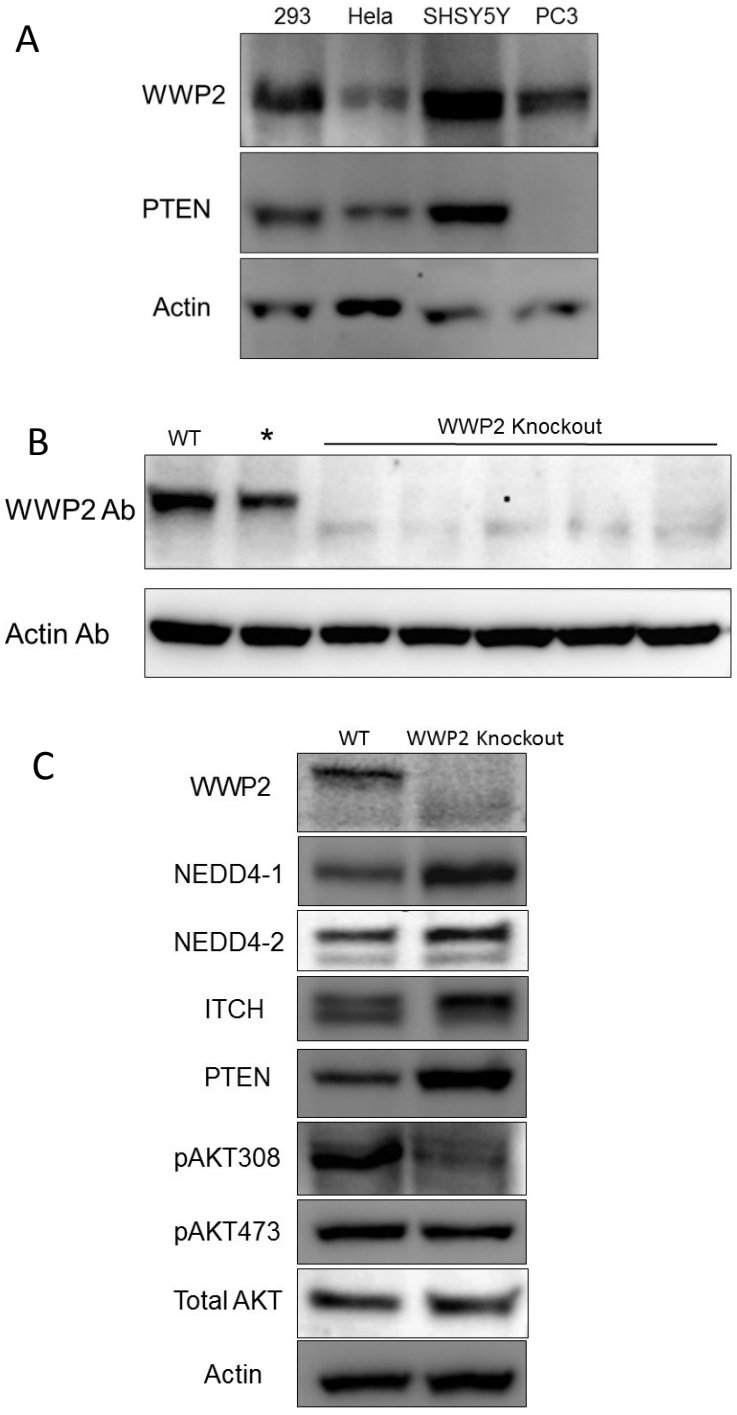

Figure 45: CRISPR knockout of WWP2 in SHSY5Y cells. (A) Western blot analysis of WWP2 and PTEN levels in HeLa, HEK293, SHSY5Y and PC3 cells. (B) Western blot analysis of WWP2 expression for the clones after CRISPR knockout. *the sample from the clone in which WWP2 was not knocked out. (C) Western blot analysis of the related protein expression level in WWP2 knockout cell line.

plausible that such compartmentalized activation mechanisms may drive specific biological outputs. Prior work on ITCH suggested that the conserved 2,3-linker WWP2 Tyr392 residue (Tyr371 in ITCH) is phosphorylated by Fyn tyrosine kinase leading to ITCH down-regulation (*142*). However, this conclusion was based on a Tyr to Phe mutation (*142*) which is silent in WWP2 but may have partly relieved autoinhibition of the 2,3-linker in the case of ITCH if the sidechain phenol is important for facilitating HECT interaction. We believe that Tyr371 phosphorylation in ITCH is more likely to be activating based on the complete set of results for the close paralog WWP2 and the ITCH linker deletion results presented here.

It is noteworthy that several WWP2, WWP1, and ITCH cancer mutations fall in the 2,3-linker/HECT autoinhibited interface and such constitutive activation of these E3 ligases may enhance tumor cell growth. Although more work will be needed to assess the precise contributions of these mutations to cancer, the degree of activation seen for these WWP2 cancer mutations in vitro are far lower than 2,3-linker deleted WWP2, which self-inactivated, but in the same range as the Y/E WWP2 mutations which led to PTEN reductions in our transfection experiments.

The tyrosine phosphorylation in the linker of ITCH has been shown to be catalyzed by Fyn, a Src tyrosine kinase(*142*). Nothing is known about the kinase for WWP2/WWP1 phosphorylation. It would be interesting to investigate the kinases that phosphorylate WWP2 Y369 and Y392, what signaling pathways they are involved in, and what biological functions they mediate. It is plausible that these two phosphorylation sites are catalyzed by different kinases and carry out distinct biological functions. It has been challenging for us to identify WWP2 Y369 phosphorylation in the cell lines I tested presumably due to the low abundance of WWP2 and probably low stoichiometry of phosphorylation. The level of tyrosine phosphorylation in WWP2 might be cell type

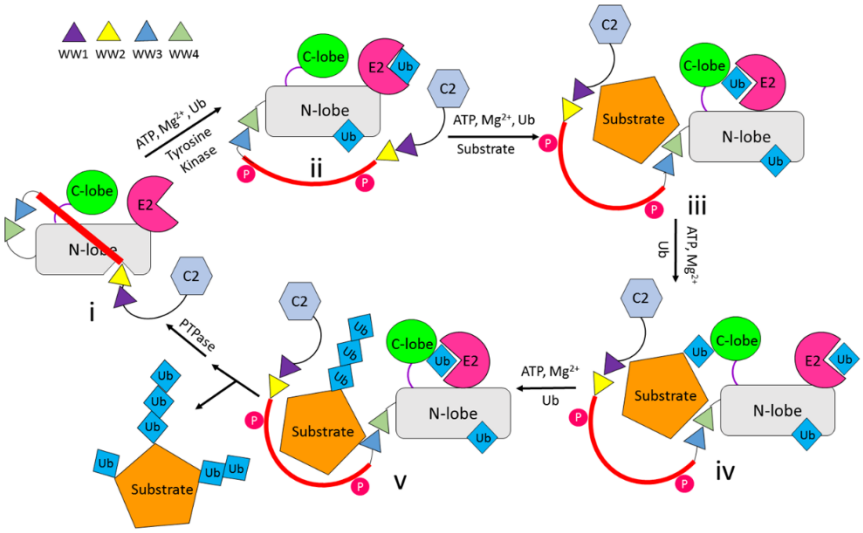

Figure 46: Proposed model of HECT E3 ligase activation. The ground-state T-shape WWP2 (i) is autoinhibited but upon phosphorylation (ii), the 2,3-linker interactions with the hinge and the ubiquitin-binding exosite is loosened allowing ubiquitin to bind. In (iii) E2-mediated ubiquitination of WWP2 takes place and protein substrate binds (the protein substrate can also be a separate WWP2 molecule). In (iv) and (v) protein substrate mono- and poly-ubiquitination occurs. After protein tyrosine phosphatase (PTPase) removes 2,3-linker phosphorylations, WWP2 returns to its autoinhibited ground state conformation (i).

specific, or transient in response to certain signaling events. Another possibility is that the phosphorylated and activated WWP2 is not stable and gets degraded quickly. Overall, a better understanding of WWP2 phosphorylation under physiological and pathological conditions will be necessary for a full picture of the biology of WWP2 and other HECT E3 ligases.

In addition to phosphorylation, our data also suggests the potential role of dimerization/oligomerization in activating autoinhibited WWP2. Dimeric WWP2 and the aggregated form of WWP2 show higher activity than monomeric WWP2 (Figure 24 and Figure 25). How apparent dimer-induced activation of WWP2, described in Section 4, relates to the 2,3-linker remains to be determined but may provide yet another cellular mechanism to ensure a proper level of protein ubiquitin transfer activity.

In summary, the internal linkers found between WW domains in WWP2/WWP1/ITCH/NEDD4-1 serve as a tunable brake for the regulation of ubiquitin transferase activity. Non-phosphorylated linker keeps the enzyme dormant, while phosphorylation or dimerization partially relieves the linker engagement and activates the ubiquitination activity. However, complete removal of the brake leads to hyperactivation and self-destruction (Figure 46). The structural and regulatory features discovered here should provide guidance to more detailed biological studies of these enzymes and aid in the drug development of modulators of the HECT E3 ligases.

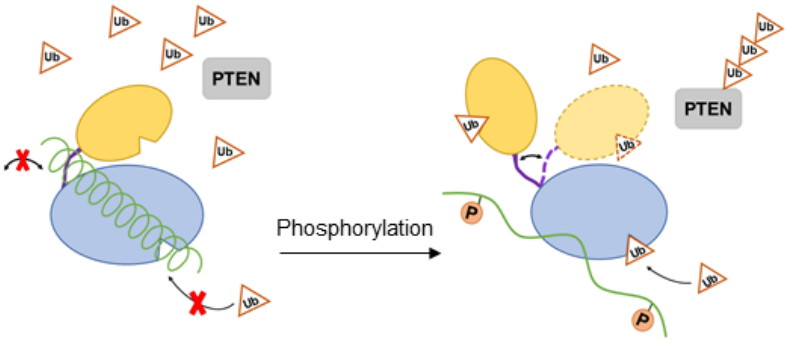

Figure 47: Proposed model of WWP2 regulation. The HECT domain of autoinhibited WWP2 is wrapped by the linker α-helix which blocks allosteric ubiquitin binding site (exosite) and constrains the hinge loop, locking the HECT domain in T-shape conformation. The activity of the HECT E3 ligase is inhibited so the substrate protein stays intact. Upon phosphorylation of the linker residues, the linker dissociates from the HECT domain, relieving the autoinhibition, so that it can catalyze the ubiquitin transfer and leads to ubiquitination and degradation of substrate protein. However, complete removal of linker causes hyperactivation and self-destruction of the E3 ligase.

References

1. S. Prabakaran, G. Lippens, H. Steen, J. Gunawardena, Post-translational modification: nature's escape from genetic imprisonment and the basis for dynamic information encoding. *Wiley Interdiscip Rev Syst Biol Med.* **4**, 565-583 (2012).
2. C. T. Walsh, S. Garneau-Tsodikova, G. J. Gatto, Jr., Protein posttranslational modifications: the chemistry of proteome diversifications. *Angew Chem Int Ed Engl.* **44**, 7342-7372 (2005).
3. D. G. Knorre, N. V. Kudryashova, T. S. Godovikova, Chemical and functional aspects of posttranslational modification of proteins. *Acta Naturae.* **1**, 29-51 (2009).
4. G. Duan, D. Walther, The roles of post-translational modifications in the context of protein interaction networks. *PLoS Comput Biol.* **11**, e1004049 (2015).
5. T. M. Karve, A. K. Cheema, Small changes huge impact: the role of protein posttranslational modifications in cellular homeostasis and disease. *J Amino Acids.* **2011**, 207691 (2011).
6. P. Beltrao, P. Bork, N. J. Krogan, V. van Noort, Evolution and functional cross-talk of protein post-translational modifications. *Mol Syst Biol.* **9**, 714 (2013).
7. T. Maehama, J. E. Dixon, The tumor suppressor, PTEN/MMAC1, dephosphorylates the lipid second messenger, phosphatidylinositol 3,4,5-trisphosphate. *J Biol Chem.* **273**, 13375-13378 (1998).
8. C. A. Worby, J. E. Dixon, Pten. *Annu Rev Biochem.* **83**, 641-669 (2014).
9. L. C. Cantley, The phosphoinositide 3-kinase pathway. *Science.* **296**, 1655-1657 (2002).

10. V. Stambolic *et al.*, Negative regulation of PKB/Akt-dependent cell survival by the tumor suppressor PTEN. *Cell.* **95**, 29-39 (1998).

11. J. Li *et al.*, The PTEN/MMAC1 tumor suppressor induces cell death that is rescued by the AKT/protein kinase B oncogene. *Cancer Res.* **58**, 5667-5672 (1998).

12. I. Sansal, W. R. Sellers, The biology and clinical relevance of the PTEN tumor suppressor pathway. *J Clin Oncol.* **22**, 2954-2963 (2004).

13. I. U. Ali, L. M. Schriml, M. Dean, Mutational spectra of PTEN/MMAC1 gene: a tumor suppressor with lipid phosphatase activity. *J Natl Cancer Inst.* **91**, 1922-1932 (1999).

14. Z. H. Chen *et al.*, PTEN interacts with histone H1 and controls chromatin condensation. *Cell Rep.* **8**, 2003-2014 (2014).

15. M. Raftopoulou *et al.*, Regulation of cell migration by the C2 domain of the tumor suppressor PTEN. *Science.* **303**, 1179-1181 (2004).

16. J. O. Lee *et al.*, Crystal structure of the PTEN tumor suppressor: implications for its phosphoinositide phosphatase activity and membrane association. *Cell.* **99**, 323-334 (1999).

17. X. Wang *et al.*, Crucial role of the C-terminus of PTEN in antagonizing NEDD4-1-mediated PTEN ubiquitination and degradation. *Biochem J.* **414**, 221-229 (2008).

18. S. J. Miller *et al.*, Direct identification of PTEN phosphorylation sites. *FEBS Lett.* **528**, 145-153 (2002).

19. D. Bolduc *et al.*, Phosphorylation-mediated PTEN conformational closure and deactivation revealed with protein semisynthesis. *Elife.* **2**, e00691 (2013).

20. F. Vazquez, S. Ramaswamy, N. Nakamura, W. R. Sellers, Phosphorylation of the PTEN tail regulates protein stability and function. *Mol Cell Biol.* **20**, 5010-5018 (2000).

21. M. Rahdar *et al.*, A phosphorylation-dependent intramolecular interaction regulates the membrane association and activity of the tumor suppressor PTEN. *Proc Natl Acad Sci U S A.* **106**, 480-485 (2009).

22. F. Cordier *et al.*, Ordered phosphorylation events in two independent cascades of the PTEN C-tail revealed by NMR. *J Am Chem Soc.* **134**, 20533-20543 (2012).

23. J. Torres, R. Pulido, The tumor suppressor PTEN is phosphorylated by the protein kinase CK2 at its C terminus. Implications for PTEN stability to proteasome-mediated degradation. *J Biol Chem.* **276**, 993-998 (2001).

24. S. Mosessian *et al.*, Analysis of PTEN complex assembly and identification of heterogeneous nuclear ribonucleoprotein C as a component of the PTEN-associated complex. *J Biol Chem.* **284**, 30159-30166 (2009).

25. N. Amodio *et al.*, Oncogenic role of the E3 ubiquitin ligase NEDD4-1, a PTEN negative regulator, in non-small-cell lung carcinomas. *Am J Pathol.* **177**, 2622-2634 (2010).

26. F. Fouladkou *et al.*, The ubiquitin ligase Nedd4-1 is dispensable for the regulation of PTEN stability and localization. *Proc Natl Acad Sci U S A.* **105**, 8585-8590 (2008).

27. S. Maddika *et al.*, WWP2 is an E3 ubiquitin ligase for PTEN. *Nat Cell Biol.* **13**, 728-733 (2011).

28. C. Van Themsche, V. Leblanc, S. Parent, E. Asselin, X-linked inhibitor of apoptosis protein (XIAP) regulates PTEN ubiquitination, content, and compartmentalization. *J Biol Chem.* **284**, 20462-20466 (2009).

29. L. C. Trotman *et al.*, Ubiquitination regulates PTEN nuclear import and tumor suppression. *Cell.* **128**, 141-156 (2007).

30. X. Wang *et al.*, NEDD4-1 is a proto-oncogenic ubiquitin ligase for PTEN. *Cell.* **128**, 129-139 (2007).

31. J. Cao *et al.*, MC1R is a potent regulator of PTEN after UV exposure in melanocytes. *Mol Cell.* **51**, 409-422 (2013).

32. X. Wu *et al.*, Evidence for regulation of the PTEN tumor suppressor by a membrane-localized multi-PDZ domain containing scaffold protein MAGI-2. *Proc Natl Acad Sci U S A.* **97**, 4233-4238 (2000).

33. M. Valiente *et al.*, Binding of PTEN to specific PDZ domains contributes to PTEN protein stability and phosphorylation by microtubule-associated serine/threonine kinases. *J Biol Chem.* **280**, 28936-28943 (2005).

34. N. B. Adey *et al.*, Threonine phosphorylation of the MMAC1/PTEN PDZ binding domain both inhibits and stimulates PDZ binding. *Cancer Res.* **60**, 35-37 (2000).

35. Y. Takahashi, F. C. Morales, E. L. Kreimann, M. M. Georgescu, PTEN tumor suppressor associates with NHERF proteins to attenuate PDGF receptor signaling. *EMBO J.* **25**, 910-920 (2006).

36. R. B. Chagpar *et al.*, Direct positive regulation of PTEN by the p85 subunit of phosphatidylinositol 3-kinase. *Proc Natl Acad Sci U S A.* **107**, 5471-5476 (2010).

37. B. Davidson *et al.*, Expression and clinical role of DJ-1, a negative regulator of PTEN, in ovarian carcinoma. *Hum Pathol.* **39**, 87-95 (2008).

38. L. He *et al.*, alpha-Mannosidase 2C1 attenuates PTEN function in prostate cancer cells. *Nat Commun.* **2**, 307 (2011).

39. L. He, A. Ingram, A. P. Rybak, D. Tang, Shank-interacting protein-like 1 promotes tumorigenesis via PTEN inhibition in human tumor cells. *J Clin Invest.* **120**, 2094-2108 (2010).

40. C. Hodakoski *et al.*, Regulation of PTEN inhibition by the pleckstrin homology domain of P-REX2 during insulin signaling and glucose homeostasis. *Proc Natl Acad Sci U S A.* **111**, 155-160 (2014).

41. B. Fine *et al.*, Activation of the PI3K pathway in cancer through inhibition of PTEN by exchange factor P-REX2a. *Science.* **325**, 1261-1265 (2009).

42. Y. Hu *et al.*, MAGI-2 Inhibits cell migration and proliferation via PTEN in human hepatocarcinoma cells. *Arch Biochem Biophys.* **467**, 1-9 (2007).

43. T. Tolkacheva *et al.*, Regulation of PTEN binding to MAGI-2 by two putative phosphorylation sites at threonine 382 and 383. *Cancer Res.* **61**, 4985-4989 (2001).

44. R. Rabinovsky *et al.*, p85 Associates with unphosphorylated PTEN and the PTEN-associated complex. *Mol Cell Biol.* **29**, 5377-5388 (2009).

45. G. Goldstein *et al.*, Isolation of a polypeptide that has lymphocyte-differentiating properties and is probably represented universally in living cells. *Proc Natl Acad Sci U S A.* **72**, 11-15 (1975).

46. S. E. Kaiser *et al.*, Protein standard absolute quantification (PSAQ) method for the measurement of cellular ubiquitin pools. *Nat Methods.* **8**, 691-696 (2011).

47. Y. Kimura, K. Tanaka, Regulatory mechanisms involved in the control of ubiquitin homeostasis. *J Biochem.* **147**, 793-798 (2010).

48. C. M. Pickart, M. J. Eddins, Ubiquitin: structures, functions, mechanisms. *Biochim Biophys Acta.* **1695**, 55-72 (2004).

49. S. Vijay-Kumar, C. E. Bugg, W. J. Cook, Structure of ubiquitin refined at 1.8 A resolution. *J Mol Biol.* **194**, 531-544 (1987).

50. L. Buetow, D. T. Huang, Structural insights into the catalysis and regulation of E3 ubiquitin ligases. *Nat Rev Mol Cell Biol.* **17**, 626-642 (2016).

51. A. Hershko, A. Ciechanover, The ubiquitin system. *Annu Rev Biochem.* **67**, 425-479 (1998).

52. D. Komander, M. Rape, The Ubiquitin Code. *Annual Review Of Biochemistry, Vol 81.* **81**, 203-229 (2012).

53. H. D. Ulrich, H. Walden, Ubiquitin signalling in DNA replication and repair. *Nat Rev Mol Cell Biol.* **11**, 479-489 (2010).

54. C. Hoege *et al.*, RAD6-dependent DNA repair is linked to modification of PCNA by ubiquitin and SUMO. *Nature.* **419**, 135-141 (2002).

55. K. Robzyk, J. Recht, M. A. Osley, Rad6-dependent ubiquitination of histone H2B in yeast. *Science.* **287**, 501-504 (2000).

56. J. Jin, X. Li, S. P. Gygi, J. W. Harper, Dual E1 activation systems for ubiquitin differentially regulate E2 enzyme charging. *Nature.* **447**, 1135-1138 (2007).

57. Y. Ye, M. Rape, Building ubiquitin chains: E2 enzymes at work. *Nat Rev Mol Cell Biol.* **10**, 755-764 (2009).

58. W. Li *et al.*, Genome-wide and functional annotation of human E3 ubiquitin ligases identifies MULAN, a mitochondrial E3 that regulates the organelle's dynamics and signaling. *PLoS One.* **3**, e1487 (2008).

59. R. J. Deshaies, C. A. Joazeiro, RING domain E3 ubiquitin ligases. *Annu Rev Biochem.* **78**, 399-434 (2009).

60. F. Bernassola, M. Karin, A. Ciechanover, G. Melino, The HECT family of E3 ubiquitin ligases: multiple players in cancer development. *Cancer Cell.* **14**, 10-21 (2008).

61. J. J. Smit, T. K. Sixma, RBR E3-ligases at work. *EMBO Rep.* **15**, 142-154 (2014).

62. D. E. Spratt, H. Walden, G. S. Shaw, RBR E3 ubiquitin ligases: new structures, new insights, new questions. *Biochem J.* **458**, 421-437 (2014).

63. J. F. Trempe *et al.*, Structure of parkin reveals mechanisms for ubiquitin ligase activation. *Science.* **340**, 1451-1455 (2013).

64. D. Rotin, S. Kumar, Physiological functions of the HECT family of ubiquitin ligases. *Nat Rev Mol Cell Biol.* **10**, 398-409 (2009).

65. M. A. Verdecia *et al.*, Conformational flexibility underlies ubiquitin ligation mediated by the WWP1 HECT domain E3 ligase. *Mol Cell.* **11**, 249-259 (2003).

66. H. B. Kamadurai *et al.*, Insights into ubiquitin transfer cascades from a structure of a UbcH5B approximately ubiquitin-HECT(NEDD4L) complex. *Mol Cell.* **36**, 1095-1102 (2009).

67. H. B. Kamadurai *et al.*, Mechanism of ubiquitin ligation and lysine prioritization by a HECT E3. *Elife.* **2**, e00828 (2013).

68. H. C. Kim *et al.*, Structure and function of a HECT domain ubiquitin-binding site. *EMBO Rep.* **12**, 334-341 (2011).

69. W. Zhang *et al.*, System-Wide Modulation of HECT E3 Ligases with Selective Ubiquitin Variant Probes. *Mol Cell.* **62**, 121-136 (2016).

70. C. E. Berndsen, C. Wolberger, New insights into ubiquitin E3 ligase mechanism. *Nat Struct Mol Biol.* **21**, 301-307 (2014).

71. E. Maspero *et al.*, Structure of a ubiquitin-loaded HECT ligase reveals the molecular basis for catalytic priming. *Nat Struct Mol Biol.* **20**, 696-701 (2013).

72. A. A. Ogunjimi *et al.*, The ubiquitin binding region of the Smurf HECT domain facilitates polyubiquitylation and binding of ubiquitylated substrates. *J Biol Chem.* **285**, 6308-6315 (2010).

73. E. Maspero *et al.*, Structure of the HECT:ubiquitin complex and its role in ubiquitin chain elongation. *EMBO Rep.* **12**, 342-349 (2011).

74. M. E. French, B. R. Kretzmann, L. Hicke, Regulation of the RSP5 ubiquitin ligase by an intrinsic ubiquitin-binding site. *J Biol Chem.* **284**, 12071-12079 (2009).

75. C. Salvat *et al.*, The -4 phenylalanine is required for substrate ubiquitination catalyzed by HECT ubiquitin ligases. *J Biol Chem.* **279**, 18935-18943 (2004).

76. S. G. Kathman *et al.*, A Small Molecule That Switches a Ubiquitin Ligase From a Processive to a Distributive Enzymatic Mechanism. *J Am Chem Soc.* **137**, 12442-12445 (2015).

77. M. Gao *et al.*, Jun turnover is controlled through JNK-dependent phosphorylation of the E3 ligase Itch. *Science.* **306**, 271-275 (2004).

78. H. Xu *et al.*, WWP2 promotes degradation of transcription factor OCT4 in human embryonic stem cells. *Cell Res.* **19**, 561-573 (2009).

79. X. Zhi, C. Chen, WWP1: a versatile ubiquitin E3 ligase in signaling and diseases. *Cell Mol Life Sci.* **69**, 1425-1434 (2012).

80. F. Huang *et al.*, Lysine 63-linked polyubiquitination is required for EGF receptor degradation. *Proc Natl Acad Sci U S A.* **110**, 15722-15727 (2013).

81. W. Chen, X. Jiang, Z. Luo, WWP2: a multifunctional ubiquitin ligase gene. *Pathol Oncol Res.* **20**, 799-803 (2014).

82. M. Scheffner, S. Kumar, Mammalian HECT ubiquitin-protein ligases: biological and pathophysiological aspects. *Biochim Biophys Acta.* **1843**, 61-74 (2014).

83. D. Aki, W. Zhang, Y. C. Liu, The E3 ligase Itch in immune regulation and beyond. *Immunol Rev.* **266**, 6-26 (2015).

84. L. Broix *et al.*, Mutations in the HECT domain of NEDD4L lead to AKT-mTOR pathway deregulation and cause periventricular nodular heterotopia. *Nat Genet.* (2016).

85. J. M. Huibregtse, M. Scheffner, S. Beaudenon, P. M. Howley, A family of proteins structurally and functionally related to the E6-AP ubiquitin-protein ligase. *Proc Natl Acad Sci U S A.* **92**, 5249 (1995).

86. D. Martinez-Zapien *et al.*, Structure of the E6/E6AP/p53 complex required for HPV-mediated degradation of p53. *Nature.* **529**, 541-545 (2016).

87. R. Ohshima *et al.*, Putative tumor suppressor EDD interacts with and up-regulates APC. *Genes Cells.* **12**, 1339-1345 (2007).

88. X. Zhao *et al.*, The HECT-domain ubiquitin ligase Huwe1 controls neural differentiation and proliferation by destabilizing the N-Myc oncoprotein. *Nat Cell Biol.* **10**, 643-653 (2008).

89. L. Zhang *et al.*, The E3 ligase HACE1 is a critical chromosome 6q21 tumor suppressor involved in multiple cancers. *Nat Med.* **13**, 1060-1069 (2007).

90. F. R. Garcia-Gonzalo, R. Bartrons, F. Ventura, J. L. Rosa, Requirement of phosphatidylinositol-4,5-bisphosphate for HERC1-mediated guanine nucleotide release from ARF proteins. *FEBS Lett.* **579**, 343-348 (2005).

91. H. Chong-Kopera *et al.*, TSC1 stabilizes TSC2 by inhibiting the interaction between TSC2 and the HERC1 ubiquitin ligase. *J Biol Chem.* **281**, 8313-8316 (2006).

92. F. R. Garcia-Gonzalo, J. L. Rosa, The HERC proteins: functional and evolutionary insights. *Cell Mol Life Sci.* **62**, 1826-1838 (2005).

93. C. I. Rodriguez, C. L. Stewart, Disruption of the ubiquitin ligase HERC4 causes defects in spermatozoon maturation and impaired fertility. *Dev Biol.* **312**, 501-508 (2007).

94. K. Hochrainer *et al.*, Highly homologous HERC proteins localize to endosomes and exhibit specific interactions with hPLIC and Nm23B. *Cell Mol Life Sci.* **65**, 2105-2117 (2008).

95. R. Kroismayr *et al.*, HERC5, a HECT E3 ubiquitin ligase tightly regulated in LPS activated endothelial cells. *J Cell Sci.* **117**, 4749-4756 (2004).

96. J. J. Wong, Y. F. Pung, N. S. Sze, K. C. Chin, HERC5 is an IFN-induced HECT-type E3 protein ligase that mediates type I IFN-induced ISGylation of protein targets. *Proc Natl Acad Sci U S A.* **103**, 10735-10740 (2006).

97. P. J. Plant *et al.*, The C2 domain of the ubiquitin protein ligase Nedd4 mediates Ca2+-dependent plasma membrane localization. *J Biol Chem.* **272**, 32329-32336 (1997).

98. O. Staub *et al.*, WW domains of Nedd4 bind to the proline-rich PY motifs in the epithelial Na+ channel deleted in Liddle's syndrome. *EMBO J.* **15**, 2371-2380 (1996).

99. J. Jiang *et al.*, Characterization of substrate binding of the WW domains in human WWP2 protein. *FEBS Lett.* **589**, 1935-1942 (2015).

100. M. C. Bruce *et al.*, Regulation of Nedd4-2 self-ubiquitination and stability by a PY motif located within its HECT-domain. *Biochem J.* **415**, 155-163 (2008).

101. G. Spagnol *et al.*, Structural Studies of the Nedd4 WW Domains and Their Selectivity for the Connexin43 (Cx43) Carboxyl Terminus. *J Biol Chem.* **291**, 7637-7650 (2016).

102. V. Kanelis, D. Rotin, J. D. Forman-Kay, Solution structure of a Nedd4 WW domain-ENaC peptide complex. *Nat Struct Biol.* **8**, 407-412 (2001).

103. H. A. Fisk, M. P. Yaffe, A role for ubiquitination in mitochondrial inheritance in Saccharomyces cerevisiae. *J Cell Biol.* **145**, 1199-1208 (1999).

104. J. M. Huibregtse, J. C. Yang, S. L. Beaudenon, The large subunit of RNA polymerase II is a substrate of the Rsp5 ubiquitin-protein ligase. *Proc Natl Acad Sci U S A.* **94**, 3656-3661 (1997).

105. N. Belgareh-Touze *et al.*, Versatile role of the yeast ubiquitin ligase Rsp5p in intracellular trafficking. *Biochem Soc Trans.* **36**, 791-796 (2008).

106. J. Y. Lu *et al.*, Functional dissection of a HECT ubiquitin E3 ligase. *Mol Cell Proteomics.* **7**, 35-45 (2008).

107. K. Huang *et al.*, A HECT domain ubiquitin ligase closely related to the mammalian protein WWP1 is essential for Caenorhabditis elegans embryogenesis. *Gene.* **252**, 137-145 (2000).

108. J. W. Astin, N. J. O'Neil, P. E. Kuwabara, Nucleotide excision repair and the degradation of RNA pol II by the Caenorhabditis elegans XPA and Rsp5 orthologues, RAD-3 and WWP-1. *DNA Repair (Amst).* **7**, 267-280 (2008).

109. D. D. Shaye, I. Greenwald, LIN-12/Notch trafficking and regulation of DSL ligand activity during vulval induction in Caenorhabditis elegans. *Development.* **132**, 5081-5092 (2005).

110. T. Sakata *et al.*, Drosophila Nedd4 regulates endocytosis of notch and suppresses its ligand-independent activation. *Curr Biol.* **14**, 2228-2236 (2004).

111. A. Laine, Z. Ronai, Regulation of p53 localization and transcription by the HECT domain E3 ligase WWP1. *Oncogene.* **26**, 1477-1483 (2007).

112. X. R. Cao *et al.*, Nedd4 controls animal growth by regulating IGF-1 signaling. *Sci Signal.* **1**, ra5 (2008).

113. Z. Huang *et al.*, The E3 ubiquitin ligase NEDD4 negatively regulates HER3/ErbB3 level and signaling. *Oncogene.* **34**, 1105-1115 (2015).

114. A. Persaud *et al.*, Nedd4-1 binds and ubiquitylates activated FGFR1 to control its endocytosis and function. *EMBO J.* **30**, 3259-3273 (2011).

115. H. Zhu *et al.*, A SMAD ubiquitin ligase targets the BMP pathway and affects embryonic pattern formation. *Nature.* **400**, 687-693 (1999).

116. M. Yamashita *et al.*, Ubiquitin ligase Smurf1 controls osteoblast activity and bone homeostasis by targeting MEKK2 for degradation. *Cell.* **121**, 101-113 (2005).

117. Y. Zhang *et al.*, Regulation of Smad degradation and activity by Smurf2, an E3 ubiquitin ligase. *Proc Natl Acad Sci U S A.* **98**, 974-979 (2001).

118. P. M. Snyder, D. R. Olson, B. C. Thomas, Serum and glucocorticoid-regulated kinase modulates Nedd4-2-mediated inhibition of the epithelial Na+ channel. *J Biol Chem.* **277**, 5-8 (2002).

119. R. Zhou, S. V. Patel, P. M. Snyder, Nedd4-2 catalyzes ubiquitination and degradation of cell surface ENaC. *J Biol Chem.* **282**, 20207-20212 (2007).

120. O. Staub *et al.*, Regulation of the epithelial Na+ channel by Nedd4 and ubiquitination. *Kidney Int.* **57**, 809-815 (2000).

121. F. J. McDonald *et al.*, Ubiquitin-protein ligase WWP2 binds to and downregulates the epithelial Na(+) channel. *Am J Physiol Renal Physiol.* **283**, F431-436 (2002).

122. H. M. Xu *et al.*, Wwp2, an E3 ubiquitin ligase that targets transcription factor Oct-4 for ubiquitination. *J Biol Chem.* **279**, 23495-23503 (2004).

123. H. Li *et al.*, Wwp2-mediated ubiquitination of the RNA polymerase II large subunit in mouse embryonic pluripotent stem cells. *Mol Cell Biol.* **27**, 5296-5305 (2007).

124. H. Kawabe *et al.*, Regulation of Rap2A by the ubiquitin ligase Nedd4-1 controls neurite development. *Neuron.* **65**, 358-372 (2010).

125. F. Fouladkou *et al.*, The ubiquitin ligase Nedd4-1 is required for heart development and is a suppressor of thrombospondin-1. *J Biol Chem.* **285**, 6770-6780 (2010).

126. S. J. Bae *et al.*, NEDD4 controls intestinal stem cell homeostasis by regulating the Hippo signalling pathway. *Nat Commun.* **6**, 6314 (2015).

127. L. Xing, M. Zhang, D. Chen, Smurf control in bone cells. *J Cell Biochem.* **110**, 554-563 (2010).

128. Z. Xu *et al.*, SMURF2 regulates bone homeostasis by disrupting SMAD3 interaction with vitamin D receptor in osteoblasts. *Nat Commun.* **8**, 14570 (2017).

129. N. Xiao *et al.*, The E3 ubiquitin ligase Itch is required for the differentiation of follicular helper T cells. *Nat Immunol.* **15**, 657-666 (2014).

130. Y. C. Liu, The E3 ubiquitin ligase Itch in T cell activation, differentiation, and tolerance. *Semin Immunol.* **19**, 197-205 (2007).

131. G. Melino *et al.*, Itch: a HECT-type E3 ligase regulating immunity, skin and cancer. *Cell Death Differ.* **15**, 1103-1112 (2008).

132. H. Li *et al.*, Itch promotes the neddylation of JunB and regulates JunB-dependent transcription. *Cell Signal.* **28**, 1186-1195 (2016).

133. L. Qiu *et al.*, Recognition and ubiquitination of Notch by Itch, a hect-type E3 ubiquitin ligase. *J Biol Chem.* **275**, 35734-35737 (2000).

134. C. Lu *et al.*, Intestinal knockout of Nedd4 enhances growth of Apcmin tumors. *Oncogene.* **35**, 5839-5849 (2016).

135. Z. Yu *et al.*, Gamabufotalin triggers c-Myc degradation via induction of WWP2 in multiple myeloma cells. *Oncotarget.* **7**, 15725-15737 (2016).

136. J. G. Jung *et al.*, Notch3 interactome analysis identified WWP2 as a negative regulator of Notch3 signaling in ovarian cancer. *PLoS Genet.* **10**, e1004751 (2014).

137. S. Wiesner *et al.*, Autoinhibition of the HECT-type ubiquitin ligase Smurf2 through its C2 domain. *Cell.* **130**, 651-662 (2007).

138. S. Mari *et al.*, Structural and functional framework for the autoinhibition of Nedd4-family ubiquitin ligases. *Structure.* **22**, 1639-1649 (2014).

139. C. Riling *et al.*, Itch WW Domains Inhibit Its E3 Ubiquitin Ligase Activity by Blocking E2-E3 Ligase Trans-thiolation. *J Biol Chem.* **290**, 23875-23887 (2015).

140. A. Persaud *et al.*, Tyrosine phosphorylation of NEDD4 activates its ubiquitin ligase activity. *Sci Signal.* **7**, ra95 (2014).

141. E. Gallagher, M. Gao, Y. C. Liu, M. Karin, Activation of the E3 ubiquitin ligase Itch through a phosphorylation-induced conformational change. *Proc Natl Acad Sci U S A.* **103**, 1717-1722 (2006).

142. C. Yang *et al.*, Negative regulation of the E3 ubiquitin ligase itch via Fyn-mediated tyrosine phosphorylation. *Mol Cell.* **21**, 135-141 (2006).

143. C. Debonneville *et al.*, Phosphorylation of Nedd4-2 by Sgk1 regulates epithelial Na(+) channel cell surface expression. *EMBO J.* **20**, 7052-7059 (2001).

144. P. M. Snyder *et al.*, cAMP and serum and glucocorticoid-inducible kinase (SGK) regulate the epithelial Na(+) channel through convergent phosphorylation of Nedd4-2. *J Biol Chem.* **279**, 45753-45758 (2004).

145. I. H. Lee *et al.*, Akt mediates the effect of insulin on epithelial sodium channels by inhibiting Nedd4-2. *J Biol Chem.* **282**, 29866-29873 (2007).

146. T. Ichimura *et al.*, 14-3-3 proteins modulate the expression of epithelial Na+ channels by phosphorylation-dependent interaction with Nedd4-2 ubiquitin ligase. *J Biol Chem.* **280**, 13187-13194 (2005).

147. B. Cha *et al.*, Protein Arginine Methyltransferase 1 Methylates Smurf2. *Mol Cells.* **38**, 723-728 (2015).

148. P. Xie *et al.*, The covalent modifier Nedd8 is critical for the activation of Smurf1 ubiquitin ligase in tumorigenesis. *Nat Commun.* **5**, 3733 (2014).

149. B. Liao, Y. Jin, Wwp2 mediates Oct4 ubiquitination and its own auto-ubiquitination in a dosage-dependent manner. *Cell Res.* **20**, 332-344 (2010).

150. I. Attali *et al.*, Ubiquitylation-dependent oligomerization regulates activity of Nedd4 ligases. *EMBO J.* **36**, 425-440 (2017).

151. B. Sander *et al.*, A conformational switch regulates the ubiquitin ligase HUWE1. *Elife.* **6**, (2017).

152. V. P. Ronchi, J. M. Klein, D. J. Edwards, A. L. Haas, The active form of E6-associated protein (E6AP)/UBE3A ubiquitin ligase is an oligomer. *J Biol Chem.* **289**, 1033-1048 (2014).

153. A. A. Ogunjimi *et al.*, Regulation of Smurf2 ubiquitin ligase activity by anchoring the E2 to the HECT domain. *Mol Cell.* **19**, 297-308 (2005).

154. T. Mund, H. R. Pelham, Control of the activity of WW-HECT domain E3 ubiquitin ligases by NDFIP proteins. *EMBO Rep.* **10**, 501-507 (2009).

155. K. Lu *et al.*, Targeting WW domains linker of HECT-type ubiquitin ligase Smurf1 for activation by CKIP-1. *Nat Cell Biol.* **10**, 994-1002 (2008).

156. S. W. Hong *et al.*, p34 is a novel regulator of the oncogenic behavior of NEDD4-1 and PTEN. *Cell Death Differ.* **21**, 146-160 (2014).

157. Z. Chen, P. A. Cole, Synthetic approaches to protein phosphorylation. *Curr Opin Chem Biol.* **28**, 115-122 (2015).

158. T. W. Muir, D. Sondhi, P. A. Cole, Expressed protein ligation: a general method for protein engineering. *Proc Natl Acad Sci U S A.* **95**, 6705-6710 (1998).

159. J. B. Blanco-Canosa, P. E. Dawson, An efficient Fmoc-SPPS approach for the generation of thioester peptide precursors for use in native chemical ligation. *Angew Chem Int Ed Engl.* **47**, 6851-6855 (2008).

160. N. H. Shah, T. W. Muir, Inteins: Nature's Gift to Protein Chemists. *Chem Sci.* **5**, 446-461 (2014).

161. K. R. Karukurichi *et al.*, Analysis of p300/CBP histone acetyltransferase regulation using circular permutation and semisynthesis. *J Am Chem Soc.* **132**, 1222-1223 (2010).

162. O. Tsoy *et al.*, Minimal genome encoding proteins with constrained amino acid repertoire. *Nucleic Acids Res.* **41**, 8444-8451 (2013).

163. H. Rohde, O. Seitz, Ligation-desulfurization: a powerful combination in the synthesis of peptides and glycopeptides. *Biopolymers.* **94**, 551-559 (2010).

164. Q. Wan, S. J. Danishefsky, Free-radical-based, specific desulfurization of cysteine: a powerful advance in the synthesis of polypeptides and glycopolypeptides. *Angew Chem Int Ed Engl.* **46**, 9248-9252 (2007).

165. J. Li *et al.*, PTEN, a putative protein tyrosine phosphatase gene mutated in human brain, breast, and prostate cancer. *Science.* **275**, 1943-1947 (1997).

166. F. Meng *et al.*, MicroRNA-21 regulates expression of the PTEN tumor suppressor gene in human hepatocellular cancer. *Gastroenterology.* **133**, 647-658 (2007).

167. H. B. Salvesen *et al.*, PTEN methylation is associated with advanced stage and microsatellite instability in endometrial carcinoma. *Int J Cancer.* **91**, 22-26 (2001).

168. X. Wang, X. Jiang, Post-translational regulation of PTEN. *Oncogene.* **27**, 5454-5463 (2008).

169. X. Wang, X. Jiang, PTEN: a default gate-keeping tumor suppressor with a versatile tail. *Cell Res.* **18**, 807-816 (2008).

170. H. Sun *et al.*, PTEN modulates cell cycle progression and cell survival by regulating phosphatidylinositol 3,4,5,-trisphosphate and Akt/protein kinase B signaling pathway. *Proc Natl Acad Sci U S A.* **96**, 6199-6204 (1999).

171. M. P. Myers *et al.*, The lipid phosphatase activity of PTEN is critical for its tumor supressor function. *Proc Natl Acad Sci U S A.* **95**, 13513-13518 (1998).

172. A. M. Al-Khouri *et al.*, Cooperative phosphorylation of the tumor suppressor phosphatase and tensin homologue (PTEN) by casein kinases and glycogen synthase kinase 3beta. *J Biol Chem.* **280**, 35195-35202 (2005).

173. M. Rahdar *et al.*, A phosphorylation-dependent intramolecular interaction regulates the membrane association and activity of the tumor suppressor PTEN. *Proc Natl Acad Sci U S A.* **106**, 480-485 (2009).

174. L. Odriozola, G. Singh, T. Hoang, A. M. Chan, Regulation of PTEN activity by its carboxyl-terminal autoinhibitory domain. *Journal Of Biological Chemistry.* **282**, 23306-23315 (2007).

175. H. N. Nguyen *et al.*, Engineering ePTEN, an enhanced PTEN with increased tumor suppressor activities. *Proc Natl Acad Sci U S A.* **111**, E2684-2693 (2014).

176. G. R. Masson, O. Perisic, J. E. Burke, R. L. Williams, The intrinsically disordered tails of PTEN and PTEN-L have distinct roles in regulating substrate specificity and membrane activity. *Biochem J.* **473**, 135-144 (2016).

177. W. Gong *et al.*, Structure of the HECT domain of human WWP2. *Acta Crystallogr F Struct Biol Commun.* **71**, 1251-1257 (2015).

178. F. Mueller-Planitz, Crossfinder-assisted mapping of protein crosslinks formed by site-specifically incorporated crosslinkers. *Bioinformatics.* **31**, 2043-2045 (2015).

179. I. Forne *et al.*, Probing the conformation of the ISWI ATPase domain with genetically encoded photoreactive crosslinkers and mass spectrometry. *Mol Cell Proteomics.* **11**, M111 012088 (2012).

180. Q. Wang *et al.*, Understanding the stereospecific interactions of 3-deoxyphosphatidylinositol derivatives with the PTEN phosphatase domain. *J Mol Graph Model.* **29**, 102-114 (2010).

181. Y. Wei *et al.*, Phospholipid-binding sites of phosphatase and tensin homolog (PTEN): exploring the mechanism of phosphatidylinositol 4,5-bisphosphate activation. *J Biol Chem.* **290**, 1592-1606 (2015).

182. A. Perren *et al.*, Immunohistochemical evidence of loss of PTEN expression in primary ductal adenocarcinomas of the breast. *Am J Pathol.* **155**, 1253-1260 (1999).

183. L. P. Weng *et al.*, PTEN suppresses breast cancer cell growth by phosphatase activity-dependent G1 arrest followed by cell death. *Cancer Res.* **59**, 5808-5814 (1999).

184. Y. J. Yao *et al.*, PTEN/MMAC1 mutations in hepatocellular carcinomas. *Oncogene.* **18**, 3181-3185 (1999).

185. F. Vazquez, W. R. Sellers, The PTEN tumor suppressor protein: an antagonist of phosphoinositide 3-kinase signaling. *Biochim Biophys Acta.* **1470**, M21-35 (2000).

186. K. L. Lorick *et al.*, RING fingers mediate ubiquitin-conjugating enzyme (E2)-dependent ubiquitination. *Proc Natl Acad Sci U S A.* **96**, 11364-11369 (1999).

187. Y. Yang *et al.*, Ubiquitin protein ligase activity of IAPs and their degradation in proteasomes in response to apoptotic stimuli. *Science.* **288**, 874-877 (2000).

188. R. Wiener *et al.*, E2 ubiquitin-conjugating enzymes regulate the deubiquitinating activity of OTUB1. *Nat Struct Mol Biol.* **20**, 1033-1039 (2013).

189. A. Saha *et al.*, Essential role for ubiquitin-ubiquitin-conjugating enzyme interaction in ubiquitin discharge from Cdc34 to substrate. *Mol Cell.* **42**, 75-83 (2011).

190. J. Rappsilber, Y. Ishihama, M. Mann, Stop and go extraction tips for matrix-assisted laser desorption/ionization, nanoelectrospray, and LC/MS sample pretreatment in proteomics. *Anal Chem.* **75**, 663-670 (2003).

191. S. Rauch, J. Martin-Serrano, Multiple interactions between the ESCRT machinery and arrestin-related proteins: implications for PPXY-dependent budding. *J Virol.* **85**, 3546-3556 (2011).

192. L. Broix *et al.*, Mutations in the HECT domain of NEDD4L lead to AKT-mTOR pathway deregulation and cause periventricular nodular heterotopia. *Nat Genet.* **48**, 1349-1358 (2016).

193. A. Escobedo *et al.*, Structural basis of the activation and degradation mechanisms of the E3 ubiquitin ligase Nedd4L. *Structure.* **22**, 1446-1457 (2014).

194. L. Chang *et al.*, The E3 ubiquitin ligase itch couples JNK activation to TNFalpha-induced cell death by inducing c-FLIP(L) turnover. *Cell.* **124**, 601-613 (2006).

195. S. Fang *et al.*, The tumor autocrine motility factor receptor, gp78, is a ubiquitin protein ligase implicated in degradation from the endoplasmic reticulum. *Proc Natl Acad Sci U S A.* **98**, 14422-14427 (2001).

196. Z. Otwinowski, W. Minor, Processing of X-ray diffraction data collected in oscillation mode. *Macromolecular Crystallography, Pt A.* **276**, 307-326 (1997).

197. CCP4, The CCP4 Suite: Programs for Protein Crystallography. *Acta Crystallographica D.* **50**, 760-763 (1994).

198. W. L. DeLano. (DeLano Scientific, San Carlos, CA, USA, 2002).

199. Z. Chen *et al.*, Enzymatic Analysis of PTEN Ubiquitylation by WWP2 and NEDD4-1 E3 Ligases. *Biochemistry.* **55**, 3658-3666 (2016).

200. S. Durinck *et al.*, Spectrum of diverse genomic alterations define non-clear cell renal carcinoma subtypes. *Nat Genet.* **47**, 13-21 (2015).

201. Y. Sato *et al.*, Integrated molecular analysis of clear-cell renal cell carcinoma. *Nat Genet.* **45**, 860-867 (2013).

202. D. Mouradov *et al.*, Colorectal cancer cell lines are representative models of the main molecular subtypes of primary cancer. *Cancer Res.* **74**, 3238-3247 (2014).

203. P. Mertins *et al.*, Ischemia in tumors induces early and sustained phosphorylation changes in stress kinase pathways but does not affect global protein levels. *Mol Cell Proteomics.* **13**, 1690-1704 (2014).

204. Y. Yu *et al.*, Phosphoproteomic analysis identifies Grb10 as an mTORC1 substrate that negatively regulates insulin signaling. *Science.* **332**, 1322-1326 (2011).

205. H. Neurath, The versatility of proteolytic enzymes. *J Cell Biochem.* **32**, 35-49 (1986).

206. M. Huse, J. Kuriyan, The conformational plasticity of protein kinases. *Cell.* **109**, 275-282 (2002).

207. C. Choudhary *et al.*, Mislocalized activation of oncogenic RTKs switches downstream signaling outcomes. *Mol Cell.* **36**, 326-339 (2009).

208. J. Palacios-Moreno *et al.*, Neuroblastoma tyrosine kinase signaling networks involve FYN and LYN in endosomes and lipid rafts. *PLoS Comput Biol.* **11**, e1004130 (2015).

209. T. Aasen *et al.*, Efficient and rapid generation of induced pluripotent stem cells from human keratinocytes. *Nat Biotechnol.* **26**, 1276-1284 (2008).

210. F. A. Ran *et al.*, Genome engineering using the CRISPR-Cas9 system. *Nat Protoc.* **8**, 2281-2308 (2013).

211. F. Scialpi *et al.*, Itch self-polyubiquitylation occurs through lysine-63 linkages. *Biochem Pharmacol.* **76**, 1515-1521 (2008).

212. B. H. Choi *et al.*, WWP2 is required for normal cell cycle progression. *Genes Cancer.* **6**, 371-377 (2015).

213. R. Bose, M. A. Holbert, K. A. Pickin, P. A. Cole, Protein tyrosine kinase-substrate interactions. *Curr Opin Struct Biol.* **16**, 668-675 (2006).

CURRICULUM VITAE FOR Ph.D. CANDIDATES

Johns Hopkins University School of Medicine

Zan Chen

Date and Place of Birth: 09/11/1989, Chongqing, China

Educational History:

Ph.D. expected	2017	Department of Pharmacology and Molecular Sciences Mentor: Philip A. Cole M. D. Ph.D.	Johns Hopkins University School of Medicine
B.M.	2012	School of Basic Medical Sciences	Peking University

Other Professional Experiences:

Research rotation	Aug-Dec 2012	Laboratory of Jun Liu	Johns Hopkins University School of Medicine
Summer research	July-Sep 2011	Laboratory of Fuyuhiko Tamanoi	University of California Los Angeles

Awards and Honors

2016 Poster Prize of Pharmacology Retreat, Johns Hopkins University

2014 Scheinberg Travel Award, Johns Hopkins University

2013 Fred & Ruth Kort Young Scholar Award, Johns Hopkins University

2012 Excellent Graduate of Peking University

2011 Award for Future Star in Medicine, Peking University

2009 Second Price, National Medical Student Forum of Experimental Innovation

2006 First Prize and Silver Medal, China High School Biology Olympiad

Publications

Chen Z, Jiang H, Xu W, Li X, Dempsey DR, Zhang X, Devreotes PN, Wolberger C, Amzel M, Gabelli S, Cole PA. "A tunable brake for HECT ubiquitin ligases." ***Molecular Cell***. 2017, *66 (3)*: 345-375. (Featured article, highlighted by *Cancer Discovery*)

Mo GC, Ross B, Hertel F, Manna P, Yang X, Greenwald E, Booth C, Plummer AM, Tenner B, **Chen Z**, Wang Y, Kennedy EJ, Cole PA, Fleming KG, Palmer A, Jimenez R, Xiao J, Dedecker P, Zhang J. "Genetically-Encoded Biosensors for Visualizing Live-cell Biochemical Activity at Super-resolution." ***Nature Methods***. 2017, *14 (4)*: 427-434.

Henager SH, Chu N, **Chen Z**, Bolduc DM, Dempsey DR, Hwang Y, Wells J, Cole PA. "Enzyme catalyzed expressed protein ligation." ***Nature Methods***. 2016*, 13 (11):* 925-927*.*

Chen Z, Thomas SN, Bolduc DM, Zhang X, Wolberger C, Jiang X, Cole PA. "Enzymatic analysis of PTEN ubiquitination by WWP2 and NEDD4-1 E3 ligases." ***Biochemistry***. 2016*, 55 (26): 3658-3666.*

Chen Z, Dempsey DR, Thomas SN, Heyward D, Bolduc DM, Cole PA. “Molecular features of phosphatase and tensin homolog (PTEN) C-terminal phosphorylation.” ***Journal of Biological Chemistry***. 2016, *291 (27):* 16160-16169.

Taylor MS, Dempsey DR, Hwang Y, **Chen Z**, Chu N, Boeke JD, Cole PA. “Mechanistic analysis of ghrelin-O-acyltransferase using substrate analogs.” ***Bioorganic Chemistry.*** 2015, *62*: 64-73.

Chen Z, Cole PA. “Synthetic approaches to protein phosphorylation.” ***Current Opinion in Chemical Biology***. 2015, *28***:** 115-122.

Wang Y, Kavran JJ, **Chen Z**, Karukurichi KR, Leahy DJ, Cole PA. “Regulation of S-adenosylhomocysteine hydrolase by lysine acetylation.” ***Journal of Biological Chemistry***. 2014, *289 (45)*: 31361-31372.

Fang Z, Li Y, **Chen Z**, Chen J, Zhu L. “Inhibition of signal transducer and activator of transcription 3 and cyclooxygenase-2 is involved in radiosensitization of cepharanthine in HeLa cells.” ***International Journal of Gynecological Cancer***. 2013, *23 (4)*: 608-614.

Chen Z, Huang C, Yang Y, Ding Y, Zhang Y, Xu M. “Inhibition of STAT3 signaling pathway is involved in the antitumor activity of Cepharanthine in SaOS2 cells.” ***Acta Pharmacologica Sinica***. 2012, *33 (1)*: 101-108.

Lin S, Li S, **Chen Z**, He X, Xu X, Zhang Y, Xu M, Yuan Gu. “Formation, recognition and bioactivities of a novel G-quadruplex in the STAT3 gene.” ***Bioorganic & Medicinal Chemistry Letters***. 2011, *21 (19)*: 5987-5991.

Posters and Oral presentations

2017	Invited speaker, 2017 Experimental Biology Annual Meeting: Mechanisms of Life, American Society of Biochemistry and Molecular Biology, Chicago, IL
Jul. 2015	Invited speaker, Gordon Conference: Post-translational modification networks, Hong Kong, China
Mar. 2015	Poster presentation, 2015 Experimental Biology Annual Meeting, American Society of Biochemistry and Molecular Biology, Boston, MA